The Design and Implementation of an all Digital Shear Sensitive Tactile Sensor

Ajit Nilakantan

B. Eng, (McGill University) 1985

Department of Electrical Engineering
McGill University

A thesis submitted to the Faculty of Graduate Studies and Research

in partial fulfillment of the requirements for the degree of

Masters in Electrical Engineering

1987/7/20

ISBN 0-315-52413-8

RESEARCH THESES/REPORTS

THESIS NO. 87 - 13TM

TITLE: The Design and Implementation of an all Digital Shear Sensitive Tactile Sensor

AUTHOR(S) Ajit Nilakantan

Department of Electrical Engineering

McGill University

Montreal, CANADA

DATE: July, 1987

GRANT OR CONTRACT:

NO. OF PAGES: 97

SUPERVISOR: Prof. Vincent Hayward

Abstract

A novel touch (*tactile*) sensing device is presented. The sensor has several advantages over those currently available on the market. It is completely digital and based entirely on standard VLSI technology and is, in addition, sensitive to both the normal and tangential components of the pressure. The sensor has the potential to achieve high resolutions and can be inexpensively mass produced. The sensor has many applications ranging from a force sensor for a robot to a mouse–like input device. This thesis outlines the design, fabrication and testing of this unique tactile sensor.

Résumé

Le but de cette thèse est de présenter un nouveau *capteur tactile* qui offre de nombreux avantages par rapport à ceux disponibles sur le marché présentement. Les caractéristiques les plus uniques de ce "tactomètre" est de n'être fabriqué qu'en utilisant la technologie 'VLSI', d'être entièrement digital et de ne pas faire appel à des techniques très particulières. Le principe de fonctionement simplifie l'interface avec un ordinateur et aussi rend possible l'obtention de hautes résolutions. De plus, le tactomètre peut détecter les composantes normales et tangentielles de la force de contact, ce qui n'est pas le cas pour la plupart des tactomètres. Le but de cette thèse est donc d'exposer le principe de fonctionement, la procédure de fabrication et de discuter les résultats d'essais expérimentaux de ce dispositif unique au monde.

Acknowledgements

I would like to offer my heartfelt thanks to the many people who gave their time and help. This thesis involved many different areas of engineering and without them, would never have been completed. I would like to begin by thanking Prof. Vincent Hayward for his guidance, numerous suggestions and unfailing support. From the VLSI department, I would like to thank Mike Howells, Prof. Rumin and Serge Gaiotti. I am also deeply indebted to Prof. Shih, Ziad Shukri, Cindy Qiu and Steve Qiu for their incredible amount of patience and time given in the solid state lab. I also thank John Lloyd, Mike Parker and Cem Eskenazi for putting up with a lot of stupid questions. From the Canadian Microelectronics Corporation, I would like to thank Peter Ellis, Gary Puukila and Dan Gale for taking care of the special requests for the sensor. I am grateful to the many people and companies who donated materials for the sensor. They are Dan Giambattisto from B.D.H. Chemicals for the polyimides, Sal Maucieri from Dow Corning Canada for supplying the silicone rubbers, Columbia Rubber for the carbon powder and Siliconex for supplying ceramic substrates. Finally, and most importantly, I would also like to thank my family for their support.

Table of Contents

Chapter 1 Introduction

As robots are required to perform increasingly complex tasks, it becomes necessary for them possess the means to perceive as well as comprehend all pertinent features in their environment. To this end, research has thus far focused a great deal on the sense of vision. It is likely that this choice within the scientific community was perhaps, to a certain extent, dictated by the lack of any other suitable sensory input devices. The only other comparable commonly available means of sensing was through a microphone. Indeed much research and progress has been made in such areas as speech recognition. There, however, seems to be no direct application of such auditory information in robotics. Hence, vision has reigned as the only viable means of observing the environment.

Vision, however, has several disadvantages associated with it. The chief is that, simply put, vision is an extremely complex process. It is probably the most highly developed and complex of the five senses in humans. A very large percentage of the the brain is devoted to visual processing, indicating how formidable the problem is. Much of the difficulty is caused by the fact that the information one wishes to extract is not readily available from an image. In robotics, one is interested in such information as the identification and classification of objects in the workspace including the determination of their shape, size, location and orientation. One also uses sensory input to generate robot motions, controlling force and velocity and also to reduce uncertainty in the model of the environment. In vision, from a two dimensional image of light intensities, one must extract three dimensional physical features of the object that are not directly related to its optical properties (Marr 1982; Nevatia 1982). This problem involves extracting shape from intensity variations (due to shading, texture, occlusion et cetera) and is further compounded by the fact that the image can vary drastically with different lighting conditions which though easier to control in a robotic environment is still subject to change.

Recently, alternative approaches have been available, most important amongst which are range sensing devices and tactile sensors. These have the advantage over vision in that they transduce features that are close to what one is interested in. A range sensor bypasses the one great hurdle encountered in vision systems in inferring three dimensional information from a two dimensional image. Range sensors will undoubtedly play an important rôle in future developments in non–contact imaging for robotics.

Carrying the logical progression of sensors further, one arrives at what are commonly known as tactile sensors. Tactile sensors are devices that give an 'image' of the pressure applied, much as a camera gives an image of light intensities, and a range sensor a depth map. Tactile sensors can be used in a wide variety of applications. If the sensor has a sufficiently high resolution, it can be used in pattern recognition. This is especially useful in identifying small objects such as nuts and bolts picked from a bin as they are obscured by the manipulator's fingers. Used in such an application, the sensor need only detect the normal component of the force and could even be binary. Another important application for a tactile sensor is in providing force feedback to better control the object being grasped by the manipulator. For instance, a sensor that is sensitive to the tangential (*i.e.* along the plane of the sensor) component of the force as well as the normal component of the force will be able to detect slippage. In addition, such a sensor would be a great aid in such tasks as insertions which ordinary non-compliant robots find difficult. A crude sensor could also be used to probe the environment in order the build a model of the work area (Bajcsy 1983; Brock and Chiu). In addition, tactile sensors have a lot of scope as graphic input devices, as an alternative to the keyboard, mouse and joystick (Buxton, Hill and Rowley 1985; Greene 1985).

The field of haptic sensing deals with such concerns. Other applications include trying to find stable grasp positions for an object in a robot's hand (Hanafusa and Asada 1977), as well as object recognition and environment modelling (Eric, Grimson and Lozano-Pérez 1984 *and* Gaston and Lozano-Pérez 1984). The sensor is also useful in the force control of objects with the current consensus being that the robot should possess some form of 'controlled' compliance; this compliance is in fact provided by the rubber skin of the sensor. Without such compliance, there would be large spikes of force when the robot comes into contact with a rigid object.

The science is still in its infancy and most sensors suffer many shortcomings amongst which are:

1. Sensitivity to external noise sources due to electromagnetic and electrostatic perturbations. In addition, many sensors are affected by temperature and the thermal conductivity of the object grasped.

2. Fabrication difficulties in scaling the device down to achieve higher spatial resolutions; many sensors are limited in the maximum attainable spatial resolution.

3. Complexity: Most sensors are analogue in nature and hence require complex and massive analogue to digital converters and circuitry.

4. I/O difficulties: To address the individual sensing elements, the sensors have a large number of wire connections. Typically, this number is twice the square root of the number of sensing elements.

5. The prohibitive costs of the sensors keeps them out of the consumer market.

6. A vast majority of the sensors are not sensitive to the shear (tangential) component of the pressure, reducing their usefulness by restricting their range of applications.

7. Many have a limited force–scale resolution.

8. Many suffer from hysteresis and non–linearity

9. Tactile sensors are often very fragile.

In this paper, we will present a novel tactile sensor that possesses many of the features required for a sensor in robotics. It compares favourably for items 1 through 8. The last two may be circumvented or be of no importance for a given application. The sensor is completely digital and VLSI based. This allows the output of the sensor/chip to be serialised eliminating the high wire count that burdens other sensors. The device that was implemented has only seven wires (which can trivially be reduced to five) and this is independent of the resolution of the device. Being VLSI based, one can incorporate other image processing features (besides the serialisation) directly on the sensor. The interface circuitry is also very simple and the chip can easily be mass produced using standard VLSI fabrication techniques, lowering its price. Finally, this sensor will be capable of giving a grey scale output of both the normal and tangential components of the applied force. It is, though, insensitive to applied torques but it is the contention of this paper that they are not as important and can be inferred from the normal and tangential forces.

Before going into the details of the sensor, we will first describe existing tactile sensing devices, their methods of transduction, their pros and their cons. This will be followed by a physical description of the sensor. From this description, we will go on to look at the actual mechanics of touch sensing in order to predict the behaviour of the sensor. This will be followed by a description of the VLSI circuit that implements the device and its simulation. Next is an outline of the actual fabrication of the device, concluded by experimental results.

Chapter 2 A Survey of Tactile Sensors

There exist many different tactile sensing devices which use radically different pressure transduction schemes. The transduction methods used are based upon a wide variety of physical properties of materials. These involve such diverse phenonema such as resistivity, capacitance, magnetic fields and optical properties of the transductive material.

So far, no method has yet emerged as by and far the most efficient, accurate and effective. There however, seem to be two that are vying for this position. The first and more dominant are schemes based on optics. They have the advantage of suffering from very little noise—that is to say, they are not influenced by strong electric and magnetic fields that would be common in a robot workplace. In addition, rapid progress in opto–electronic technology will undoubtedly lead to an increased use of this technology. Close behind are tactile sensors based on resistivity. These, however suffer from hysteresis and hence are not as popular.

It would be impossible to give an exhaustive overview of all tactile sensors because of their diversity and number. So in this chapter, for each transduction method we will give a few typical sensors in order to give a sense of their capabilities, their advantages and their disadvantages.

2.1 An Optical Based Sensor

Optical based sensors are quite popular because of the high resolutions that are possible and their insensitivity to external noise. Below, illustrated, is a typical method of transduction (Bejczy 1984). It involves having pairs of fibre optic strands arranged in an array. One fibre transmits light which is reflected off the device's elastic cover while the second is connected to a photodetector. Normally, with no pressure applied, the light is reflected entirely into the second fibre. When pressure is applied, however, the light is deflected away from the second fibre. As illustrated, the sensor would give only a binary output—contact or no contact. The scheme can be modified slightly so that by measuring the amount of deflection, one would be able to get a grey scale measurement of the applied pressure.

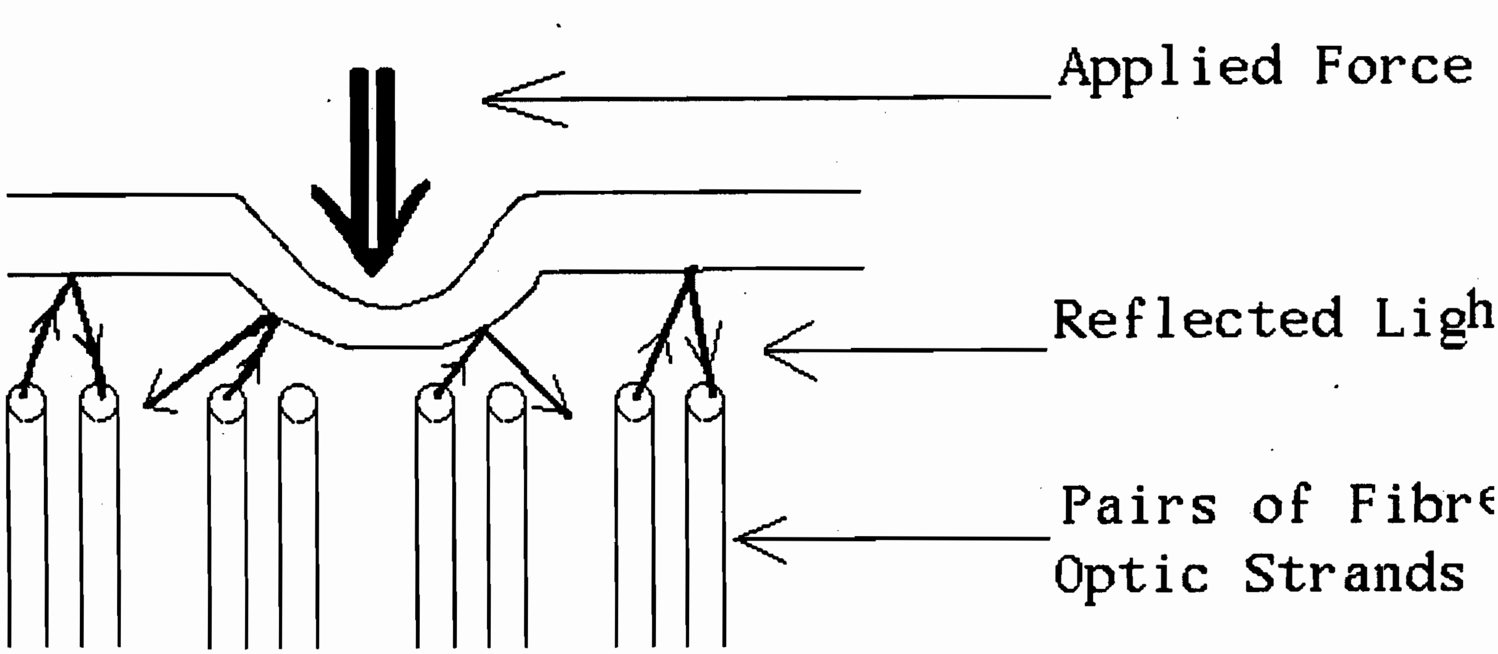

Figure 2.1 A Fibre Optic Tactile Sensor.

The main disadvantages of this scheme is that there are a large number of I/O connections. In addition, scanning the optical array may pose a problem and it may require a large number of A/D converters. On the other hand, optical sensors are immune to electromagnetic noise sources and hence are quite popular.

2.2 Sensors Based on Contact Resistance

Almost as popular as optical sensors are tactile sensors that utilise the piezoresistive properties of conductive rubber. All sensors in this family base the transduction process two phenonema: one is a decrease of resistance due to an increase in contact area caused by the deformation of the rubber under pressure; the other is a decrease in resistance due to a compression of the rubber also caused by pressure. We will give an example of each type of sensor.

One of the simplest tactile sensors is illustrated below. The top layer is a sheet of resistive rubber. Underneath the skin is an array of metal probes which measure the resistance between two points. When the rubber is pressed, it compresses, so the resistance between two adjacent electrodes decreases (non–ohmically). Thus a map of the pressure can presumably be derived from the map of resistances obtained.

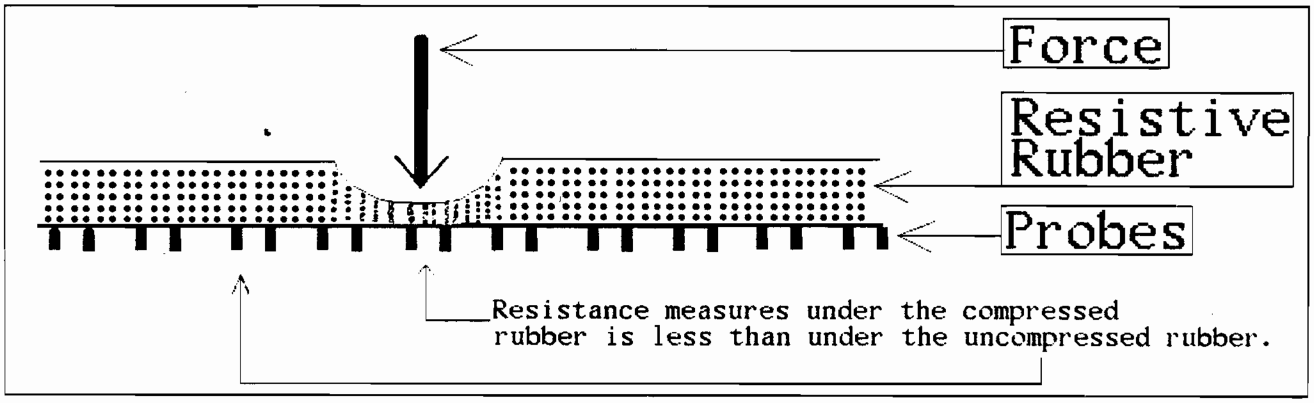

Figure 2.2 A Simple Piezoresistive Tactile Sensor.

One potential problem with the sensor is that it is not too clear how one transforms the array of resistances into one of forces. It is hard to give an accurate model of the inherently non–ohmic behaviour of the resistive rubber. Ohmic materials normally *increase* in resistance when the cross–sectional area decreases, but here we are hoping for a *decrease* in resistance since the rubber is compressing while its cross–sectional area decreases. Also, from a practical point of view, good quality rubber with uniform resistance and good mechanical properties is hard to obtain. Such rubbers normally suffer from hysteresis and poor resistive properties.

On the other hand, this circuit has been implemented on VLSI. The probes are simply the top metal layer of the chip exposed via overglass cuts. Such an arrange-

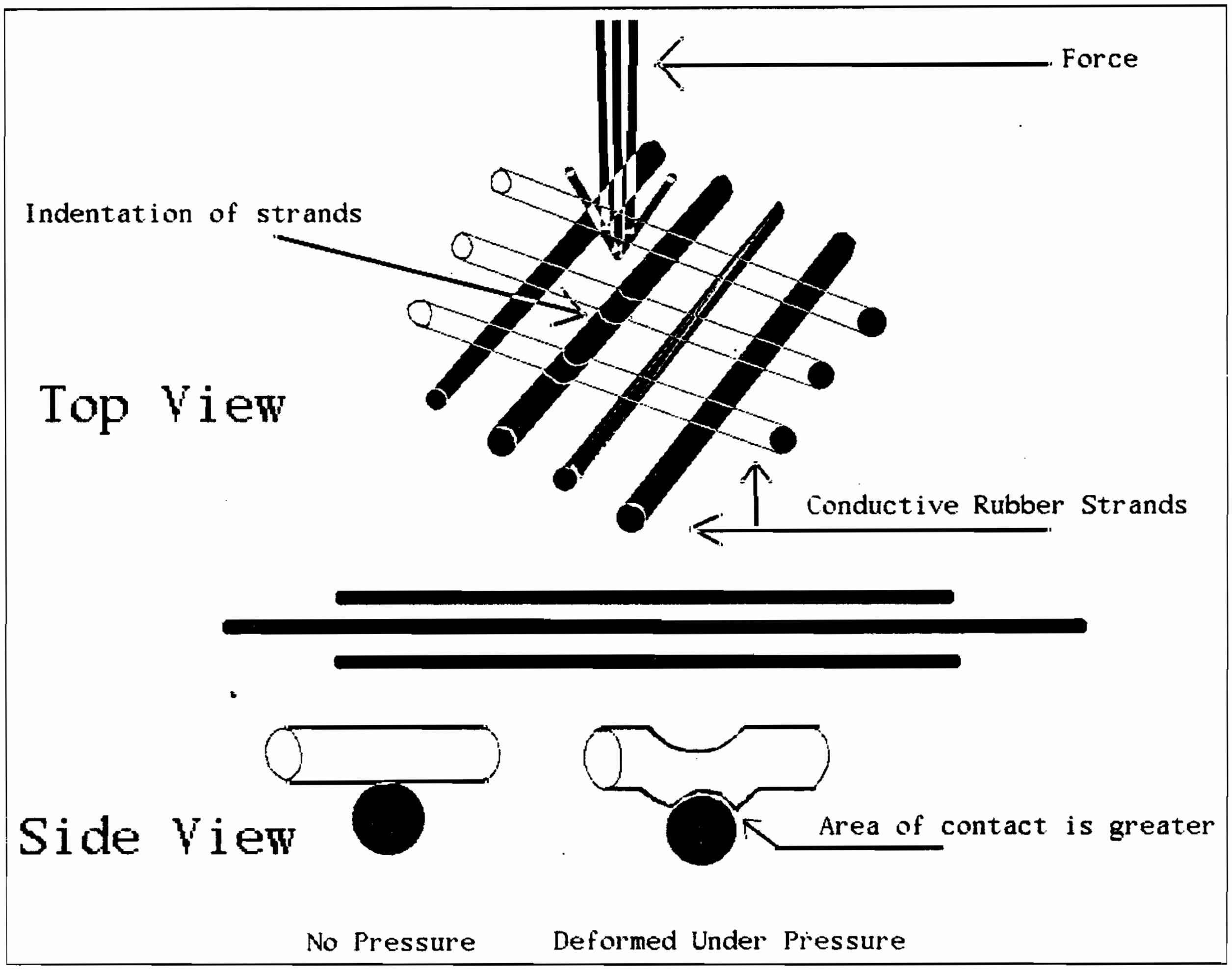

Figure 2.3 A High Resolution Resistive Tactile Sensor.

ment also permits onboard processing of the tactile image and greatly simplifies the routing of the wires. For instance, the output can be serialised, giving a very low wire count (Raibert and Tanner 1982).

Another interesting device is proposed by (Hillis 1982). This device consists of a 'fabric' of resistive rubber strands of wire. The unique feature about this sensor is that it can be woven to form a glove for the robot's end–effector. The operation of the sensor is straightforward. Normally, with no applied pressure, there is a very small area of contact between the top level and the bottom level of fibres, the fibres being cylindrical. Under pressure, however, the top level will press down on the bottom layers, deform and increase the area of contact, decreasing the contact resistance.

As with the previous design, the sensor is quite hard to model. In addition, it has a large number of wires; an **N** by **N** grid would have **2N** resistive rubber strands and require just as many wires. Also, the A/D conversion is made especially hard by the fact that the individual resistors are hard to address. Complex current driving circuits are needed to electrically isolate the resistors.

This sensor also has a more serious problem due to 'cross–coupling.' This is because the sensor can be modelled as an array of resistors, *but* we only have access to the $\mathbf{N^2}$ resistors from **4N** wires at the ends of the cylindrical rubber strands. This is what creates a great addressing problem, since the resistance of any one resistor along the measured path affects the total resistance. Note that this problem does not occur in the previous design (at least it is much less severe). This is because in the former design, one can explicitly measure the resistance between two points. There is still some degree of cross–coupling but it is nowhere near that which occurs in this design. The usual procedure is to assume that the coupling has the effect of giving the tactile image a Gaussian blur but it is not clear that this is the actual result.

2.3 A Piezoelectric Tactile Sensor

This sensor, (Wallace and Goldenberg), utilises a piezoelectric material(PVF_2) as its method of transduction. The operation of the sensor is straightforward (though some interesting steps must be carried out in fabricating the the piezoelectric material itself). The sensor consists of an array of squares of a piezoelectric plastic–like compound PVF_2 sandwiched between a plastic skin and a common ground plate. In addition, each PVF_2 square has a wire lead at the top. When pressure is applied to the the skin, the piezoelectric material compresses, resulting in a generated voltage. This voltage is measured to give the *change* in pressure.

The one main drawback of this sensor is that is measures only the change in pressure; a steady state tactile reading is not possible. To get a steady state reading, one would have to integrate the previous readings, but this leads to 'drift.' If the pressure readings vary slowly, the change will not be picked up by the tactile sensor and the tactile model of the image will be incorrect. It has also been shown, however, that the variation of pressure can be just as important as the actual pressure in many applications—for instance, during sliding motions.

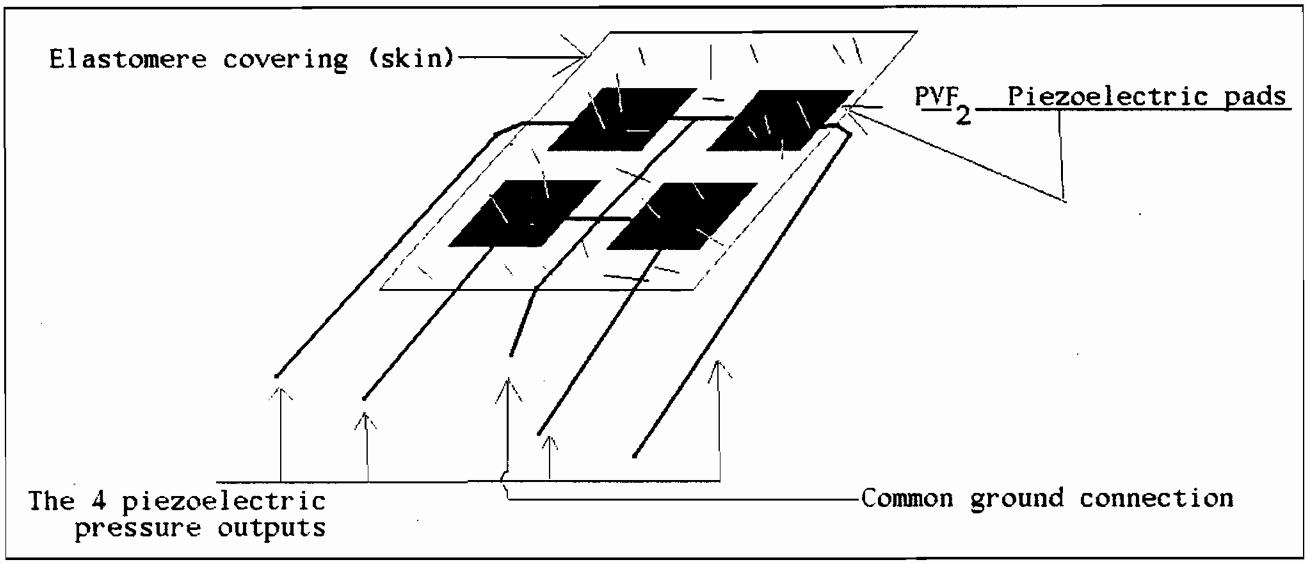

Figure 2.4 A Piezoelectric Tactile Sensor.

2.4 A Capacitive Based Tactile Sensor

This sensor, (Boie 1984), involves an array of small parallel capacitive elements. These capacitors are simply two strips of metal separated by a thin compressible dielectric gap. The principle of its operation is obvious. When pressure is applied, gap between the plates decreases, increasing the capacitance.

Needless to say, this sensor has several drawbacks. As with most of the previous sensors, it has a high wire count. Its A/D circuitry is also quite complex. But most of all, its major flaw lies in its sensitivity to noise inducible through static electricity or radioactivity. This cannot but increase as the device gets scaled down to meet greater resolution requirements.

2.5 A Torque Sensitive Sensor Based on Magnetic Dipoles

Next is an interesting design that utilises magnetic dipoles suspended in an elastic medium (Hackwood *et al.* 1983).

When pressure is applied to the sensor, corresponding dipoles are displaced slightly and what the sensor does is measure this change. Four magnetoresistive wires

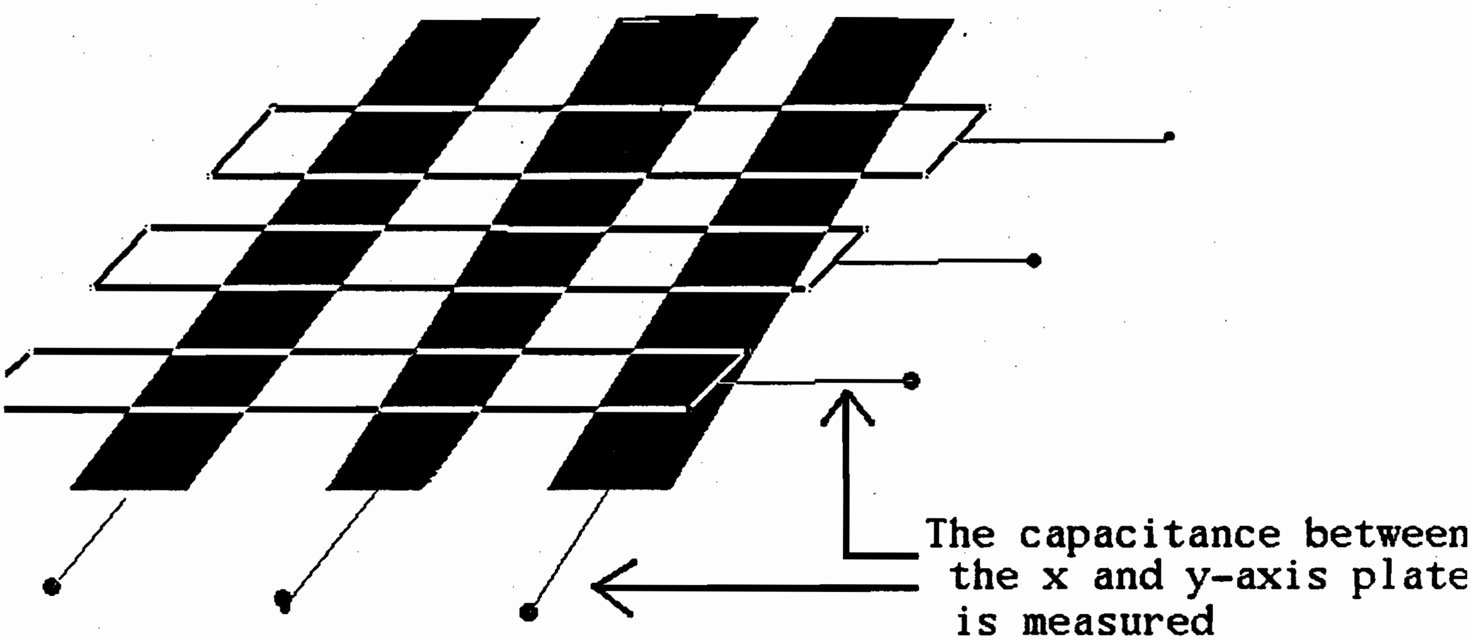

Figure 2.5 A Capacitive Tactile Sensor.

are placed around each dipole. Their resistances vary with the strength of the magnetic field generated by the dipole, enabling one to infer the location of the dipole. This will give the normal, tangential as well as angular displacement of the dipole giving us the normal *as well as* the tangential and tortional components of the force. This is quite a bit more than the previous sensors which could obtain only the normal force ignoring tangential forces and torques.

The sensor has an obvious problem that is susceptible to magnetic noise which could come from metallic objects or strong electric motors. There is also, however, a hidden problem in that the torque readings it gives are necessarily doomed to be prone to noise and inaccuracy. We will expand upon this in a coming section discussing the mechanics of tactile sensors.

2.6 An All Digital VLSI Tactile Sensor

Finally, we come upon a very clever design that we base our tactile sensor upon (Raibert 1984). This design is unique in that it requires no special A/D converters;

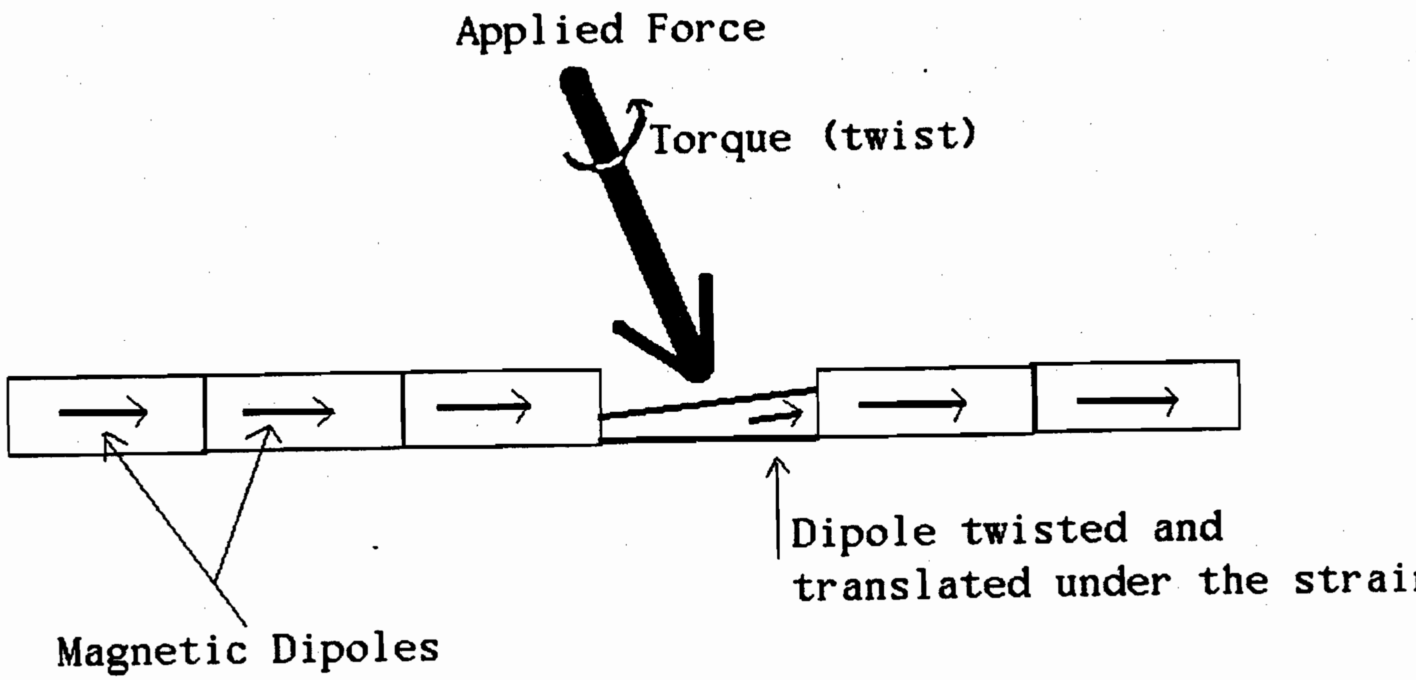

Figure 2.6 A Torque Sensitive Sensor.

as the name indicates, it is 100% digital. This surprising fact is a result of the way it transduces ~~pressure in~~to digital signals.

The sensor has a number of triangular notches engraved in the overglass of a VLSI device, exposing a number of electrodes from the top metal layer of the chip. The whole device is then covered with a stretched out sheet of elastic conductive rubber that is grounded. The principle of its operation is that when the rubber is pressed, it will tend to touch down first at the base of the triangle since the aperture is greatest there. As the amount of pressure increases, the rubber will deform more and proceed on towards the opposite vertex (see the following illustration). Thus to determine the pressure one just has to count the number of electrodes that are touched by the conductive rubber. This simple principle does away with the need for complicated analogue to digital converters since the measurement at each probe is binary, contact or no contact.

Due, however, to the unsymmetrical nature of the triangular notches, the sensor is nonisotropic. That is, the triangular notches cause different responses to equal pressures but in different directions. Thus this device is intended to measure only normal pressure but it has the bad property that it does not ignore the tangential component.

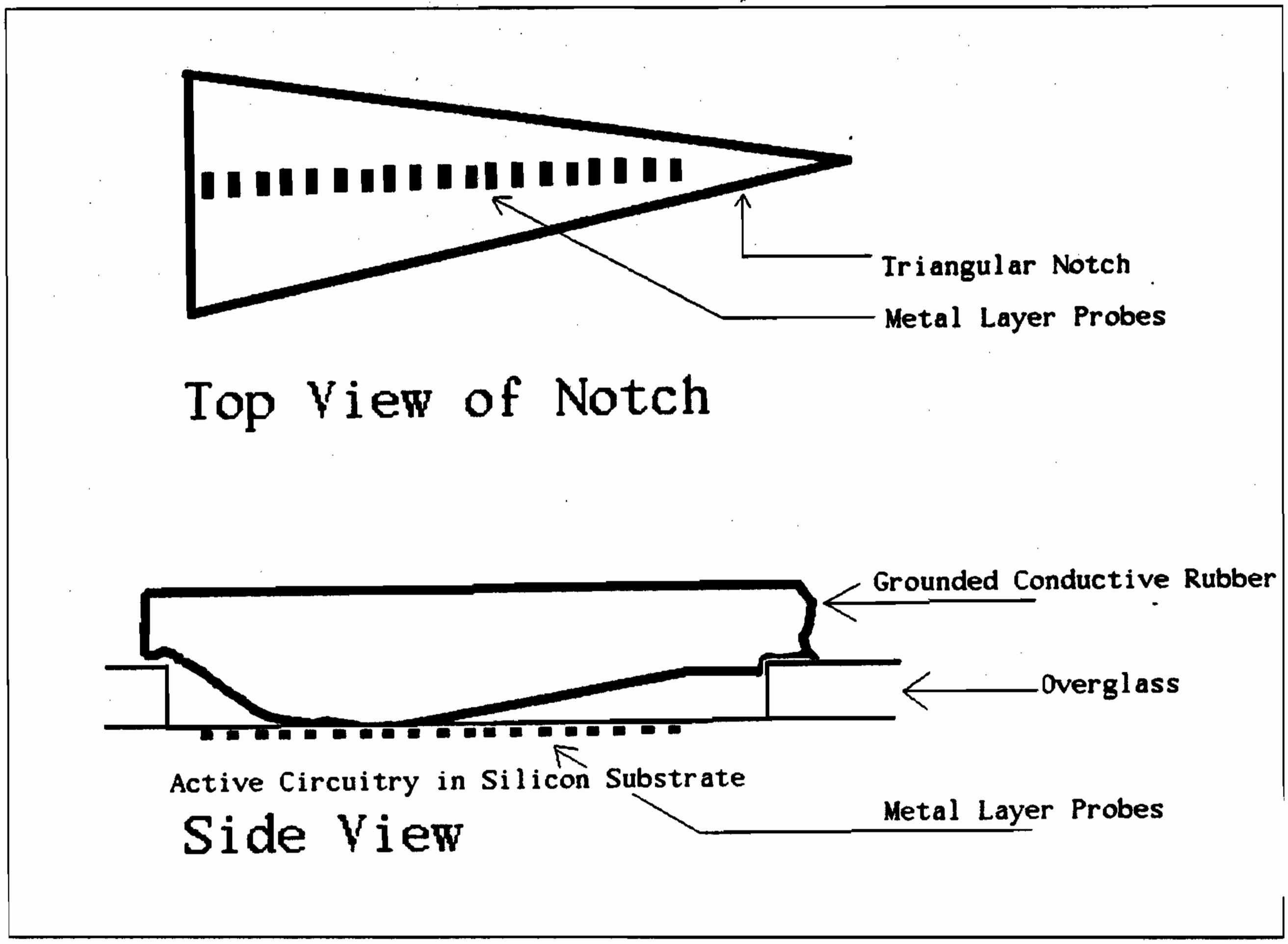

Figure 2.7 An all Digital VLSI Tactile Sensor.

Rather, the presence of tangential forces will cause the sensor to give inaccurate and erroneous results. For example, if the pressure has a tangential component along the axis of the triangle in the direction of the vertex, then it will misleadingly be interpreted as a large force since it will tend to cover more probes. Conversely, a tangential component in the opposite direction will falsely indicate a small force. Also, this sensor was never successfully fabricated. Difficulties were encountered in etching the notches in the overglass SiO_2 layer. In the proposed sensor, we attempt to solve these problems by modifying the original design as is explained in the coming section.

Chapter 3 The Proposed Tactile Sensor

We now propose a tactile sensor based upon that described by (Raibert 1984). The main difference between our tactile sensor and Raibert's is that the latter device utilised triangular notches while ours uses circular holes. This may not seem to be a great difference, but it does provide one major additional feature which is that now the sensor is shear sensitive. Paradoxically, the nonisotropic behaviour of Raibert's sensor translates into an ability to measure tangential forces in the proposed sensor.

The operation of the sensor is best explained with a picture:

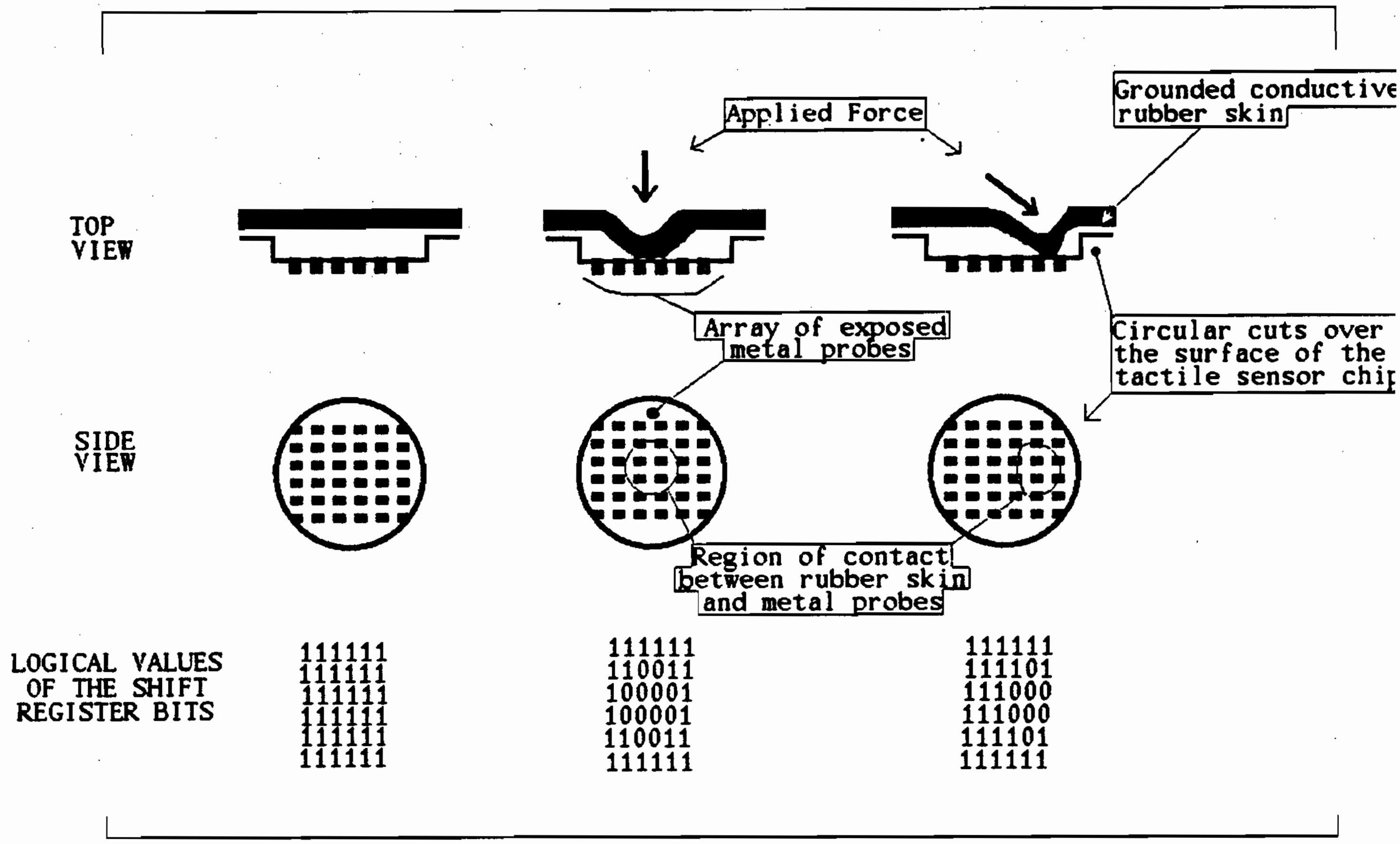

Fig~~ure 3.1~~ The Proposed Sensor.

The idea behind it is similar to Raibert's tactile sensor. Initially, without any pressure applied, the rubber is stretched out taut so it does not touch any of the 'probes.' When a normal pressure is applied to the rubber, it will deform and start squeezing through the hole. Once the pressure reaches a certain threshold, the rubber will touch down on the surface of the wafer. If the pressure is perfectly perpendicular then by symmetry, the rubber will touch the center of the circular cut first. As the pressure increases, we intuitively expect the rubber to deform more, spreading out and making contact with more probes. Thus, we expect to measure the normal force by *counting* the number of probes that touch the rubber skin.

The sensor becomes interesting when the force has a tangential component. Now, the rubber will not deform straight down but will be skewed along the direction of the tangential component of the force. Thus our hopes lie in that we expect to derive information about the tangential component of the force by measuring this offset. These predictions are formalised in the next chapter where we come up with a mathematical model of the device and derive first order approximations for the sensor response. That is to say, given a certain binary array map at a tactile 'pixel' we want an inverse transformation to derive the forces that would cause such a response. In addition, this sensor does not *directly* measure the torques at each pixel. We will show, nonetheless, that this is no great impediment and that information about the torques can be derived from a map of normal and tangential force vectors, and vice versa. Furthermore, we will also show that direct measurements of the torques, as done in (Hackwood et al. 1983) is the incorrect approach as the results will be noisy and inaccurate.

From the outset, one can foresee several obstacles that will have to be overcome in order to get a working and reliable sensor. To begin, there are a number of problems which arise from the fragility of the sensor. There is the problem that the VLSI chip will not be able to withstand the physical abuse during normal operation; the stresses caused by pressing down on the skin may cause lines to break and lead to circuit failure. In addition, large areas of the chip are unprotected with an overglass layer, exposing these regions to contamination. There is also the danger that when the rubber skin is pressed onto the chip, it will slowly erode the metal probes—this may be especially true if there are frequent changes in the tangential component of the force, which will cause the skin to slide across the probes. The metal layer of the chip is usually on the order of only 1 to 2μ thick so this could be a major factor in determining the longeivity of the sensor. Next, there is the problem that the sensor will be damaged by static electricity. The static can arise from a wide variety of sources and is an unavoidable hazard, though the conductive rubber skin may provide some form of shielding. The design is currently being based on the CMOS technology, one that is particularily static sensitive. If this turns out to be a major problem, alternate technologies may have to be considered or protective measures will have to be taken.

Despite the numerous potential problems, the design has a large number of very attractive features, not the least of which is its unique use of VLSI technology. The use of VLSI also provides the opportunity for greatly increased spatial and force resolutions as well as the option of adding high level processing circuitry directly onto the sensor ranging from data compression to edge detection and pattern recognition. In addition, if the sensor's concept can be demonstrated to be sound, a number of designs based on a similar idea are possible. These will be discussed in a later chapter.

The sensor also has a large number of parameters that can be used to shape its response. For instance, one can alter the size and depth of the holes, the density and distribution of the probes as well as the mechanical properties of the rubber skin, including its thickness, elasticity and tension. The effects of these factors will have to be determined by experiment as the processes involved are too complex to model accurately, analytically.

Finally, the choice of VLSI technology to fabricate the sensor is not absolutely necessary. It is attractive and convenient as it affords one a very high degree of miniaturisation with the added bonus of permitting one to add additional information processing circuitry onboard the sensor. If the fragility of the sensor turns out to be a significant factor, one other obvious choice of technology is the use of printed circuit boards (PCB's). The resolution offered by this technology is many times lower than that of VLSI (though fast rising) and there are greater problems faced in wire routing. The use of this technology may be dictated by its greater robustness.

Chapter 4 The Mechanics of Friction and Touch Sensing

This section will explore the theory behind the mechanics of the sensor in order to better understand and predict its behaviour. In general, the mechanics of a touch sensor are extremely difficult to model accurately. Invariably, one is forced to make a variety of simplifying assumptions so as to arrive at a simple analytic solution. One very common practice is to try to decouple the system as much as possible so that the net response can be thought of as a sum of independent components.

A feature that is necessary in almost every sensor is a skin–like rubber covering. Such a covering is required not only for the protection of the device, but also enhances its response. In fact the skin is part of the very principle of touching. Touch essentially characterises the physical phenonema which occur when two objects with different intrinsic stiffness come into contact; here a soft rubber skin comes in contact with a rigid object. For example, without a skin, if the tactile sensor comes in contact with the edge or corner of an object, it will be subjected to enormous stresses which would damage the device. When a noncompliant sensor comes in contact with a hard surface, the number of contact points will be small and at these points of contact, the force will be very high. Thus, for example, one would find it impossible to differentiate between a spherical object and a corner of a cube or even between a flat face and isolated points. This is the case since only three points of contact are necessary for the stable grasping of an object; the rubber skin serves to dissipate the force.

Unfortunately, the rubber skin is one of the hardest components of the sensor to model accurately. The rubber skin is most often modelled as just a Gaussian blurring. Thus to obtain the 'actual' pressure map, one would just have to apply a deblurring operator on the map given by the force sensing devices (Kinoshita and Hattori 1984).

Thus in many sensors, there is a neat physical decoupling of the sensor. One just has to accurately model and understand the behaviour of the pressure transducing device and basically ignore the rubber skin, for the moment. Later on, various image enhancing techniques can be used to recover the original image.

In this sensor, however, the mechanics of the rubber play an integral part in the response of the device. The rubber skin, in this sensor, exhibits two forms of behaviour, one on a *macroscopic* level and one one a *microscopic* level. On a global (or macroscopic) scale, the rubber can still be modelled as a Gaussian blurring operator. This is in the sense that the rubber will smear out the applied pressure map. Deblurring techniques identical to those used in vision (Hummel, Kimia and Zucker 1983) can be employed to restore the original tactile image.

On a more local scale—on the scale of a 'pixel,' the microscopic effects take place and it is these microscopic effects that give the sensor its interesting response. To predict the behaviour of the sensor, we will first give a simple first order approximation of what happens when a force is applied to the skin of the VLSI sensor. This model will give us an idea of what to expect and lend credence to our instinct that the sensor is indeed sensitive to tangential forces.

Consider a point pressure being applied on a sheet of rubber over the center of a circular hole (as we have in our sensor). A reasonable approximation is that the resulting deformation in the rubber would have a Gaussian profile. The approximation is also justified since the hole is so shallow as compared with the diameter of the cuts. This deformation, however, is obstructed by the bottom of the holes—the surface of the wafer. The resulting region of contact depends upon the amount of force applied, its direction (*i.e.* its normal and tangential components), the mechanical characteristics of the rubber and the depth of the cuts. Taking advantage of the fact that the depth of the hole is so small, we can approximate the the region of contact by the area cut off by the plane at a height **d**, the depth of the hole. Furthermore, one can use a first order spring–like approximation of the rubber. Working in two dimensions, since everything is radially symmetric, when a normal force (F) is applied the deformation of the rubber can be approximated by:

$$y(x) = -\kappa F e^{-\sigma x^2}$$

κ is the 'spring constant' or the first order approximation of the stiffness of the rubber.

σ is the blurring factor. It depends on the thickness of the rubber skin as well as its mechanical properties. **x** is the distance radially form the center and **y** is the vertical deformation of the rubber, *provided* that it does not hit the bottom of the hole. When it does hit the bottom, we ignore the complex boundary effects and assume the resulting profile will still be a Guassian but the bottom simply cut off.

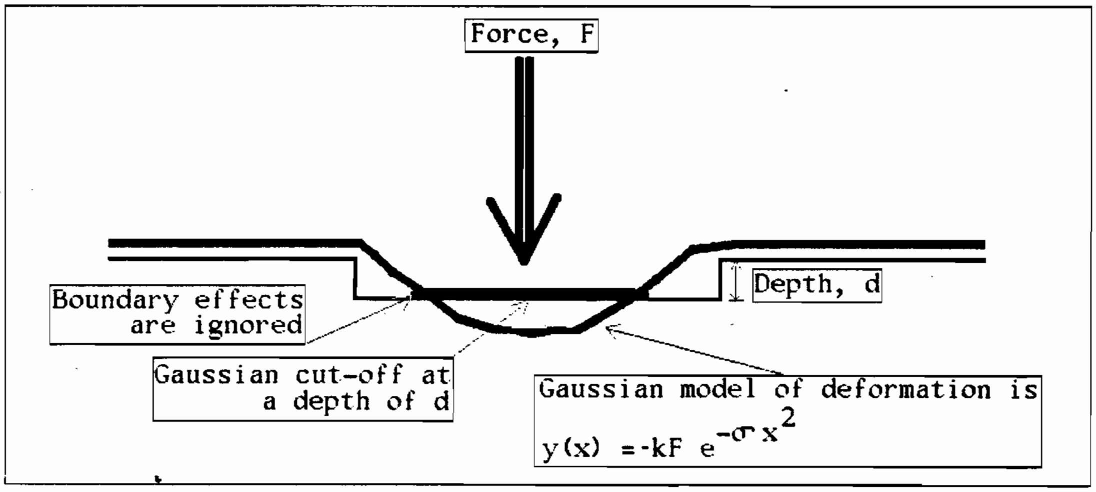

Figure 4.1 The First Order Approximation of the Deformation Caused by a Normal Point Force over a Circular Membrane.

Thus, at a depth **d**, we have,

$$y(x) = -d = -\kappa F e^{-\sigma x^2}$$

Therefore

$$\begin{aligned} x^2 &= \frac{1}{\sigma} ln(\frac{\kappa F}{d}) \\ &= \frac{1}{\sigma} ln(\frac{\kappa}{d}) + \frac{1}{\sigma} ln(F) \\ &= \text{threshold } + \frac{1}{\sigma} ln(F) \end{aligned}$$

Since the area of contact is πx^2, we have the interesting result that, after a certain threshold, *the area of contact increases in proportion to the logarithm of the normal force.*

Now, consider a slight tangential component to the force as illustrated below. If the angle, θ made by the net force, **F**, to the normal, **N** is small then we can make a gross approximation. We can assume that the displacement of the 'center–of–mass,' Δx of the area of contact, will vary directly with the tangential component, **T**. This approximation is valid if the depth of the hole, **d**, is, as we are assuming, small compared to the diameter of the hole so we can consider only the linear terms. The constant of proportionality is, as before, κ, the first order stiffness of the skin. In this case, we are modelling the skin by a spring.

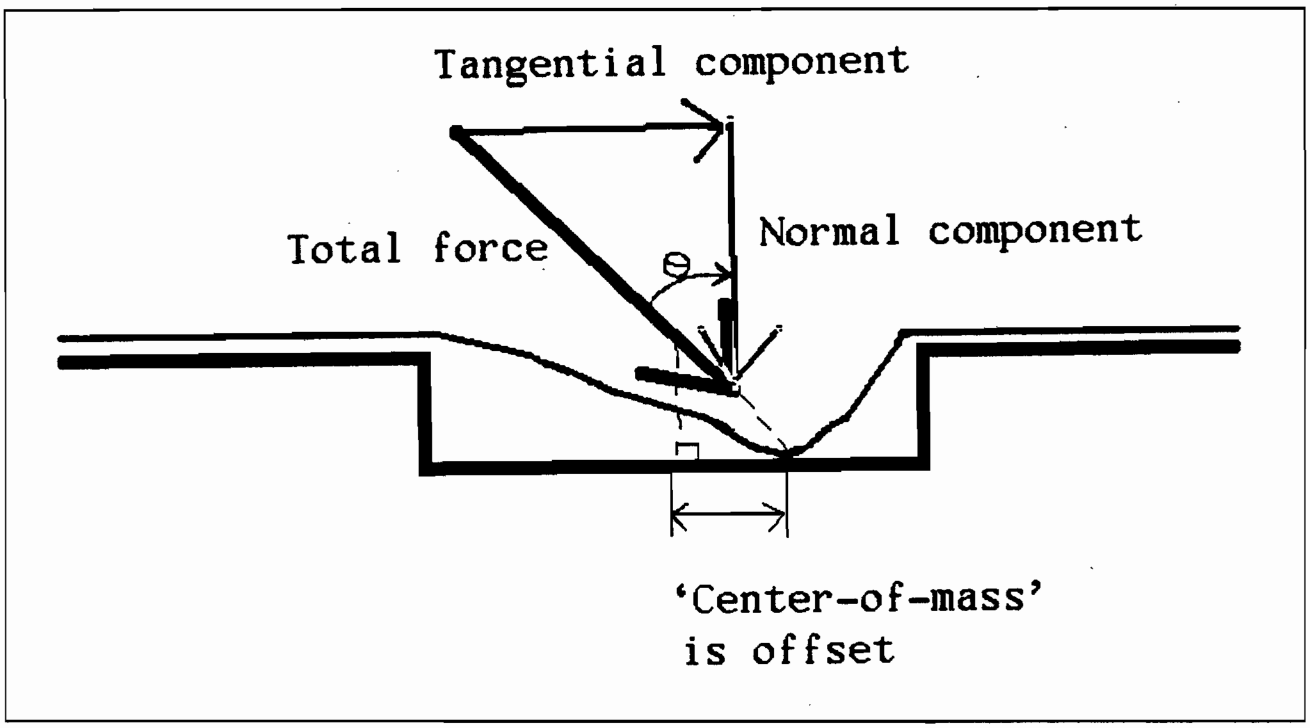

Figure 4.2 The First Order Approximation of the Deformation Caused by a Small Tangential Force.

Thus to summarise, we are able to relate the normal and tangential forces to the 'mass' and the 'offset of the center–of–mass' of a single tactile sensing element. The mass can easily by calculated; it is the total number of probes that are touched by the rubber skin. Similarly, the offset of the center–of–mass is the distance of the centroid of the area of contact, from the center of the circular cut. Thus,

$$\text{Mass} \propto ln(\mathbf{N})$$

$$\text{Center–of–mass} \propto \mathbf{T}$$

A more accurate model is presented in (Fearing and Hollerbach 1985). The model is accurate enough to predict the fringe effects that occur when a rigid object presses against a rubber sheet. Such fringe effects include the bulging of the rubber along the edge of the object which will cause 'negative' stresses. It gives the stresses formed in the rubber when a point force is applied to an infinite plane of rubber sheet. The basic premise in the model is that the stresses are distributed uniformly radially around the direction of force. However, the model can only derive the resultant stresses in the rubber, not the displacements which we are interested in. This is because superposition holds only for stresses, not displacements. The example given is that the net displacement that occurs when two points indent a rubber skin by 1mm is not the sum the displacements that are created by the points individually. The resulting stress profile is *not* a Gaussian as we had predicted. Qualitatively, however, the stress profile is very close to a Gaussian. The model, however, is based on the assumption that the rubber is infinite in length and this is clearly not so in the microscopic model, although the lateral dimensions are large compared with the vertical depth of the hole. In addition, neither model takes into account the boundary conditions at the edges of the circular hole and at the bottom.

It would not be reasonable to expect either one of these models to come close to predicting the response of the sensor—there are just too many factors to be taken into consideration. Nonetheless, we do have certain expectations about the sensor's behaviour, and we can use them as a starting point. The only true model will have to be, and will be, derived by experimentation.

In closing we note that the sensor predictions were based on the assumption that the force was directed over the center of the circular cut. If a force is directed off-center, or an object only partially covers a sensor site, then these sensors will be wildly off, more than likely indicating the presence of very large tangential forces. This fault, however, is shared by many a other sensor design. The edge effects are sure to give erroneous results for many optical sensors such as (Bejczy 1984). The magnetic dipole sensor by (Hackwood et al. 1983) will also exhibit such edge effects.

4.1 A Note on Measuring Torques

Most sensors choose to completely ignore torques, at least in the pixel level. The only sensor that is torque sensitive is the one based on magnetic dipoles (Hackwood et al. 1983), discussed in a previous section. However, we will show that it is not necessary to directly measure the torques and that furthermore, such measurements will probably be inaccurate and prone to noise.

The VLSI sensor is not able to directly measure torques so we will argue here that such information is redundant in that one can derive the torques from the force field. So, based on the previous observation about torque measurements, we lose nothing by having a sensor that is torque insensitive.

This is because, the global torque about an arbitrary point is simply the vectorial sum of the force vectors *crossed* with the radius vector. One can extend this and arrive at a *map* of torques, $\tilde{\tau}$, much as we have a map of forces, $\vec{F}$. We arrive at this by simply applying the curl operator on the force field since,

$$\vec{\tau} = \lim_{C \to 0} \oint_C \vec{F} \times \vec{R}.$$

Because of noise, we will probably have to average (*integrate*) over a larger path, that is, not let the closed path, C, collapse to a point.

Another approach would be to directly measure the torques at each pixel point. This has one major problem associated with it in that due to physical constraints, the developed torques are of a secondary order. That is to say, a force sensor measures linear deformations formed at each pixel but a torque sensor must measure angular deformations which are a magnitude smaller. Thus any device that directly measured torques would have to be much more accurate than a similar force measuring device and would be subjected to much more noise.

For example, consider a rigid object being held and twisted against the rubber skin of a sensor. This twist will create an elementary torque $\boldsymbol{\Delta}\tilde{\tau}$ at a point, $\tilde{\mathbf{p}}$, in the z-direction. It will also cause an elementary angular deformation $\boldsymbol{\Delta}\theta$ to be formed at that point as well. Now, if the object is large, *i.e.* an order of magnitude larger than the size of the sensors, this angular deformation will cause linear stresses along the object as well. At a distance **r** from $\tilde{\mathbf{p}}$, the rubber will be stretched a distance $\mathbf{r}\Delta\theta$. Thus to keep the rubber from stretching and applying too great a stress, one would be forced to apply torques that are constrained by the size of an object; large objects—those as large as the tactile sensor would have to cause only small angular deformations.

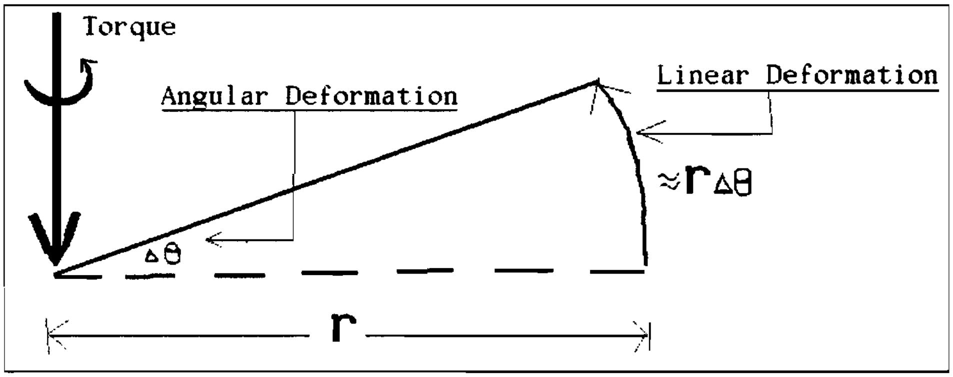

Figure 4.3 The Linear Deformation Induced by an Angular Deformation.

To summarise, to get 'measurable' torques, one would have to work with objects that are as large as the torque sensing devices. This, however, is dangerous for the tactile sensor since such objects are likely to pierce the skin and damage the sensor. An object so small that would give such an angular deformation would be akin to a drill and would go right through the rubber skin. Thus we lose nothing by having a sensor that does not directly measure torques since that information can be derived directly from the forces.

Chapter 5 The Design of the VLSI Circuit

Having explored the theory behind the sensor, we now go into the details of the VLSI circuit. Unlike the developed theory which was essentially independent of the technology used to implement the sensor, the laid out circuit is very much tied in with such matters. However, as we shall see, the circuit is exceedingly simple so the 'problem' of having to redesign the sensor each time the VLSI fabrication technology advances is minimal.

We will begin by giving a brief overview of the CMOS VLSI technology that was used to implement the sensor. A reader familiar with VLSI design can skip the next section without loss of continuity.

5.1 VLSI Fabrication Technology

5.1.1 An Introduction to CMOS VLSI Design

Complementary MOS (CMOS) is presently the dominant VLSI technology. Its popularity stems chiefly from the fact that CMOS circuits use very little power. In some design strategies, the power used by a chip can be made to be directly proportional to the clock rate. Thus in some applications (such as watches, clocks and calculators), where a low clock rate is tolerable, the chips consume a negligible amount of power. Also, CMOS circuits can be very tightly packed onto silicon wafers. The miniaturisation technology has not bottomed out yet; it appears likely that circuit dimensions can be decreased by an order of magnitude yet. Current technology allows minimum dimensions around 3 microns ($1\mu = 10^{-6}$m). That is to say, 3μ is the minimum dimensions achievable in the silicon foundry. This is usually applicable to transistors, so it would mean that the smallest transistors would be 3μ by 3μ.

CMOS gets its name from the two types of transistors which are used, the pMOS and nMOS field effect transistors (FETs.[1]) These MOSFETs behave in a complementary fashion. MOSFETS are voltage controlled transistors which can be modelled as switches (to be contrasted with current controlled bipolar transistors). The MOSFET is a three terminal device[2]. The voltage applied to the *gate* controls the 'switch' between the *drain* and *source* terminals of the transistors[3]. For an nMOS transistor, if the gate voltage is low (*i.e.* 0 volts) then the source is effectively 'cut–off' from the drain; the switch is open. When the voltage is high (*i.e.* 5 volts), the 'switch' closes allowing the signal input at the drain to pass through and to be output at the source. The nMOS transistor is not, however, a perfect switch when it is closed. It passes a low input well but a high input is degraded—there is a voltage drop of about 0.7 volts (depending upon fabrication parameters). The pMOS transistor behaves in an exactly opposite way. When the gate voltage is high, the transistor is cut–off. When the gate voltage is low, the transistor is turned on. It passes a high signal well but a low input is degraded, raised by approximately 0.7 volts. This is illustrated below.

These basic building blocks can be used to build more complex logic devices, the simplest of which, an inverter is illustrated below.

The inverter's operation is straightforward. When the input is low, the nMOS

---

1 There are really two types of MOS transistors, *enhancement* mode and *depletion* mode devices. An enhancement nMOS transistor is normally cut–off with a zero gate potential, whereas a depletion mode transistor still conducts (*i.e.* it has a negative threshold voltage). Similarly, a pMOS enhancement mode device is cut–off with a high gate voltage ($\approx$5 volts), but a depletion mode transistor is still in the active region. In this paper we will, without exception, restrict the discussion to *enhancement* mode transistors.

2 There is an additional terminal but we will, for the most part, ignore the *substrate connection*. In our design, as in most, the nMOS substrates are always grounded and the pMOS substrates are always tied to V_{DD}, the power supply.

3 MOS transistors are completely symmetric; the drain and source can be interchanged though it is customary to refer to the positively biased end of the transistor as the drain.

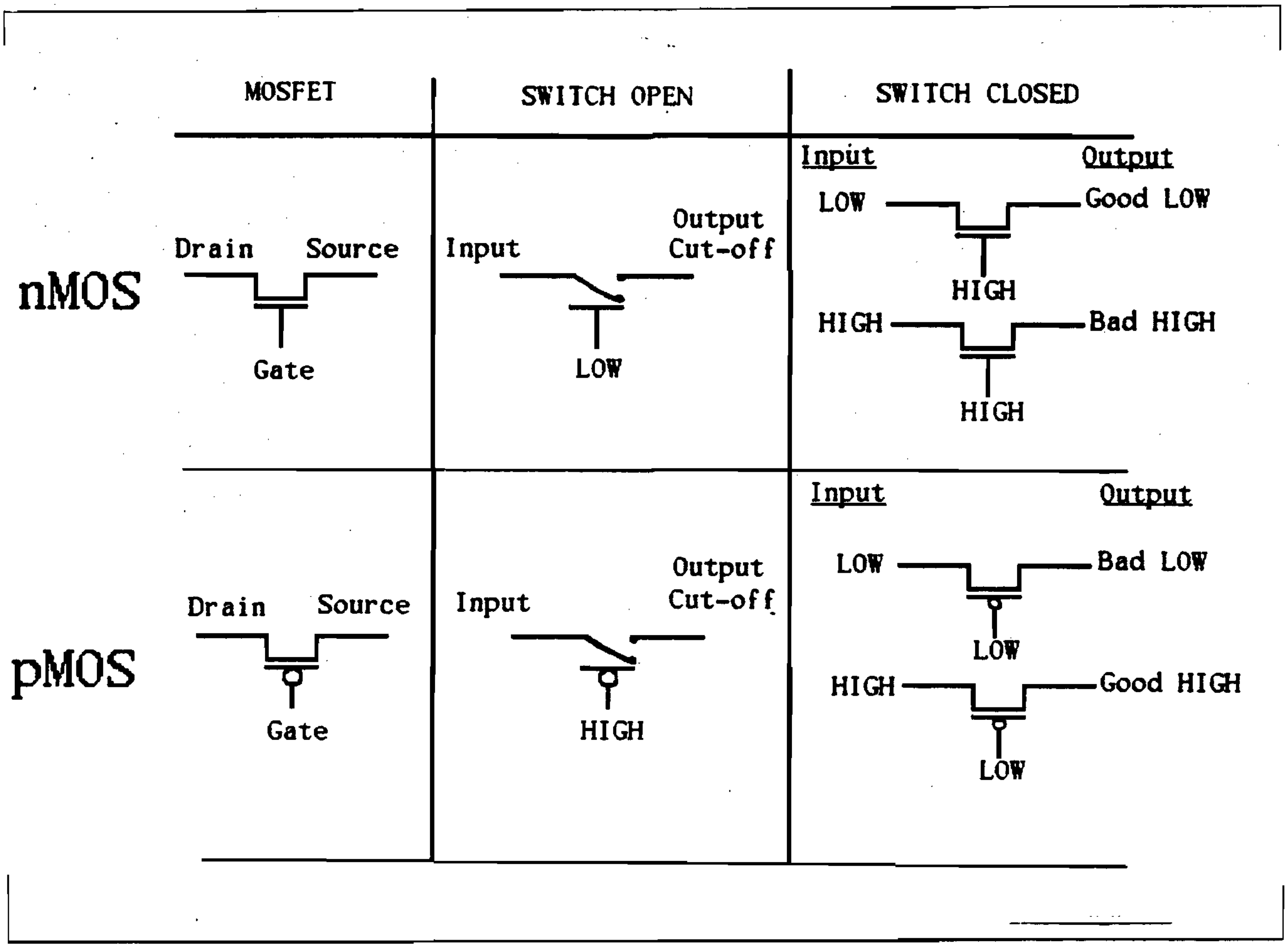

Figure 5.1 The Behaviour of MOSFET Switches.

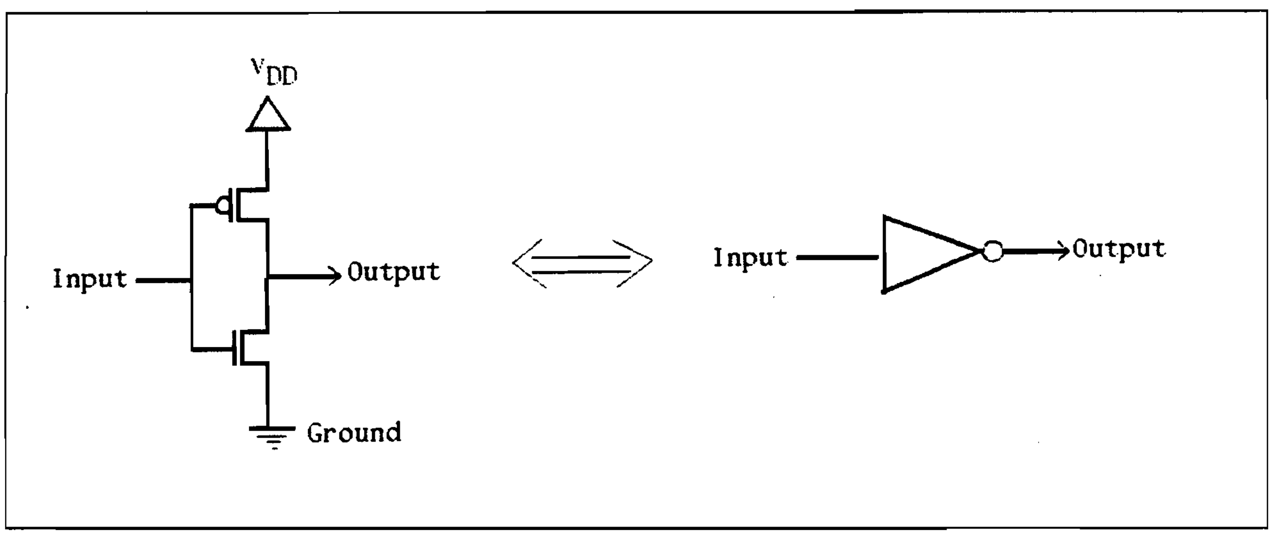

Figure 5.2 A CMOS Inverter.

transistor is cut–off and the pMOS transistor is turned on, passing V_{DD} † and giving a 'good' high output. Similarly, a high input cuts–off the pMOS transistor and turns on the nMOS transistor which passes the ground voltage, giving a low output without any degradation.

There are two points of interest. First is that the input draws almost no current since it drives the gates of the MOSFETs. Secondly, one of the two transistors is always cut–off so there is never a conducting path from V_{DD} to Ground (the effective resistance of a cut–off transistor is for all intents and purposes infinite). The only time there is a conducting path is when the input changes (on a clock transition). Thus the circuit draws almost no power; there are only sharp spikes of current during the brief transition times.

One additional point of note is that in some circuits, the voltage drop/rise that occurs across a transistor (also called a *pass transistor*), is tolerable. For example, if the output of an inverter (which is *always* at the 'full' logic values) passes through an nMOS pass transistor, then a high will be lowered by approximately 0.7 volts, while the low voltage remains, essentially, unchanged. If this corrupted signal, is immediately input to another inverter then the output of that inverter will regain the original undegraded signals. This is because a drop of 0.7 volts is not enough to switch the inverter over to the incorrect state. Taking the pass transistor into account, the inverter can be biased by ratioing the two transistors so that the 50% voltage is 2.5 volts (or $\frac{1}{2}V_{DD}$). Depending upon process parameters, as many as three pass transistors may be cascaded, though it is not really recommended. In our tactile sensor design, just a single level nMOS pass transistor was used and extensive simulations showed that it had no effect upon circuit performance.

5.1.2 An Introduction to CMOS VLSI Fabrication

The fabrication of a wafer involves the transformation of an abstract transistor level representation of a circuit into the actual physical devices. Current photolithographic techniques base the fabrication on one of the two following cycle of steps.

† V_{DD} refers to the power supply or high voltage. V_{SS} refers to the ground or low voltage.

○ Adding and etching a layer onto the wafer.

- First a layer of material we wish to add as a new layer is coated over the wafer. This coating is is usually obtained through *sputtering* (vapourisation) or through oxidisation (by heating the wafer in an oxygen/water vapour atmosphere).

- Now, we desire to selectively remove certain areas of this coating and we achieve this by first applying a coating of *photosensitive resist* over wafer (and over the layer we want to remove). The resist must have the property that the compound that etches it (the *developer*) must not etch the layer underneath, and conversely the etchant for the lower layer must not affect the resist; being otherwise would defeat the purpose of the resist.

- Next, we selectively *expose* the photoresist to some form of radiation, causing a chemical change in the exposed regions. In a photolithographic process, photomask is used to expose the resist to ultraviolet (and, more commonly, X–ray) radiation. The photomask is simply a very high quality image of the desired regions we want exposed, mounted on a clear glass plate. Depending on the type of photoresist used, a corresponding negative or a positive photomask will have to be used. A positive photoresist is one that breaks down when exposed. Consequent development will wash away the exposed regions, leaving the unexposed regions intact, over the wafer. Similarly, a negative photoresist becomes resistant under the exposed regions, while the unexposed regions are dissolved by the developer.

- Now that we have the specific regions of the original material exposed, we etch it, using an etchant that does not affect the photoresist. This step is often tricky since the etchant may also dissolve lower layers—the development time must be carefully calibrated.

- Finally, we remove the rest of the photoresist with a *stripper*, leaving, unaffected, the desired patterns of the original material on the wafer.

- Alternatively, one may want to just *dope* selected regions by adding trace impurities, changing that region's electrical characteristics.

    - Here one begins by coating the wafer with photoresist.

    - Next, as before, one exposes the photoresist, and develops it, leaving exposed, the regions in the wafer we want to dope.

    - The wafer is doped. Many methods are possible; common methods include diffusion (through heating the wafer in a doped atmosphere) and ion bombardment, which directly applies the impurity ions to the wafer. Note that in this case, the photoresist is used to prevent the impurities from doping unselected region.

    - Finally, as before, we strip the photoresist leaving the doped regions.

These above steps are applied repeatedly to the wafer resulting, finally, in a completed chip.

We will outline these steps, very briefly and greatly simplified, for a single metal layer 'p–well' process which was, in fact, used to fabricate the wafer.

• The p–well process begins with a moderately doped n–type wafer. The wafer is then split into two regions, one containing the nMOS transistors (on a p–type substrate) and the other containing pMOS transistors (on an n–type substrate). The wafer is already n-type so the first step is to define the p–type regions (or p–wells) and dope them with p-type material (*e.g.* Boron).

• Next, the regions that are to become the drains, sources and channel regions of the devices are processed. This layer is often synonomously referred to as the diffusion layer, field oxide and device well. In this thesis, we will refer to it as the *diffusion layer* (not to be confused with the general process of diffusion).

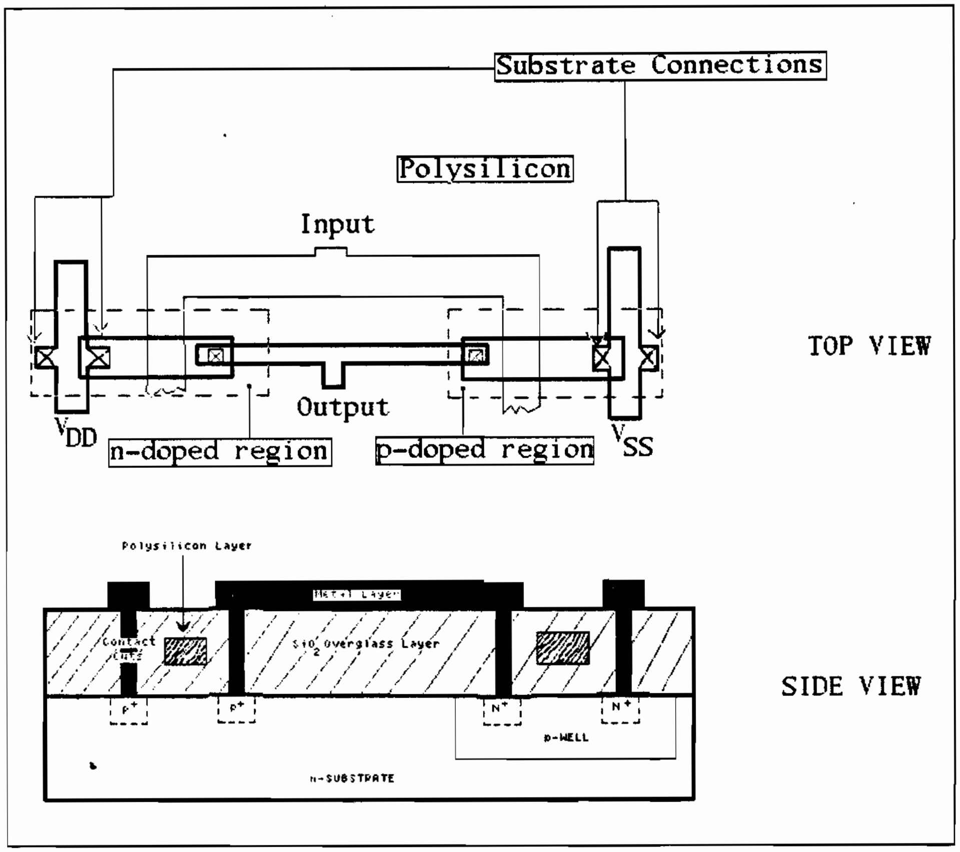

Figure 5.3 The Physical Structure of CMOS Transistors. (*From (Weste and Eshraghian 1985) page 75.*)

• Next, two guard masks are used over the non-active regions (those outside the device wells). The first, the p–guard, is used to set the threshold voltages in the p–well. Similarly, the n–guard sets the threshold voltages in the n–type substrate.

• Following this, a fairly thick layer of insulative field oxide (SiO_2) is deposited over the wafer.

• Next a thin layer of *gate oxide* is grown over the transistor's active region.

• Covering the gate oxide, forming the gates of the transistors, is the *polysilicon layer*. The polysilicon can also be used for interconnections over the field oxide (which insulates it from lower layers, specifically diffusion).

• Next the N^+ and P^+ masks are used to heavily diffuse the diffusion regions in the p-wells and the n-substrates respectively. Note that the polysilicon layer covers the gate channel, preventing it from being doped.

• The steps so far have defined all the transistor structures; the remaining steps mainly involve metalisation. First, we deposit a thick layer of SiO_2 to separate the *metal layer* from the rest of the circuit. Where we want a contact between metal and polysilicon, or metal and diffusion, or metal and substrate, we form a *contact cut* to that layer, through the SiO_2.

• Next, a layer of metal (aluminium), is deposited over the whole wafer. The metal is able to sink down through the contact cut, to make contact with the lower layers. The metal can also be used as a bridge to join two different layers or to allow a polysilicon line to cross a diffusion region without forming a transistor.

• The final step is the *passivation* process. Here a fairly thick layer of over-glass (SiO_2) is deposited over the whole wafer. Holes are only etched over the metal bonding sites and probe points. The purpose of this layer is to protect the chip against mechanical and chemical damage.

Finally, we will summarise the purpose, use, and characteristics of each layer from a VLSI designer's point of view, rather than from that of a VLSI fabrication engineer. The three most interesting 'layers' are the diffusion, polysilicon, metal and contact cuts. We use the term layer very loosely, for what we are in fact referring to is a mask–level description of the process. For example, the contact cut is not a layer as such, but the contact cut processing corresponds to a photomask operation. That is to say, the regions where there are to be contact cuts will correspond to one photomask. Thus, the VLSI designer works at the photomask level.

The masks which correspond to the doping operations are not of as great an interest. This is because, they are really dictated by the placing of the pMOS and nMOS transistor. Most designers separate, physically, the placement of the pMOS and nMOS transistors, so that the p–wells and n–substrate regions do not wildly intertwine, and the regions are fairly large†. The only important point to note about the substrates is that they should always be ties to the appropriate potential, through a *low resistance path*. The n–substrates should be grounded and the p–substrates tied to the power supply. This is necessary to prevent latch–up.

† This also helps prevent latch–up

When a polysilicon line crosses a diffusion line, the result is a transistor. The polysilicon forms the gate, and the two ends of the diffusion become the source and the drain. Depending upon which substrate the well is in, the transistor is pMOS or nMOS.

Of the three layers, the metal has the least (almost negligible) resistance. The diffusion and polysilicon layers have quite high resistances ($\approx 25\Omega/\square$ for diffusion and $\approx 50\Omega/\square$ for polysilicon). Long diffusion lines, however, are not recommended because of their high capacitance and RC constant. Polysilicon's RC constant is about an order of magnitude less, while that of metal is again negligible for the purposes of our design.

5.2 The VLSI Circuit

During the course of the project, chips were laid out for four different VLSI technologies. Two designs based on the NMOS process were not fabricated since that technology was in the process of being phased out. In its place, three CMOS chips were sent for fabrication. Two used a 5 micron process and the other, a higher resolution 3 micron process. The NMOS designs will not be discussed here as they were never fabricated.

As mentioned, the circuit is embarassingly simple, basically just one long N-bit shift register (N being the total number of probes in the circuit). Being a prototype sensor, it was decided to keep the circuit as simple as possible so no special processing circuitry (other than the serialiser) was incorporated. If the design shows promise, such features can be added in later submissions. The chip has a single output—that of the shift register. In addition, there are a small number of input lines for control signals, synchronisation, clocks and power supply. The register latches on the 'values' of the probes (*i.e.* whether it is touching the skin or is 'floating') and shifts out these binary values.

Ideally the entire surface of the silicon could be covered with the shift registers, making maximum use of the available area. Illustrated below is such a layout of a 2 by 2 array tactile sensing elements, each with 64 probes.

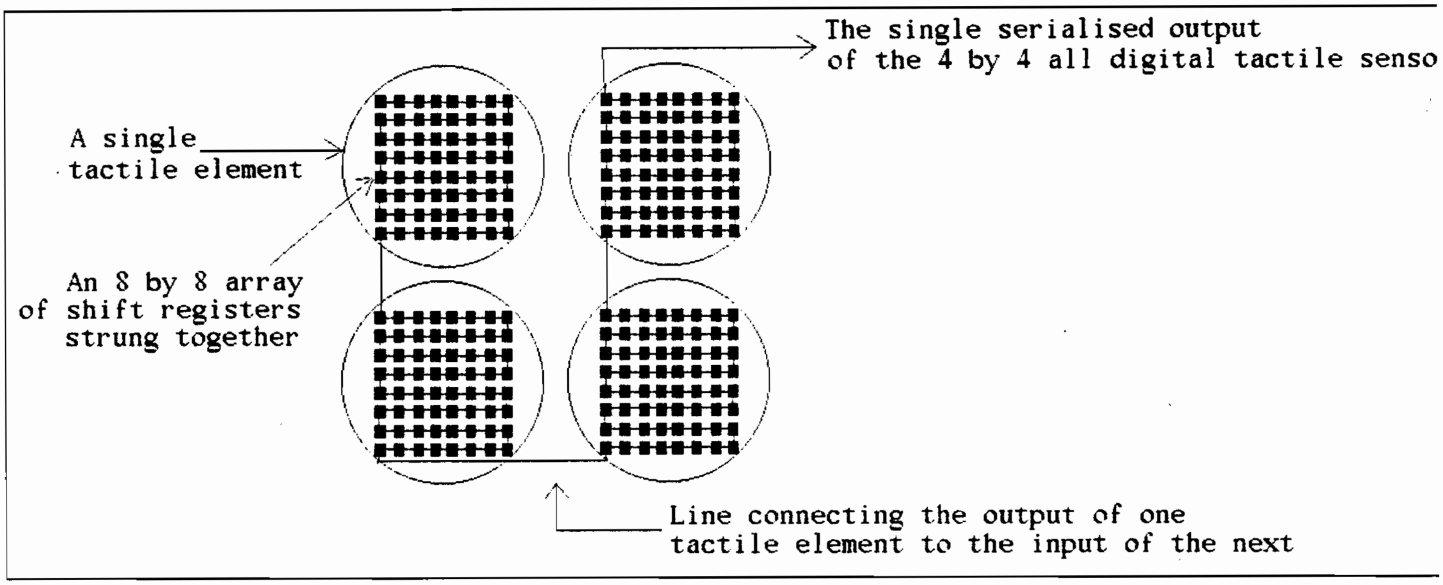

Figure 5.4 An Ideal Efficient Layout of the Tactile Sensor.

So, besides the I/O pads, the chip consists of a single simple cell repeated N times. Thus the onus of the design rests on effectively designing and laying out a single bit of a shift register.

The approach used in the design was to not worry about area of the chip. Rather, many dimensions were deliberately oversized, often being up to three times the minimum sizes stipulated by the design rules. This was done with the hope of increasing the robustness and yield of the chip. The yield can be as low as 30% straight out of a silicon foundry (Weste and Eshragian 1985). This is further exacerbated by the fact that the chip will be subject to unusual (for a VLSI circuit) stresses and, anyhow, it is just an experimental prototype. This oversizing was mainly applied to the metal layer. Being the topmost layer of the wafer, the metal lines must travel across very unevent territory and hence, more than any other layer, are prone to shorts and breaks.

The shift register is based on a simple and commonly used circuit. The aim is to build an N-bit parallel loadable shift register. We start with a simple linear shift register—a single bit is shown below.

This dynamic shift register uses the gate capacitance of the inverters as memory storage for one clock cycle. The register uses two phase non–overlapping clocks.

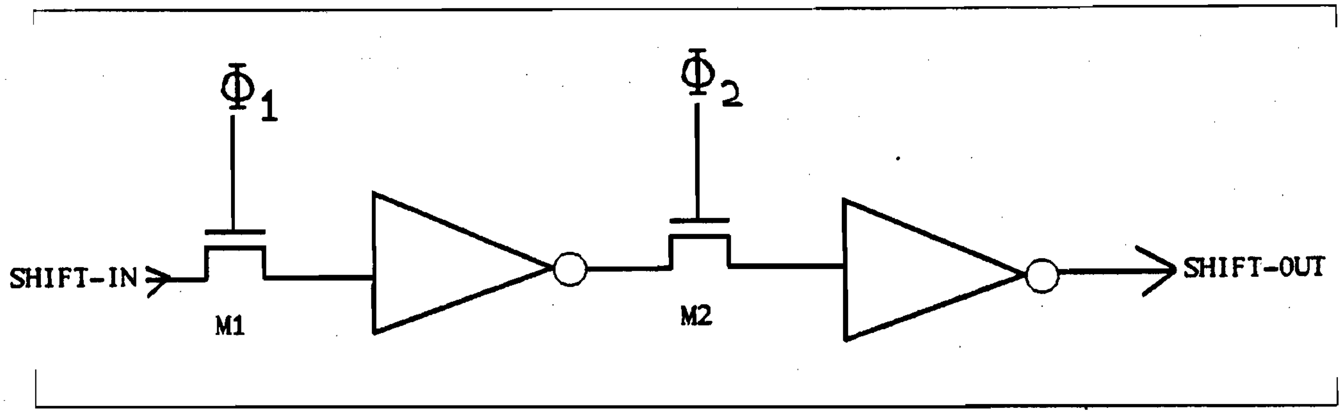

Figure 5.5 A Simple Linear Shift Register.

Data is shifted in when Φ_1 is high and shifted out with Φ_2 high. In the interim, when both clocks are low, charge is retained in the gate capacitance of the inverters. A shift register of any length is possible, simply by cascading these bits, forming a long chain.

Onto this, we add a circuit that will enable us to load the bits of the shift register (in parallel) with the 'values' of the probes. Here again, we chose the simplest possible circuit. It is basically just a pull–up resistor that can be tristated (electrically isolated) when not needed. The 'resistor' is in reality an active load—a pMOS transistor (M3) with its gate grounded. The two transistors (M4 and M5), normally cut–off, are turned on when the bit needs to be loaded; otherwise, the loading circuit remains tristated. The whole circuit is illustrated below.

Thus in 'normal' shifting operation, **load** is low and $\overline{\textbf{load}}$ is high and the circuit behaves like an ordinary two phase linear shift register. To load the bits in parallel, Φ_1 is held low (decoupling the bits) and Φ_2 is held high (connecting the inverters) while the pull–up circuitry is activated by turning **load** high and $\overline{\textbf{load}}$ low. The entire loading operation just takes *one* clock cycle so one does not have to worry about a bouncing signal and other transient effects.

So, in summary, when loading the register, if the probe is 'floating' (*i.e.* the probe is not touching the grounded conductive rubber), the inverter I2 will be precharged high. If the probe is grounded, touching the rubber skin, then I2 is precharged *low*. Thus in the shifted output, a low signifies contact, a high no contact.

Finally, there is one obvious alteration needed in the layout of the circuit. Since the CMOS process used has only a *single* metal layer, all the active circuitry

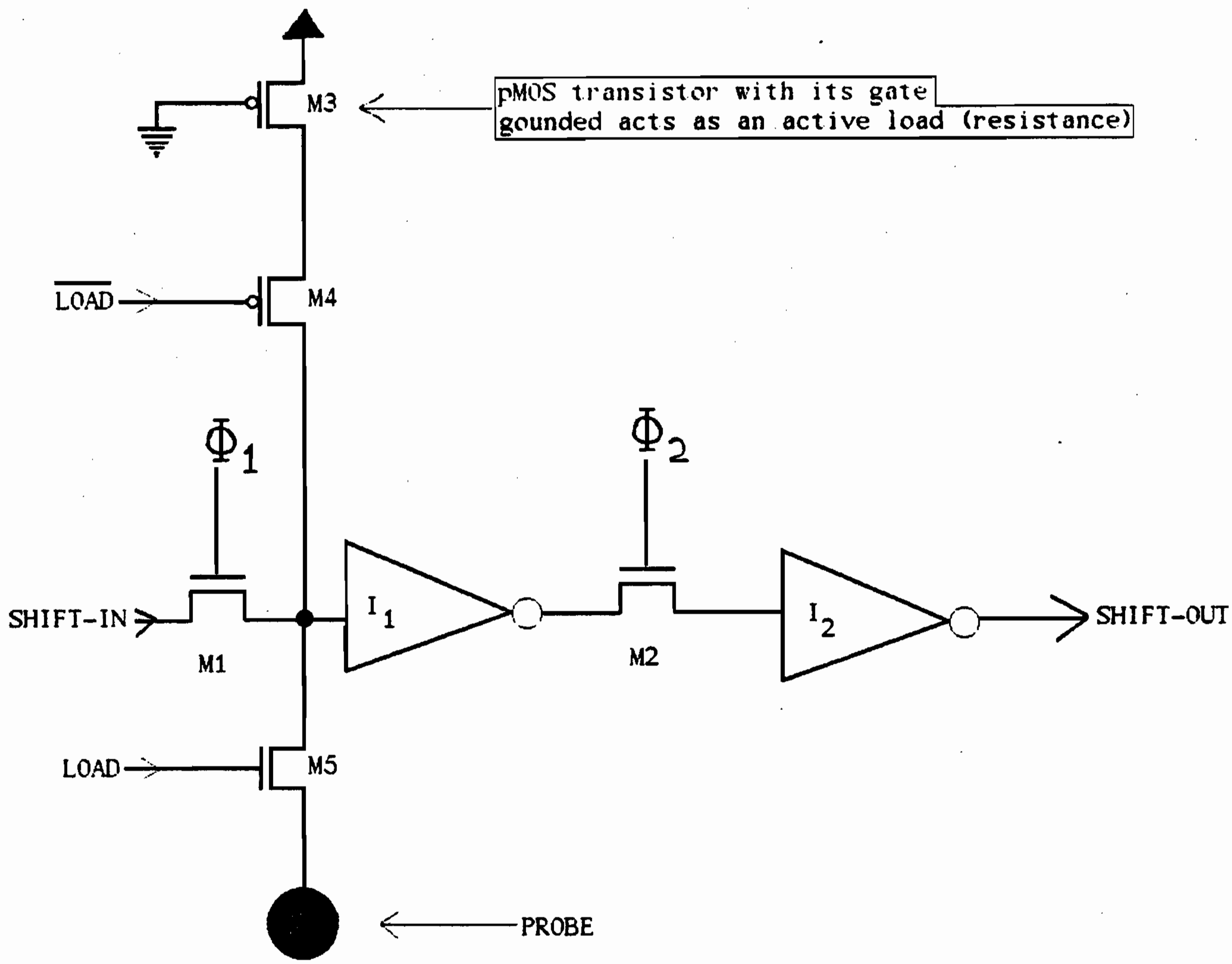

Figure 5.6 A One Bit of a Parallel Loadable Shift-Register.

must be pushed away from the circular holes. This is necessary as otherwise when the conductive rubber touches the probes, it will also touch other metal lines and short out the entire circuit. The resulting layout is shown below.

Unfortunately, such a layout results in a lot of wasted silicon area. In addition, one more factor must be taken into account when designing the shift register. This is caused by having the long polysilicon lines connecting the probes to registers. The polysilicon layer has a high resistance and the pull-up circuit take that into account. When the conductive rubber touches the probe, there will be about 1000Ω in the path

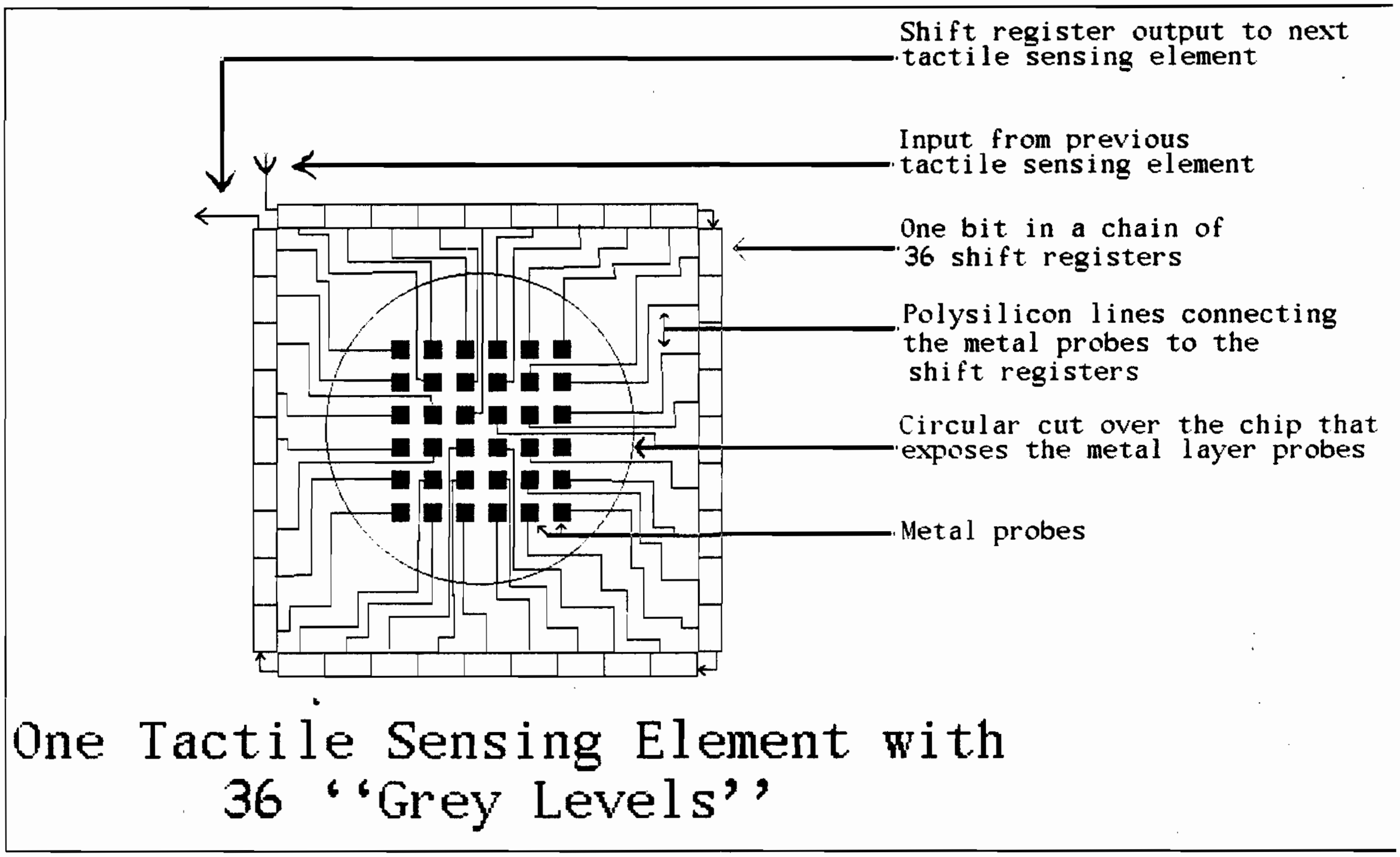

Figure 5.7 A Single Metal Layout of the Sensor

from the probe to the register. This resistance should be low enough to pull *down* the voltage of the pull-up transistor. The SPICE circuit simulator showed that to get a 'cut-off resistance' of 14KΩ the transistor ratios M3–5μ:5μ, M4–5μ:15μ and M5—5μ:5μ suffice. That is to say, if the resistance from the probe, through the conductive rubber skin, to ground is less than 14KΩ then it is recognised as a contact. The SPICE program and the simulation results are included in Appendix B.

Chapter 6 The Fabrication of the Sensor

6.1 The Fabrication of the VLSI Wafer

The VLSI circuit was laid out using an interactive graphic editor, KiC, which allows one to manipulate simple geometric structures. These structures form the masks used in the photolithography steps performed at the VLSI fabrication centre. This description is converted to the standard Caltech Intermediate Form (CIF) format. This file is nothing more than a translation of the geometric structures given by the KiC editor. This 'language,' standard throughout the industry contains a complete geometric description of the layout.

In addition to the SPICE simulations of the shift registers, a circuit extractor, `mextra`, was used to verify the laid out design. The circuit extractor returns a SPICE input file. It was not, however, possible to perform a chip level simulation due to memory and time constraints. Nonetheless, `mextra` served several useful purposes. Used on the KiC layout of a single bit of a shift register, we manually reconstructed the circuit represented in the SPICE output and verified that it matched our expectations. Furthermore, `mextra` could be used to check continuity between points. One common error in VLSI layout is that the designer improperly connects cells together or even omits some connections. Using `mextra`, it was possible to check for very obvious mistakes such as shorts between the I/O lines and to check that the power, ground and control signals are properly distributed to all the cells.

The CIF file was then sent, via electronic mail, to the Canadian Microelectronics Corporation (CMC) where the design was merged with other projects from universities across Canada. The wafers then get fabricated courtesy of Northern Telecom. The turn around time from submission of the file to the reception of the wafers was roughly three months.

In the end, returned were ten halved wafers, along with the overglass photomask which is necessary in later steps of the fabrication of the sensor. Approximately half these wafers came with a protective overglass layer; the rest had that processing step omitted at the foundry. This was done so that as many factors as possible could be varied and their effects on the resultant sensor noted. Ordinarily, the chips are returned in a forty pin open covered package. The reason for having the chips returned unpackaged along with the overglass mask will be apparent in the next section.

6.2 Application of the Polyimide Coating

6.2.1 Some History

Here, the original approach taken by (Raibert 1984) was to deposit a *very* thick layer of SiO_2 overglass on the chip as part of the final step of the VLSI fabrication process. After this nonstandard passivation step, the overglass would be etched to create the notches.

There are several fatal flaws associated with this approach. First is that the necessary overglass thickness is quite large—Raibert aimed for a thickness of 10 microns (Raibert 1984). This is an order of magnitude more than the standard overglass thickness. In the Northern Telecom silicon foundry, the overglass is only 0.900 microns thick. The deposition of such a thick layer leads to many problems. To begin with, the 'sputtering' process used to coat the wafer with SiO_2, heats the substrate. Consequently, sputtering over extended periods of time will damage the chip. Furthermore, etching such a thick overglass with any degree of accuracy is virtually impossible. This is because hydrofluoric acid is used to etch and dissolve the SiO_2. This acid is extremely strong. If left on a little too long, it will also etch away the top metal layer.

Consequently, we decided to take a different approach. Instead of using overglass as an insulative separator, we used a recently developed material—a photosensitive polyimide, the use of which we will now describe. With polyimides, one can achieve passivation layers ranging from 2.2 to 80μ.

6.2.2 An Introduction to Polyimides

Photosensitive polyimides are polymer plastic–like materials that are gaining popularity in the VLSI community. This is due to their excellent mechanical and electrical properties, giving rise to numerous applications. Initially, polyimides come as an unpolymerised liquid. This liquid is photosensitive—exposure to light (specifically ultraviolet) causes it to polymerise and harden. It acts as a negative photoresist in that the part that is exposed to the ultraviolet becomes impervious to solvents; the unexposed polyimide can be washed away creating patterns on the wafer's surface. Because of this, the material must be handled in safe yellow–light conditions.

Processing starts with *spin–coating* the wafer with the 'raw' polyimide liquid after which, it is dried by *softbaking* (also called *prebaking*). This leaves a thin partially polymerised coating of polyimide on the wafer. The wafer is then placed under a *photomask* and exposed to ultraviolet radiation. After exposure, the wafer is rinsed in a *developer* which removes the unpolymerised polyimide, leaving the exposed polyimide. Finally, the polyimide is *cured* by heating it to a high temperature in an inert gas atmosphere. This causes the polyimide to completely *imidise* and stabilise chemically. That, in a nutshell, describes the use of the polyimide—we will describe, in greater detail, the steps that were actually carried out during the fabrication of the sensor.

Presently, polyimides find their greatest use as the passivation layer in VLSI circuits. A coating of the polyimide on the wafer will protect the circuit from mechanical damage and corrosion. Another related application is to act as an α–particle barrier in densely packed circuits, especially memory chips. The coating prevents so called 'soft' errors which are caused by alpha particles from the chip's packaging. These charges particles bits in a dynamic memory to change value by knocking out electrons in the memory cells. These errors are soft because no permanent damage is done—the errors are intermittent and random. Thick coatings of high purity polyimide over sensitive areas can serve to stop alpha particles from penetrating the circuit.

Another important application is as a dielectric gap between different (usually metal) layers of a wafer. Polyimides are well suited for this because of their high degree of *planarisation*. That is, when the wafer is coated with polyimide, it forms a very even and flat layer. This is quite unlike SiO_2. A SiO_2 overglass layer is very thin ($\approx 1\mu$), less than the thickness of the metal layer ($\approx 2\mu$) so the profile of the wafer is very uneven. This creates problems when additional layers are deposited on top of the overglass; the bumpy profile increases the chances of breaks and shorts occurring in the lines. Polyimides seem to offer a solution to this problem. Other applications include the fabrication of masks and ion implantation barriers.

Thus polyimides seem to be quite well suited for the relatively simple application we have in mind. All we desire is an even coating of plastic over the wafer, 10 to 100μ thick. In addition, we must be able to etch, precisely, holes in the plastic exposing the top metal layer over the force sensors as well as over the pads. The use of the polyimide is straightforward and, below, we detail the steps that were carried out.

6.2.3 The Application of the Polyimide

The photosensitive polyimide behaves and is used much like any other normal *negative photoresist*. The main difference is that it is not necessary to remove it—the polyimide is durable and strong and can be left on the wafer. We now outline the application of the polyimide on the wafer.

1. Pretreatment We begin by cleaning the wafer with acetone and trichloroethylene and spinning it dry. This removes grease and dust from the wafer. We then immerse the wafer, for 15 seconds, in an adhesion promoter (Selectiplast© HTR AP–2) and spun dry. The adhesion promoter aids in keeping the polyimide from lifting off the wafer when it dries.

2. Coating This and the next three steps must be performed in safe yellow light conditions to prevent the exposure of the polyimide. In this step, a thin coating of polyimide is applied on the wafer. As with photoresists, it is *spin coated*. This is one reason why it is preferable to work with wafers, rather than having the chips diced and bonded.

The coating starts by placing a few drops of the liquid polyimide on the wafer. The wafer is then placed on a spinning machine where, held by suction, it is spun at a high speed for a short period of time. This removes excess polyimide leaving a thin coating on the wafer.

The thickness of the polyimide can be controlled by varying the speed of the spinner as well as the time spent spinning. High speeds and spinning times lead to thinner coatings. A table giving the thickness of the coating versus the spin time and speed is given in the polyimide documentation (Merck Electronic Chemicals) but, unfortunately, the results obtained in the lab were much too variable. The reference guide could only serve to give a a rough estimate of the resultant thickness. This was largely due to the fact that the polyimide rapidly decays (by imidising) at room temperature. Hence the material must be stored refrigerated at 4^oC. This causes the polyimide to become very viscous, making it hard to judge the thickness after spinning. This, however, is a minor problem as the chip is only experimental. Furthermore, one can always accurately measure the thickness 'after the fact' with a microscope. A variety of speeds and times were tried, ranging from 600 r.p.m. for 20 seconds to 4000 r.p.m. for 30 seconds.

3. Softbaking. In this step the wafer, with its polyimide coating is dried by heating it in a convection oven. The heating causes the polyimide to partially polymerise, causing it to harden as well as decrease in weight and volume—the thickness of the coating shrinks slightly. This step must be carried out carefully. If heated at too high a temperature, the polyimide will completely cross–link, losing its photosensitivity. In addition, the material will shrink too fast, causing cracks to appear. Best results were obtained by heating the wafer at 65^oC.

The baking time depends directly on the thickness of the polyimide. The documentation recommends 8 hours baking for an 80μ coating down to 1 hour for a 10μ coating thickness. Since we did not have too much control over the thickness, the bake time had to be found by experimentation. For the thickness that we were aiming for, 40μ, 4 hours baking time was recommended and most of the wafers were baked that long. Here too, one must be careful not to over or under bake the wafer. If it is left in the oven for too short a time, the polyimide coating will not dry completely and stick to the mask in the next step. If left in too long, there is danger that the polyimide will imidise too much and become photoinsensitive, or worse yet, will oxidise and start cracking.

4. Exposure After the prebaking, the wafer is ready for exposure. It is placed in an exposure machine under the overglass photomask that was supplied by Northern Telecom. A minor problem was encountered here as the mask supplied was a positive mask. A negative copy of the mask was fabricated by a photomask manufacturer and this negative mask was used throughout the experiments. The wafer is then properly aligned under the mask using the pads as references. Once aligned, the wafer is brought flush up against the mask.

Now the wafer is finally ready to be exposed to the ultraviolet light. Here again, experimentation determined the optimum exposure time. Best results were obtained when the wafer was exposed for 90 seconds; extremely thick coatings required 120 seconds.

5. Development The wafer is now ready do be developed. That is, using an organic solvent (Selectiplast© HTR D–2 developer), areas of the polyimide that were not exposed to ultraviolet radiation are stripped away while the exposed parts are left intact. Here, following the recommendations of the documentation, good results were obtained by immersing the wafer in the developer with the aid of an ultrasonic bath for 30 seconds. The wafer was fairly robust against overdevelopment so if traces of polyimide were still visible (under a microscope) over the sensor hole or pads, the wafer was developed for another 15 seconds.

This is quite different from the etching of SiO_2, where the strong hydrofluoric acid is employed. There, if the acid is left on too long, the metal layer will dissolve along with the overglass. With the polyimide, the organic solvent used does not affect the metal layer. Once the wafer is developed to satisfaction, it can once again be handled in plain light.

6. Curing The final step is to cure the polyimide. That is, the wafer must be heated in an inert gas, or preferably in a vacuum, gradually to a high temperature and slowly cooled back down. This heating and cooling must be carried out very carefully and slowly. One must ramp the temperature from room temperature to $450^{o}C$ over the period of four hours and then ramp the temperature back down for another four hours. We found this eight hour operation impossible to carry out in the lab because the right type of oven was unavailable. The oven that seemed most suitable was a high temperature baking oven used for oxidisation. This oven could not be accurately controlled at lower temperatures, nor could it be evacuated. Consequently the heating and cooling of the wafer was too uneven and the polyimide oxidised. This caused the polyimide to crack and peel off the wafer. Hence, we decided to omit this step in fabricating the sensor. The consequences of this are not grave for our project since the sensor is only experimental. As a result, the polyimide coating that results will not possess great thermal, mechanical and chemical stability but it is enough for short term use, enough to verify whether the sensor operates.

6.3 Bonding

The penultimate step is to bond the wafer onto a ceramic substrate. This involves bonding gold wires from the pads of the chip to leads that can be connected to testing circuitry. This seemingly simple procedure caused more problems than expected. Many sensors were destroyed by the wire bonding machine when the gold wire did not 'stick' to the chip's pads.

An ultrasonic bonding machine was used to bond the chips. The machine has a thin gold wire that is threaded through a ceramic capillary. The end of the wire has a small ball which was created by an electric arc. This ball prevents the wire from unthreading; it is held against the tip of the capillary. Underneath the capillary, the wafer is held tight on a hot plate. Using a microscope and a mechanical joystick, one can position the hot plate so that the capillary is directly over a bonding pad; that pad is now ready to be bonded.

Releasing a trigger, the capillary comes down, pushing the gold ball on the end of the wire against the pad site with a certain force. Simultaneously, a pulse of ultrasonic energy is channelled through the capillary, vibrating the wire ball. Then, automatically, the machine lifts the capillary away from the pad. The gold ball is pressed against the pad for a very short period of time, on the order of only 1 second. This series of motions results in a *ball bond*.

We now have one end of the wire bonded onto a pad site of the chip. The rest of the wire is still threaded through the capillary. Next, we move the capillary over a bonding site for the packaging. Once positioned, we release a trigger and the capillary, as before, comes down with force on the bonding pad accompanied with a pulse of ultrasonic energy. The type of bond made, however, must necessarily be different. This is because now there is no ball at the end of the capillary—the end of the wire is bonded onto a pad of the chip. A different method is used to bond the wire here. The bond, called a *wedge–bond* is formed by moving the capillary laterally, sliding it across the boding site on the ceramic substrate. This breaks the wire off, leaving a wedge shaped bond. Finally, an 'electric flame off' arm swings across. It creates an electric arc which melts the gold wire, leaving a small ball at the end. Thus, the machine is ready to make another set of bonds.

There are many parameters in the bonding process which must be tuned to get a good bond. One is the temperature of the hot plate which holds the wafer. The purpose of the hot plate is to soften the metal on the pads. This aids the bonding process by making it easier for the gold wire to 'stick' to the pads. Too high a temperature, however, will damage the chip and, furthermore, can cause the aluminium pads to oxidise, making bonding more difficult. To find the best setting, we started with a low temperature and worked upwards. 'Good' results were obtained at 125^oC though, sometimes, the temperature had to go as high as 140^oC.

Three other parameters are also important in the bonding process. They are the *bonding force*, the *ultrasonic pulse's energy* and the *duration of the ultrasonic pulse*. These three control parameters, together, mainly serve to break the thin, but hard, oxide layer that covers the metal bonding pads. There are two sets of such controls, one for each bonding cycle. That is, one set is for the first ball bond, and the other set is for the second wedge bond.

Naturally, it is desirable to have these settings as low as possible. This is because too high a setting will be destructive. For instance, too much force will puncture the bonding pad, shorting it to the substrate. Experimentation showed, however, that the ultrasonic energy had the worst effects upon the pads. Through the microscope, one could see holes 'drilled' through the metal by the high frequency vibration of the capillary.

Unfortunately, the the ball bonds to the aluminium pads on the wafer were hard to make. The wedge bonds to the gold pads of the ceramic substrate were much more easy to make. This is because gold bonds better to gold than to aluminium. Furthermore, the polyimide coating of the wafer had an adverse effect upon the bonding.

It appears as though the polyimide was not always removed completely over the pads. This is evidenced by the fact that it is quite easy to bond untreated wafers—wafers that have not been coated with polyimide. This layer, though very thin, was resistant. Because the wafer is placed on a hot plate on the bonding machine, it appears as though the residue imidised, making it all the more hard to penetrate. Because of this, the ultrasonic power settings and bonding force had to be set high. This resulted in the damage of many wafers whilst bonding.

6.4 The Rubber Skin and Packaging

A standard method was used to make the conductive rubber and that is to add fine carbon powder to an elastomere compound. This was carried out on a trial and error basis. Best results seemed to occur with a mixture of `Sylgard`[1] silicone compound, `Silatic 739 RTV`[2] plastic adhesive and carbon powder. The silicone elastomere tended to give the skin good elastic properties while the adhesive contributed to its strength. The compound was allowed to set in a mold. As a result, a skin with reasonable mechanical and electrical properties was obtained. The skin was soft and flexible but still quite durable. The addition of the carbon also gave it quite a low resistance. During the course of experimentation, however, it was discovered that the resistance obtained was not quite low enough. This required the addition of more carbon powder to the elastomere which resulted in poorer quality rubber. The rubber tended to have a more brittle quality and a more uneven surface. The quality of the rubber turned out to be very difficult to control in the lab and this is later reflected in the experimental results.

As for the packaging of the sensor, it was basically omitted, the justification being that the sensor is only experimental. The chief aim is to see whether it is feasible to construct such a sensor so work in actually packaging the device can be postponed. In future designs provisions should be made that will enable one to stretch the rubber skin over the sensor, but in this prototype, the skin was placed over the chip with no tension.

---

[1] ©Dow Corning Canada.

[2] ©Dow Corning Canada.

Chapter 7 Testing

Once the sensor is fabricated, the next step is to test it. Being completely digital, the sensor is very easy to test; we can use standard digital test equipment. Much to our disappointment, we very quickly discovered that the sensor did not work. We successfully fabricated and wire–bonded eight sensors with varying thicknesses of polyimide coating and tested them with a Hewlett–Packard 8180A digital data generator. The test patterns applied were simple; they were the same ones used in the SPICE circuit simulations, consisting of the loading pulse, normal and inverted, the two phase clocks, ground and a 5 volt power supply. The output was monitored with a 20 Mhz. oscilloscope and a grounded sheet of rubber skin was placed over the chip. The clock speeds used varied from 100KHz to 2MHz. The input signals are illustrated below.

Unfortunately, in every experiment, save one, the sensors were completely 'dead.' That is to say, when pressure was applied to the rubber skin, the output remained stationary. In most cases, it was stuck high, though occasionally, stuck low. These experimental result were very disappointing in that they provided absolutely no concrete answers about why the sensor failed. Rather, they posed a number of disquieting questions ranging from a basically faulty concept to an incorrect design to faults induced by mishandling of the wafers in the process of the sensor's fabrication. Because there were no test cells aboard the chip (a *very* serious oversight on the part of the author), very little useful hard information, as such, was learned from the experiments. In the next section, however, we will hypothesize a number of possible reasons for the sensor's failure and propose remedies that can be effected in future designs. One sensor, however, did momentarily show some sign of life for a few seconds, but it too suddenly froze. Thus, because of the designer's shortsightedness, there are really very few leads to go on to determine the cause of the sensor's utter failure and in the next section, we are forced to almost blindly guess the cause and propose effective remedies.

7.1 Post–Mortem

To begin at the beginning, it appears as though many devices were damaged even before any 'post–processing' with the polyimide was attempted. This was perhaps due to the fact that the wafers were mailed 'loose' from the silicon foundry. The half–wafers were not securely held in the packaging—the wafers could shake around in the plastic containers. This physically damaged many chips as, using a microscope, one could easily see many scratch–like marks over the wafers; many broken metal lines were quite visible under magnification. Approximately half the chips had to be immediately discounted because of this. (They were, nevertheless, still used to practice the polyimide application process and the wire bonding). The mechanical shock incurred in transporting the wafers could also have resulted in damage invisible under a microscope, though, since it is the topmost level, it is probable that such damage was mostly confined to the metal layer.

It is also possible that chips were damaged by punch–through, the puncturing of the thin oxide layer over the gate by a high voltage arc. This effect damages individual transistors and is caused by static electricity. Since the wafers were sent without special protection, and no special protective circuitry was added, the occurrence of punch–through is a distinct possibility. On the other hand, punch–through does not explain the *complete* failure of the chips. It only affects single transistors so one would still expect a certain amount of response. This is because the circuit is a single long chain of shift registers. If one register is defective, the bits before that register are effectively lost, however, one can still expect the register after that defective bit, all the way to the pad to function. Thus, a certain amount of shifting will still take place, not explaining why the outputs were completely stuck.

Another possibility is that the polyimide was not completely removed over the sensor sites. This problem became apparent during the bonding of the chips; a thin residual layer of polyimide was left over the pads and it imidised on the hot plate of the bonding machine, leaving an unwanted hard coating. The same could be occurring over the sensor cuts. As a result, when the conductive rubber is pressed into the holes, it will not be able to ground the probes. Thus, the probes will remain pulled up and the output will always be high—and this is what was observed on most of the chips during the testing.

~~There is,~~ however, one problem with this explanation. It stems from the fact that the 'sensor cuts' in the polyimide are many times larger than the cuts over the bonding pads. Because of this, the polyimide at the center of the circular sensor cuts is more easily removed than the polyimide over the bonding pad openings; the sloping edge profiles of the etched polyimide will have less of an effect over the larger holes. Nonetheless, traces of residue polyimide could be the culprit in the failure of some of the chips.

One step in the fabrication that subjected the sensors to extreme stress was the wire bonding. This step was thought to be straightforward and simple, which was why it was attempted at McGill University. The application of the polyimide coating, however, had a deterious effect upon bonding operation. As explained in a previous section, the power settings for the ultrasonic bonding machine had to be set very high. Consequently, it is very likely that some bonding pads were damaged, most probably by shorting them to the substrate. The loss of any one of the chip's input signals would immediately kill the output because of the non–fault–tolerant nature of the shift register.

Finally, we come to what, in the author's opinion, appears to be the most likely cause of failure in many of the chips. This problem, which was previously alluded to, is *latch–up*. Latch–up used to be a serious problem in CMOS circuits, which is one main reason why designers had been slow in accepting it in favour of bipolar and NMOS technologies. Basically, latch–up occurs when the parasitic bipolar transistors in the circuit become active and essentially form a short circuit from V_{DD} to Ground. Often what happens is that, if the short is not complete, then the circuit will freeze (hence the name latch–up), requiring one to reset the chip by powering it down and back up again.

Latch–up usually occurs where there are large amounts of current and high voltages, and this is most often around the I/O pads. In our tactile sensing chip, though, there are very few 'traditional' I/O pads. However, the *probes* in the tactile sensing elements can be thought of as input pads. This was not taken into account in the design of the chip—the probes were left unprotected. The reason for this was that it was assumed that the conductive rubber would *shield* the probes since the skin is always grounded.

Unfortunately, what seems to have occurred is that when the probes became grounded through contact with the skin, there was excessive signal 'bounce.' This is to be expected since the polysilicon lines that connect the metal probes to the shift registers (in the single–metal design) are very long. Consequently the lines have a high RC constant. This was foreseen in the design but only the resistance was considered to be a 'problem.' The justification for this was that we were only interested in the steady–state response of the latching circuitry (which comprised of the tristate pull–up transistor). This is due to the fact that the parallel loading of the shift register takes only *one* clock cycle—we do not have to wait for the signal to settle. In fact we *cannot* wait for the signal to settle because it is *constantly* changing; we do not expect the pressure applied to the sensor to remain the same.

7.2 Recommendations

Based on the results obtained in the first trial, we can offer several recommendations that can be incorporated in future designs. To summarise the results above, it appears that the main problems lay in bonding, punch–through and latch–up. Thus in the future, close attention must be paid to these factors when designing the chip.

To begin with the bonding problem, the most obvious solution is to have the chip bonded at the silicon foundry. Because of the greater experience of the technicians and higher quality bonding machines there, better bonded chips are sure to result. Another step commonly employed by VLSI designers is to place a polysilicon sheet under the pads. This serves to protect against 'pin–hole' punctures which occur when small holes in the SiO_2 insulative layer short the metal layer to the substrate. Because of the large metal area over the pads, there is a greater probability of a pin–hole type fault. TO protect against latch–up and punch–through, it is also advisable to add protective diodes to the probes and provide more substrate connections. In addition, it is very important that we provide test cells to make debugging possible.

To summarise, the following modifications in the design of the sensor are proposed.

- Add test cells and probe points allowing one to probe into the sensor and pinpoint the location and cause of failure.
- Have prepackaged and prebonded chips sent to us from CMC. A large error was made the first time in having only (unbonded and undiced) wafers sent back as this forced us to rely wholely on the bonding process at McGill. Having packaged chips also facilitates the verification of the test cells. Finally, with packaged chips, it may also be possible to apply the polyimide directly, thereby completely circumventing the bonding procedure at McGill.
- Provide extra static electricity protection.
- Provide a polysilicon protective layer under the pads to protect against punch–through.
- Increase the dimensions of the circuit in hopes of increasing the yield of the VLSI fabrication process.

These proposals were all implemented in the next batch of sensors submitted to the CMC. The application of the modifications and the results obtained are discussed in the next section.

Chapter 8 Round Two

In this section, we discuss the fabrication and testing of the new and improved sensor. Most of the steps, from design to testing, are identical to those carried out on the first version and , hence, will omit the discussion of these common steps. The basic principle involved in the sensor as well as the overall design of the circuit remains completely unchanged. Thus the redesigning did not take a very long time.

The philosophy behind the second design was to forget about getting a working *array* of tactile sensors on a chip immediately. Rather, the second version was designed with debugging in mind† so there were only two tactile sensing elements on the chip. We decided to use the standard 40–pin open cover package provided by CMC, so the rest of the pads were used by assorted test circuits. Indeed, there was a tendency to go overboard with the test circuits with even the pad drivers having probe points on them, though this is somewhat justifiable in light of the disappointing experience with the first batch. The result was a chip that had a lot of wasted space (the test cells are very small, but they use many pads) but really left no stone unturned as far as pinpointing errors goes.

8.1 Design

The recommendations proposed in the previous chapters were carried out on two chips, the main difference between the two being that the second contained diode protection,

---

† This is normally the other way around! The first design is intended to locate bugs so that a working product can be obtained in future designs!

while the first had, basically, the same design as the original submission with the exception of the numerous test cells and probe points. The layout of the first chip is illustrated below.

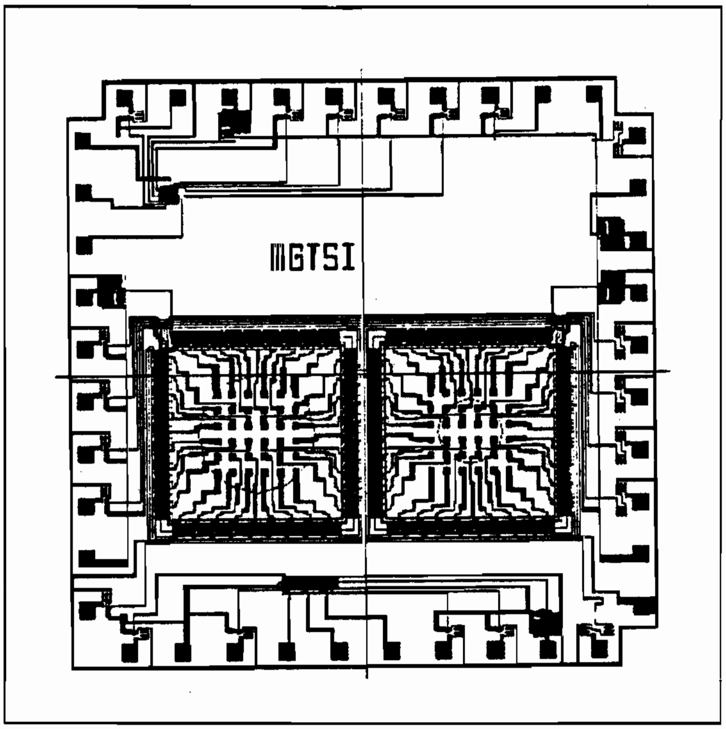

Figure 8.1 The KiC layout of the tactile sensing chip.

The chip contains the following:

- Two tactile sensors with different sized holes in order to study the effect of the hole size on the sensor's response.

- At the top is a *single* shift register bit with two probe points inside. The main purpose of this cell is to verify the operation of the pullup circuitry and determining the 'cut–off resistance' of the sensor, *i.e.* the maximum resistance that would be perceived as a path through ground, or equivalently the maximum resistance that the conductive rubber can have so that the circuit reacts when it makes contact with the probes). Recall that the simulations indicated a cut–off resistance of 14KΩ. The circuit with its probe points is shown below.

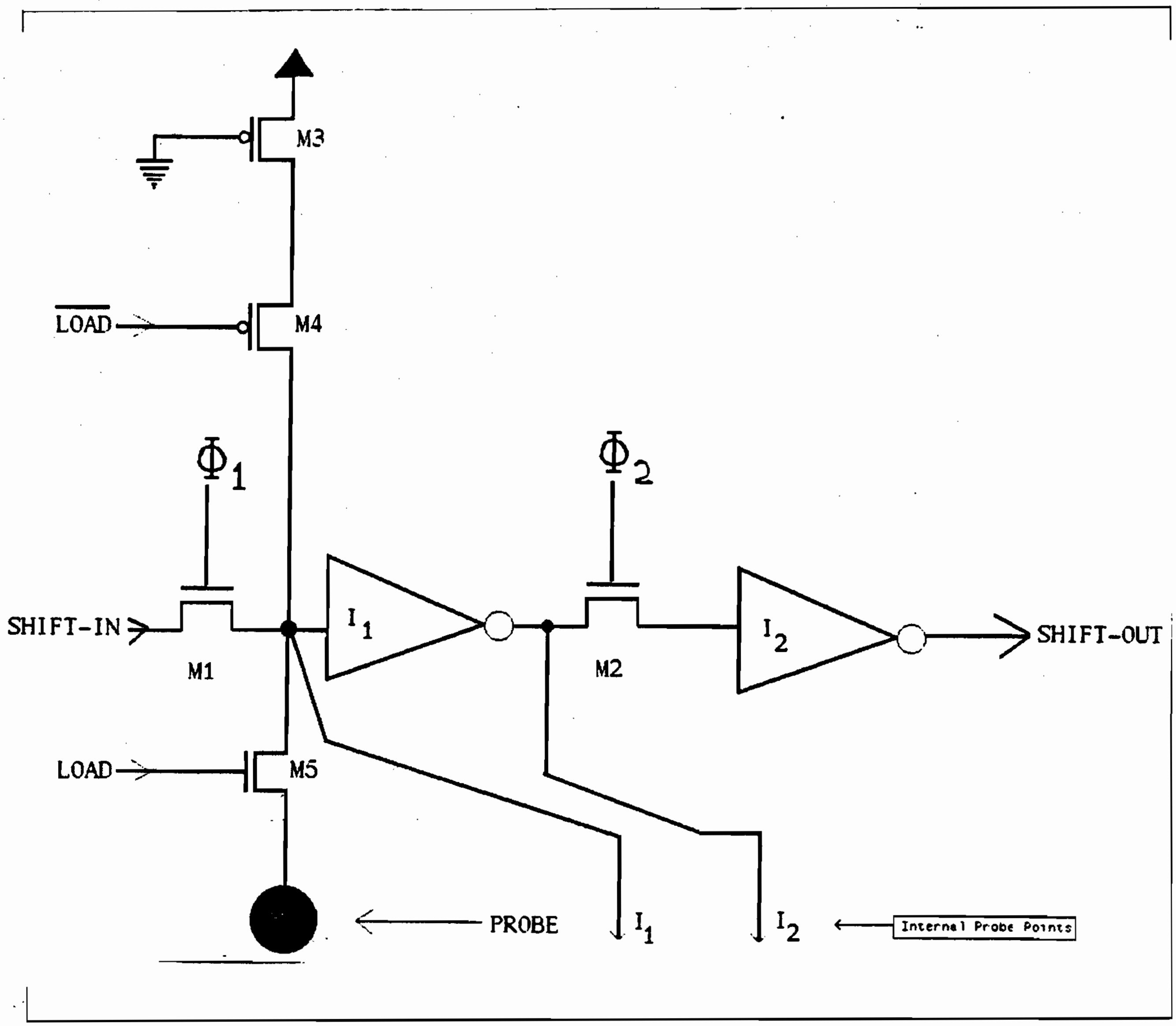

Figure 8.2 A One Bit of a Parallel Loadable Shift-Register Test Cell with Two Internal Test Points.

- At the bottom is a test cell that comprises three shift registers linked together. This circuit is intended to simulate the tactile sensor; the probes of the test cell are directly controllable as they are routed to three pads. Thus one can verify the operation of the of the shift register by applying varying resistances to the probes, sending a load signal and observing the output of the last register as it shifts out three times.

- The top right hand corner contains nothing more than the I/O pads with probes points at input and output. These stupid cells were the result of the paranoia that followed the failure of the first design—everything was under suspicion as the cause of the sensor's failure. In fact, this chip has two different types of input pads. One is the standard pad with protective diodes and current limiting resistance. This is a fairly reliable design but, because the circuit extractor, `mextra`, does not recognise diodes, it was decided to layout an alternative input pad that had no protective diodes. Thus we were able to completely verify the operation of this pad, though in reality, it will probably be inferior to the original as it provided no protection against reverse biasing or voltage spikes. This problem did not occur with the output pads as the circuit extractor worked on it and we were able to verify its operation with the SPICE circuit simulator. The tactile sensor with the large hole uses the normal input pad, while the smaller sensor uses the diodeless input pad.

The second design differs in that the probes of the sensor are provided with diode protection. Each probe has two shunting diodes to V_{DD} and Ground, using a design similar to that used in input pads. The circuit for a single bit of the shift register is illustrated below. It is identical to the first design's shift register except for the diodes. At the time of design, however, two metal layers were available for the design so the entire sensor was laid out in the area–efficient manner that was discussed in Section

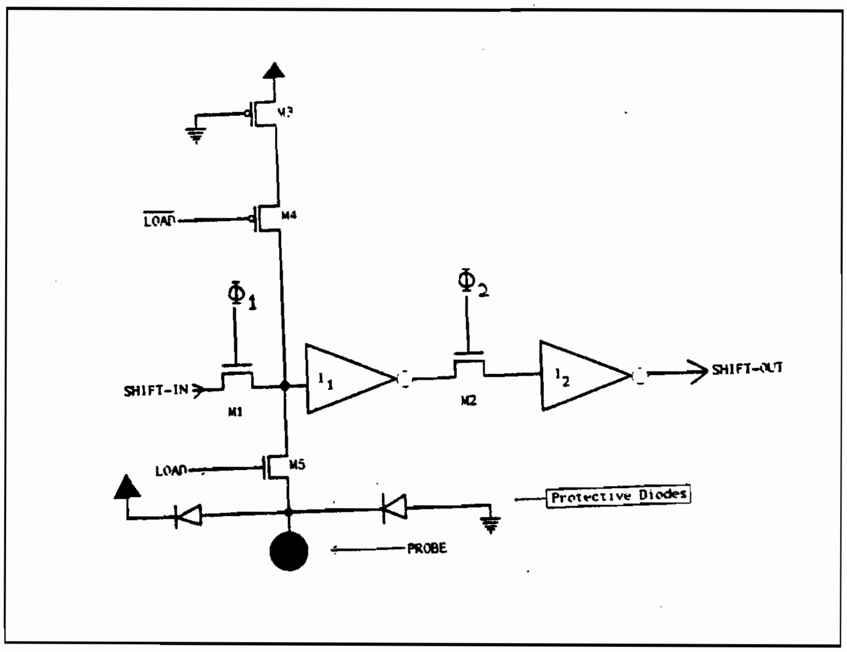

Figure 8.3 A shift register with diode protection at the probes.

The design with the protective diodes was fabricated and packaged chips were returned, however, due to the unavailability of the overglass mask, we did not perform further experiments on the chip; the experimental results in the following sections, will all be based on the the first design.

8.2 Polyimide Application

Here, unlike in the first trial, we have two options open. As before, we could apply the polyimide to the unbonded wafers, or we could attempt to directly apply it onto the bonded and packaged chip, saving us the trouble of bonding the (and in the process, perhaps damaging) the wafers. We decided to do both. Several wafers were diced and polyimide was applied as before. These wafers, however, were to be used only as a last resort—greater hope was placed upon the packaged chips.

Before applying the polyimide, the chips were first tested in order to determine whether the application of the polyimide is what caused the failure. The tests performed were straightforward and are described in the next section.

Next polyimide was applied directly to the bonded chip. This is somewhat of a tricky process; it was thought that this would be impossible to do which was why no bonded chips were asked for in the first submission. The chip is bonded in a standard 40 pin dual inline package with a removable cover. Removing the cover exposed the chip which is in a slight ($\approx$2 mm) recess. To begin, the polyimide is applied over the bonding wires. This serves the important purpose of protecting the fragile wires from breaking off when pressure is applied to the sensor. Furthermore, the polyimide acts as an insulator, preventing the wires from shorting with conductive rubber skin. Next, a few drops of polyimide are spincoated at a very low speed with the spinning machine. By necessity, the spinning speed had to be very slow, as the chips flies off the machine very easily. The maximum speed used was 500 r.p.m. for short periods of time ($\approx$5 sec). The resulting coating was very thick and it was very difficult to calibrate the process in order to get predictable thicknesses. Also, since the chip in a recess, the polyimide applied over the wires tended to flow back down adding to the thickness over the chip. The thick coatings, however, did, to a certain extent, help the exposure process, as we shall soon see.

The next step was the softbaking. Since the thicknesses were so great, extremely large baking periods were employed; we found that $10\frac{1}{2}$ hours at 65^oC gave a good degree of polyimidisation. It is useful to note that the polyimide behaves quite well even if it is overbaked (by as much as 3 hours) but underbaking yields very bad results; the polyimide is attacked fiercely by the developer, stripping away even exposed regions.

Next comes the exposure of the polyimide. This was complicated by several factors. To begin, the exposure machine is not really equipped to deal with packaged chips. It is intended to only expose the thin wafers. A few contortions were necessary to fit the package and, fortunately, they were quite painless with the machine used. The next problem was that there was quite a gap between the polyimide layer and the photomask. This gap was on the order of 1 mm but surprisingly good results were obtained, nonetheless. In fact, the reason why bonded chips were not asked for in the first submission was that we thought that this step would be impossible—the alternative chosen was to attempt the bonding at McGill *after* the wafer had been coated with polyimide.

It seems that two factors helped in giving us good results. First was that the features that we want etched have very large dimensions (relatively speaking). The polyimide can be etched to give features as fine as 5μ, but in our application, the minimum feature size was 500μ (the diameter of the smaller of the two holes). Note that we did not even have to etch over the pads as the chip had already been bonded. The second factor in our favour was that a very thick coating of polyimide was applied over the chip and this reduced the gap between the polyimide coating and the photomask. There are, however, a number of drawbacks associated with thick polyimide coatings—the main one is that it leads to problems in alignment. The raw polyimide is a colourless thick liquid, but after the softbaking, it hardens and changes colour to a dark bluish purple. The resulting coating is almost opaque so aligning the photomask over the chip becomes very difficult; reference markings on the chips are almost competely obscured. The process was applied to four chips. It was a complete failure on one chip; it appears as though it was not baked for a sufficiently long period of time so when it was developed, large amounts of exposed polyimide was stripped away. The results on the other three chips were excellent for the larger hole (diameter = 900μ) but, in all three, the smaller hole (diameter = 500μ) was not cleanly etched away. The results of the coating process are included in Appendix D.

8.3 Testing

We now come to the final and crucial step of determining if the modifications were of any avail. The testing proceeded gradually. The first test checked whether the sensor was alive. And a simple but very effective test was used here. Since the tactile sensor is essentially a shift register, the most obvious way to test it is to load it with a set of values and compare them with the shifted out values. We, however, do not have direct control over the bits in the shift register, but we do know that when nothing is touching the probes, the shift register bits will be loaded with a high value. Thus if the input to the *first* bit of the shift register is low, then we expect to see, after the loading pulse, 36 high bits shifted out followed by low bits, until the next loading cycle. These tests were performed at a speed of 100Khz.

This simple test was applied to the chip that was ruined during the polyimide application. The sensor with the large hole passed the test, but the smaller one failed it. It turned out that in *all* the chips, the smaller sensor was dead; its output was always high. It is very likely that this was caused by the fact that for the smaller sensor, the standard input pad was not used. As previously explained, an input pad with no diode protection was used because of suspicions input pads used in the original failure. It seems that the smaller sensor was damaged by static electricity punch–through while the original input pad driver functions properly. The large sensor, however, passed the test in all four chips which was quite encouraging.

Next, the operation and robustness of the shift register was tested using a three–bit shift register cell. Three 'probes' for the shift register are directly accessible at the pins of the chip; the input to the first bit is not controllable, being permanently grounded. Thus a test much like that applied to the sensors is applied here, except that now we can simulate the 'probes' being grounded. We sent a loading pulse followed by four or more shift cycles. The fourth bit and every bit after that was low as expected. The other three bits were all individually controllable; leaving a probe high caused the respective bit to be high, grounding the probe causes the bit to be low.

The shift register design having passed the functional test, we proceeded to a simple parametric test, using the cell consisting of a single bit of the register. This test is intended to determine the 'cut–off resistance' of the shift register's pullup circuitry. This is achieved by having a variable resistance from the probe to ground, and observing the output and internal test points, I_1 and I_2, while loading and shift–out pulses are applied. As predicted by the simulations, the cut–off resistance is near 15KΩ. The results are illustrated below; the graph shows the relationship between the resistance of the path from the probe to ground, versus the voltage that is shifted out by the shift register.

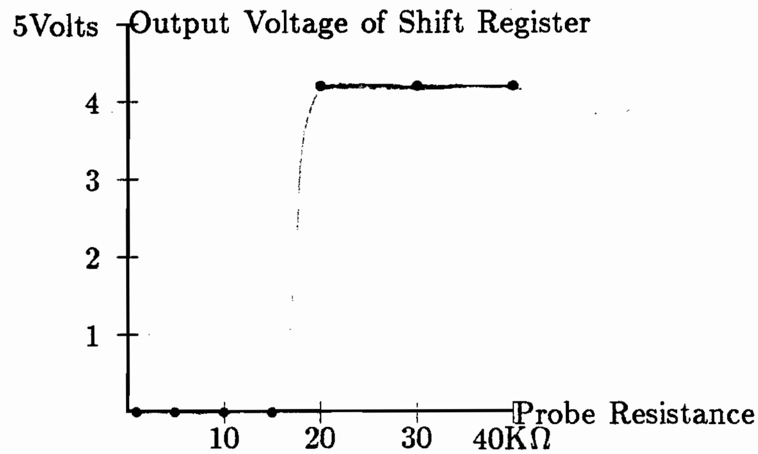

Figure 8.4 The experimentally determined 'cut–off resistance' of the shift register.

Finally, having convinced ourselves that the individual cells function as expected, we now proceed to the testing of the actual sensor. It is worth mentioning, first that in the previous tests, the cells exhibited a remarkable degree of resilience. Recall that this design has no special diode protection within the sensor itself. In addition, the probe points (I_1 and I_2) as well as outputs of the triple and single cells are directly routed to pads with no special drivers. Thus it seems that the circuit is not overly sensitive to static punch–through or fatal latch–up. This is very encouraging as previously it was thought that they were major contributors to the first design's failure. Thus at this point, it seems that the wire bonding step was what ruined the previous batch as this is the only major difference between the two designs.

We begin the testing with a qualitative study of the sensor's response. We placed a sheet of rubber that had a corner clipped to a grounded wire over the chip and pressed on it. However, it soon became apparent that the rubber had too high a resistance and the sensor gave no response; it simply shifted out 36 high bits followed by a number of low bits as though nothing were touching the probes. The obvious solution to this problem was to make a better quality conductive rubber but this was more difficult than expected. As outlined previously, the main problem experienced was that adding too much carbon powder to the elastomere, while decreasing its resistance, makes the rubber very hard and inelastic. Ultimately, adding too much carbon results in a brittle and fragile rubber that crumbles apart easily. Finally, we had no effective means of measuring the conductivity of the rubber. The resistance of the path from the probe to ground is a complex function of the area of the probe, the area of contact between the rubber and ground and the shape and conductivity of the rubber skin. Here, the area of the probes is known and is very small, while the area of contact between the skin and ground can be increased to a certain extent. The conductivity of the rubber can be increased by adding carbon powder to the elastomere, but here again there is a limit. Also, once the carbon powder is added, we used a very inaccurate method to measure its conductivity—we just used a potentiometer to get a very rough idea of the rubber's resistance. We stopped adding carbon powder when the resistance between two points, with the meter's probes penetrating the rubber by a few millimeters, dropped to 10KΩ. This, albeit inexact, procedure gave us a rough idea of the rubber's conductivity and attempts to further decrease the resistance only resulted in very poor quality rubber.

To counter this sudden obstacle, we used something of a last minute 'hack.' So far, we have based the design of the sensor upon the assumption that the rubber skin is grounded. It appears now, however, that the rubber does not have a sufficiently low resistance to be able to pull the pull-up circuitry down. Thus to assist the pulling–down, we added a *negative bias* to the conductive rubber. We first simulated the effects of small negative biases on the cut–of resistance of the pull–up circuitry and, as expected, the cut–off resistance rose. With bias of -1.5 volts, the simulations (Appendix B) predict a cut–off resistance of 30KΩ. And indeed, with such a bias, the sensor responded to different pressures.

At first, the sensor's output was monitored on an oscilloscope but this proved to be inconvenient as the signal was not always periodic which made the triggering and display unstable. Instead, the Hewlett–Packard 8182A Digital Data Analyser was used. The analyser was able to capture and store several frames of the output. In addition, the testing sessions were video taped, allowing one to record and analyse the results at leisure. Several sample outputs of this trial session are illustrated below.

Frame 1:

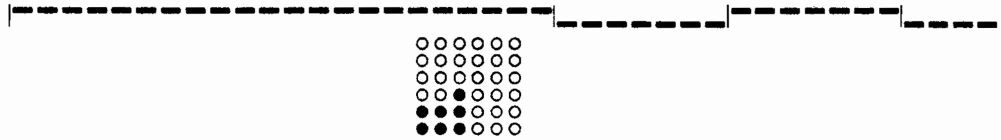

Frame 2:

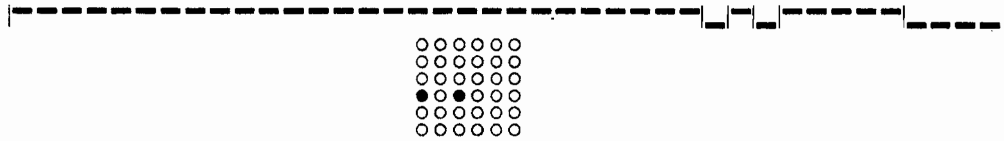

Frame 3:

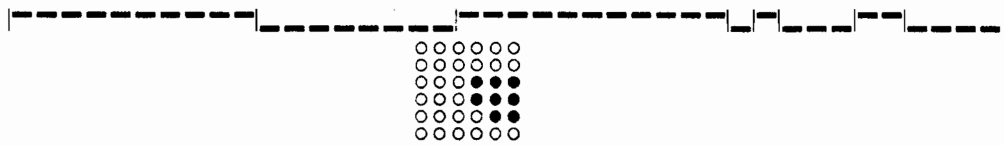

The three frames, above, show the tactile sensor's single digital output, underneath which is the top view of the map of the 6×6 array of probes. A '•' indicates that the skin is touching the probe, while a '∘' indicates that that probe is not touched (*i.e.* the sensor's output is respectively low and high). The output, read from left to right, gives the bit values of the probes. There are 40 shift cycles, and as expected, the last 4 bits shifted out are low since the input to the first bit of the 36–bit register is grounded. The order in which other bits shifted out corresspond to the probes is not straightforward because of the cock–eyed way in which the sensor was laid out. The diagram below shows the mapping—bit #1 is shifted out first and bit #36, shifted out last, has its input grounded.

Finally we come to the quantitative experiments performed on the sensor. The purpose of these experiments was to get some sort of calibration for the sensor, using the rough model presented in Section 4 to come up with a response curve. These tests are really be twofold since we expect the sensor to behave differently to forces with differing tangential components. We begin by studying just the response to normal pressure and use the setup illustrated below.

The same setup is used to test the response to tangential pressures. The chip is placed on a 40–pin DIP receptacle through which the signals can be accessed. This receptacle is mounted on a 255*mm* by 150*mm* rectangular board. A small sheet

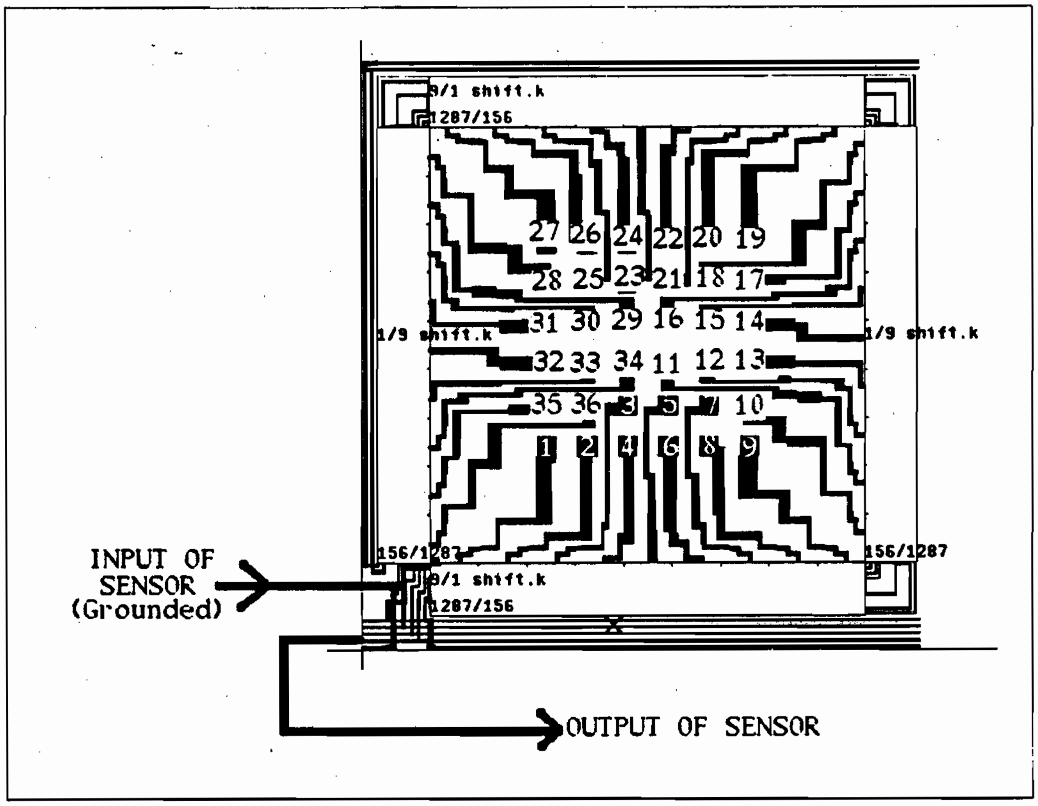

Figure 8.5 The mapping between the shifted bits and the tactile sensor's probes.

of rubber skin is placed over the chip and a corner of it is clipped to the negative bias DC power supply. Next, a small disc with a diameter of $1.0cm$ is placed on the skin over the sensor with the large hole. The purpose of this disc is to create a uniform pressure over the sensing site. Thus to calibrate the sensor's response to normal pressure, the mounting board is kept in a perfectly level position while weights are gradually added on the disc. Thus the pressure applied is equal to the mass of the weights times the gravitational constant divided by area of the disc, excluding the fringe effects. Measuring tangential responses is quite similar, except that the board is kept inclined. The tangential pressure varies with the sine while the normal pressure varies with the cosine of the angle the board is inclined. Two sensors were calibrated, each with holes approximately $0.5mm$ deep. The same rubber skin was used for both and it was $3mm$ thick. The raw results of such experiments are given in Appendix A and are summarised and analysed here.

To begin, a few subjective remarks about the experiments. As already mentioned, the quality of the rubber was found to be poor with respect to both electrical and mechanical properties. The poor electrical properties were remedied with the nega-

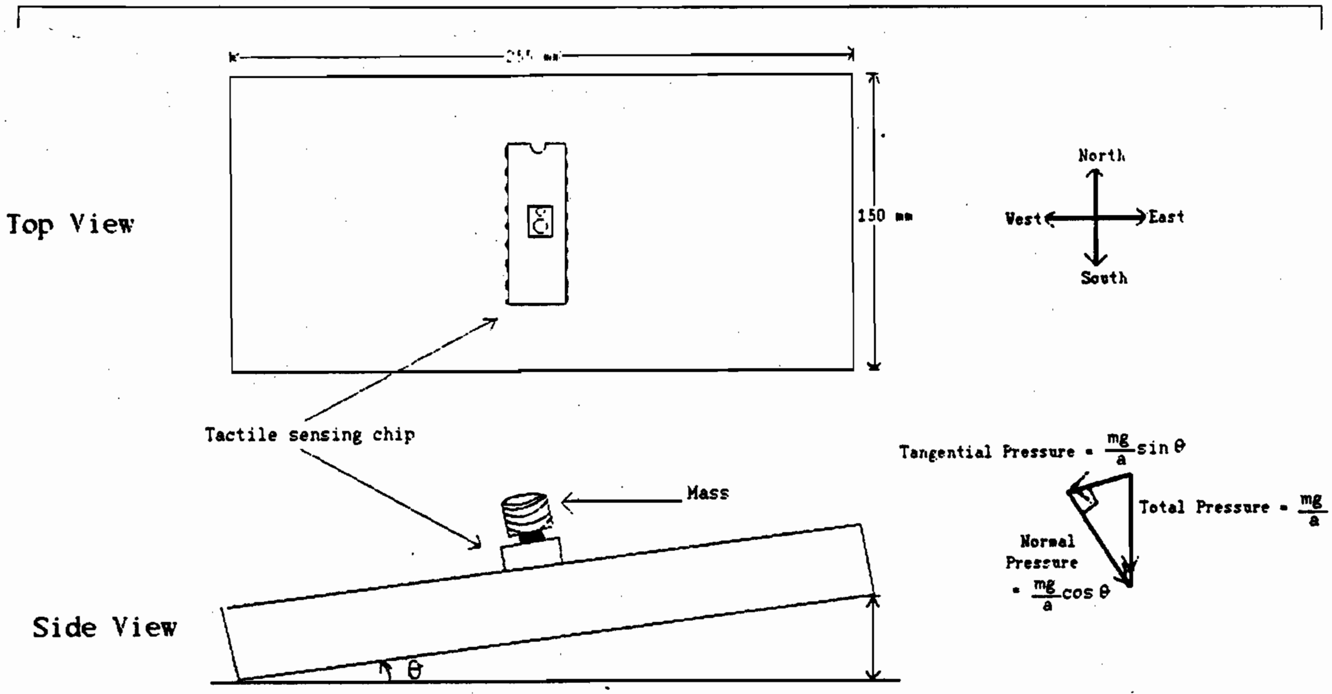

Figure 8.6 The testing setup. Shown are the top and side views of the board used to hold the chip, here, raised on the east side to give a tangential force in the 180^o direction.

tive biasing but, unfortunately, there exist no such quick fixes for the rubber's elasticity. The addition of fairly large quantities of carbon powder resulted in a stiff rubber skin. In addition, due to the lack of adequate molding facilities, the surface of the skin was not very smooth. Nonetheless, since the area of the tactile sensing hole is so small, during the testing, regions of the skin that were smooth were found and placed over the hole. Next, we did not have too much control over the depth of the sensor holes etched in the polyimide, resulting in holes on the order of $1mm$ deep. What these lead to is the fact that the sensor's response was *very* erratic. To begin, because of the deep holes and stiff rubber, the sensor required a very high threshold pressure before it exhibited any response. Furthermore, once the pressure had reached this threshold, there is a lot of response as many probes are touched by the skin. Thus the chip acted almost like a binary sensor, indicating whether or not the pressure applied is more than the threshold and it did not give as much indication, as hoped, about the tangential component. Also, since this threshold is so high, the two sensors which these experimental results are based on, were destroyed during the testing. Finally, the chips did latch–up several times during the testing and was evidenced with the output of the sensor becoming stuck high. This was easily remedied by powering the chip down and immediately back up again. Three times, however, this was accompanied by a sudden increase in the current, going as high as 1 ampere. The first chip still managed to survive the first power surge, but the second time it happened, the chip died with the output always stuck high. The second chip died immediately when the latch–up was accompanied by the power surge.

We now summarise the results in tabulular form. Recall that from the cursory analysis performed previously, we expect the 'mass' of the area touched by the rubber in the hole (*i.e.* the number of probes) to vary with the logarithm of the normal pressure applied, while the offset of the 'center–of–mass' from the center of the hole will vary with the tangential pressure.

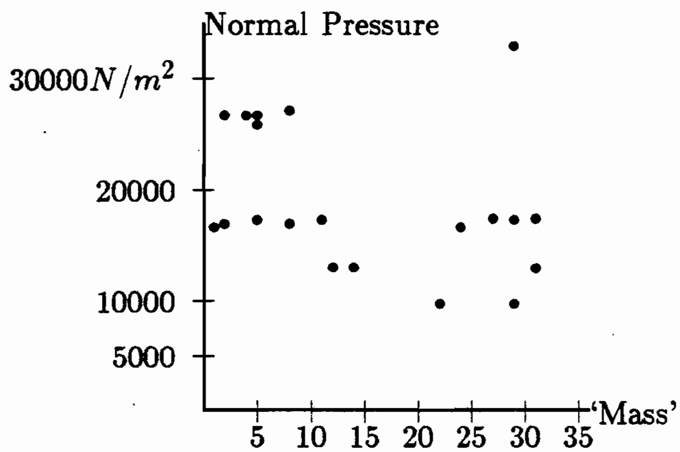

Figure 8.7 The normal pressure *vs* the 'mass' of the region of contact.

The points in the graph seem almost random, but two facts are apparent. First is that the threshold of the sensor is about 10000N/m^2. When the normal pressure applied passes this threshold, the sensor responds, but with a wide range of 'masses.' Secondly, there appears to to be two clusters in the graph on either side of the mass=15 boundary. The explanation for this is that when there is a large tangential component to the pressure, 'edge–effects' will affect the 'mass.' This is illustrated below with an example taken from the experiments.

Mass	Normal Pressure ($Newtons/meter^2$)
1	16583
2	16904
2	26665
4	26665
4	26665
5	17219
5	25842
5	26665
8	27090
8	16904
11	17229
12	12952
14	12952
22	9706
24	16583
24	16583
27	17384
27	17384
27	17384
29	9682
29	17219
29	32833
31	12920
31	17341

Table 8.1 "Mass" *vs.* Normal Pressure

East Inclined by $45mm$ Total Pressure= $27090N/m^2$
Normal Pressure= $26665N/m^2$ Tangential Pressure= $4779N/m^2$
Angle of Inclination= 10.16^o Direction of Pressure= 180^o

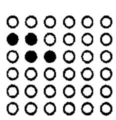

Mass= 4
Center–of–mass= (-180μ, 120μ)
Offset of the center of mass= 216μ in direction 146^o

In the figure, there is a large ($4779N/m^2$) tangential component (towards the left side of the page) which, as predicted, does cause an offset of the 'center of mass' towards the left. There is also, however, a large normal pressure ($26665N/m^2$) but because the region of contact is at the boundary of the hole, it gives a deceivingly small mass of 4. We can test this hypothesis by discarding pressures with a large tangential component. Using $2000N/m^2$ as a threshold, we get the following graph.

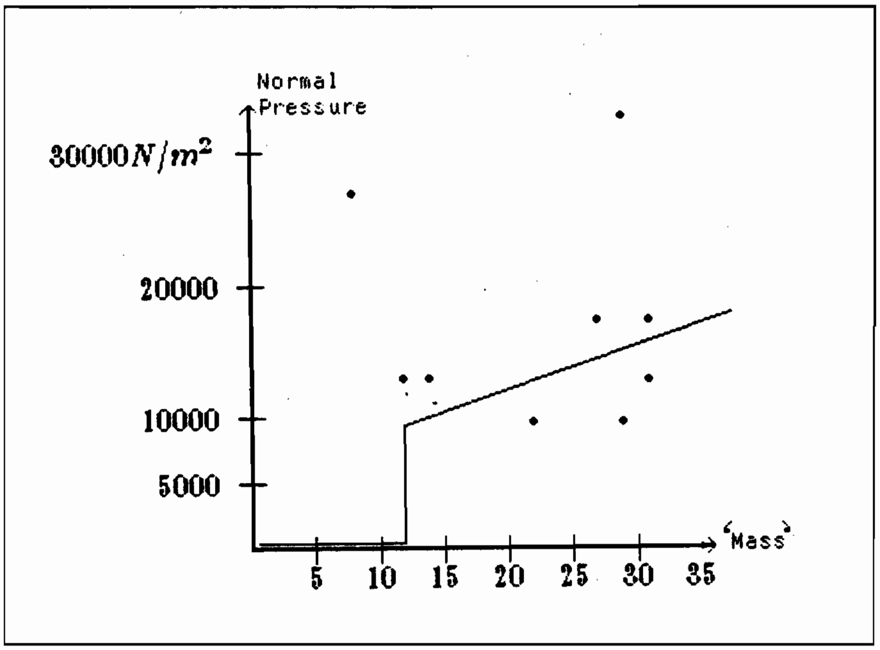

Figure 8.8 The normal ~~pressure vs the~~ 'mass,' below the threshold of $2000N/m^2$ for the shear pressure.

This graph seems to be more reasonable, but there still exist a few spurious points—there is no way of getting around irregularities in the rubber skin's surface. Nonetheless, with a little imagination, we can fit a line through the points; there are too few points to be able to fit the expected logarithmic relationship, though. Thus a simple model for the sensor is:

If the Tangential Pressure $< 2000N/m^2$ then

$$\begin{aligned} \text{Pressure} &= 10000 + 348 * \text{Mass}; \text{Mass} > 12 \\ \text{Pressure} &< 10000 \qquad\qquad ; \text{Mass} \leq 12 \end{aligned}$$

with units of $Newtons/meter^2$.

Analysing the relationship between the offset of the 'center-of-mass' and the tangential component of the pressure is more complicated because there are are actually two parameters involved. They are the offset of the center–of–mass as well as the direction in which it is offset. Correspondingly are the magnitude of the shear pressure as well its direction. We expect the direction of the center–of–mass to correspond exactly with the direction of the tangential component and the magnitude of the offset to vary directly with the magnitude of the tangential component. There are, however, bound to be discrepencies with the predicted direction and actual direction when the tangential component is small, since when the latter is zero, the direction is undefined. Very curiously, in the experiments, we *never* had a case when the offset was zero, giving an undefined direction, even when there was no shear component. This is most probably attributable to the skin's roughness, giving unsymmetric responses. The table below summarises the behaviour of the sensor to tangential pressures. The offset is given in microns (the distance between the probes is 120μ).

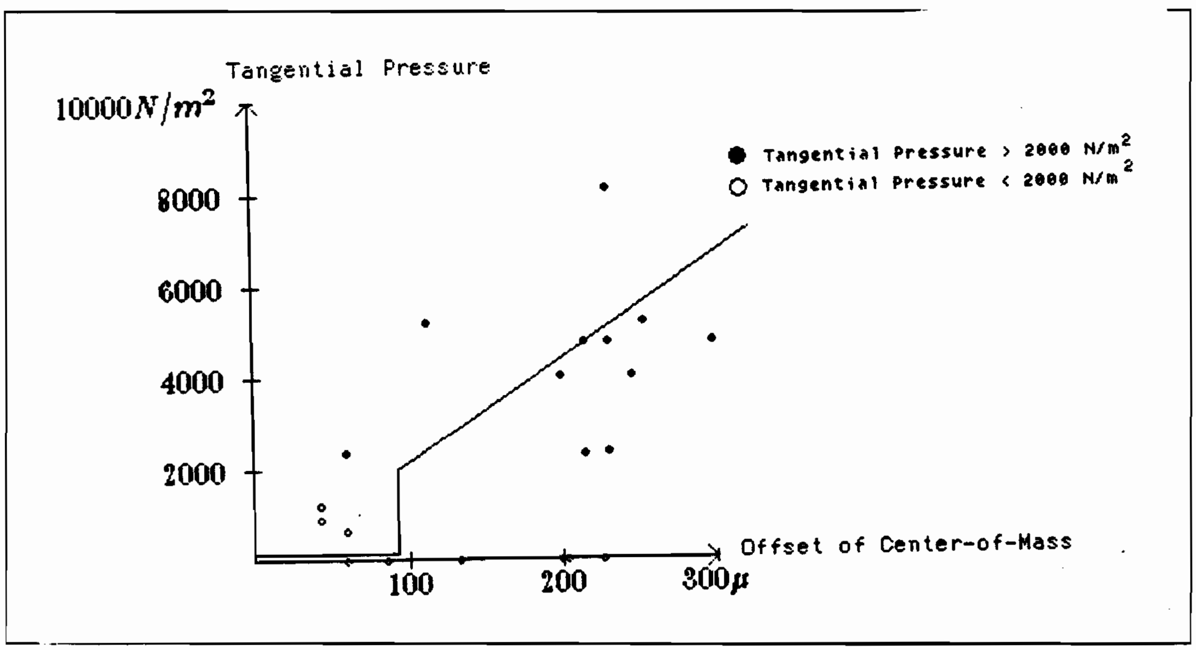

Figure 8.9 Graph of tangential pressure *vs* the offset of the 'center–of–mass.'

Just as with the normal pressures, the relationship between the offset of the center–of–mass and the shear component of the pressure is not very obvious. Two facts, however, are apparent in the table and in the graph. In the table, one can see that the

Offset (μ)	Tangential Pressure ($Newtons/meter^2$)	Direction of Offset	Actual Direction	Discrepency in Direction
204	0	-158^o	Undefined	—
227	0	-139^o	Undefined	—
134	0	-117^o	Undefined	—
87	0	-94^o	Undefined	—
87	0	-94^o	Undefined	—
61	0	-80^o	Undefined	—
200	0	167^o	Undefined	—
61	679	-80^o	90^o	170^o
44	906	-67^o	90^o	157^o
44	1216	-67^o	90^o	157^o
216	2317	-94^o	Undefined	—
231	2386	152^o	180^o	28^o
61	2386	-80^o	180^o	100^o
247	4055	-170^o	90^o	100^o
200	4055	166^o	90^o	76^o
216	4779	146^o	180^o	34^o
231	4779	152^o	180^o	28^o
300	4779	143^o	180^o	37^o
216	4779	146^o	180^o	34^o
255	5216	167^o	90^o	77^o
114	5216	135^o	90^o	45^o
114	5216	-105^o	90^o	165^o
231	8128	152^o	90^o	62^o

Table 8.2 Offset of the "Center-of-Mass" *vs.* Tangential Pressure

discrepency between the predicted and the actual direction of the tangential component is very high when the tangential pressure is less than $2000N/m^2$. As previously mentioned, this is to be expected as the direction becomed undefined as the magnitude of the shear component approaches zero. Secondly, if one excludes points which have a tangential component less than $2000N/m^2$ from the graph, there does seem to be a linear relationship between the offset of the center–of–mass and the shear pressure. Here too, there is a threshold below which the sensor gives unreliable results and above which it behaves approximately linearly. Thus a relationship similar in form to one for the normal pressure is obtained.

If the Tangential Pressure $\geq 2000 N/m^2$ then

$$
\begin{aligned}
\text{Tangential Pressure} &= 2000 + 28.5 * (\text{Offset of the Center–of–Mass}) \\
&\qquad ; (\text{Offset of the Center–of–Mass}) > 90\mu \\
\text{Tangential Pressure} &< 2000 \\
&\qquad ; (\text{Offset of the Center–of–Mass}) \leq 90\mu
\end{aligned}
$$

with units of $Newtons/meter^2$.

So to conclude this section, we have been able to find a simple linear relationship between the normal component of the pressure and the 'mass' of the region of contact, defined as the number of probes touched by the skin. A similar relationship was also found between the shear component and the offset of the 'center–of–mass' from the center of the hole. The two relationships are *not* in fact independent as a high tangential component will, due to boundary effects, decrease the 'mass' of the region of contact. Also, there is a threshold ~~with the~~ normal pressure as the rubber skin must first penetrate the hole before the sensor even starts responding. The latter threshold is very high because of the stiffness of the skin and the depth of the hole.

Finally, it is interesting to note the strange skewed symmetry in the way the sensor responds to normal and tangential forces. When the tangential forces are large, the sensor gives inaccurate readings for the normal pressure. On the other hand, when the tangential pressure is small, it gives inaccurate tangential pressure readings—it only responds predictably to the shear force only when it higher than a threshold.

In the next section we propose further improvements as well as alternate approaches that can be implemented in future design and will follow that with several concluding remarks.

Chapter 9 Recommendations and Proposals for Future Designs

In the previous section, the basic principle behind the all digital shear sensitive tactile sensor was shown to be sound and fabrication viable. Nonetheless, several disappointments were experienced in the course of testing the sensor and flaws were discovered which could severely limit potential uses of the sensor. In this section we propose remedies for these flaws.

One of the most serious drawbacks of the sensor is its fragility. This is, of course, to be expected since the sensor is, after all, a VLSI circuit with microscopic definitions. The chief cause of the two sensors' failures is very probably due to the high thresholds which required one to apply very large forces but that aside, there still seems to be a flaw in the design of the circuit as the chip still experiences latch–up. From another viewpoint, though, the sensor was more robust than initially expected since it was provided with no diode protection at the probes. One way or the other, the problem of latch–up can be easily rectified in future designs by adding more substrate connections and adding diode protection to the probes.

The aforementioned high thresholds also severely limit the applications of the sensor. In addition, there is the problem in the way the normal and tangential responses are coupled. This seems to be inherent in the design but there are means to reduce the interaction. To begin, it is very important that much more attention be paid to the quality of the rubber. In future designs, it would also be very prudent to increase the 'cut–off resistance' of the shift register. This can be achieved by increasing the length to width ratio of the active pullup pMOS transistor. This would increase the area of the shift register cell but, on the other hand, rubber skins with very good mechanical properties can be used since not as much carbon powder would need to be added. In the author's opinion, the cut–off resistance should be made as high as possible—the limiting factor is the increase in area of the circuit. With a more pliable rubber skin, the threshold is bound to decrease. Another obvious way to decrease the sensing threshold is to decrease the depth of the hole; the same end can also be reached by increasing the diameter of the hole.

There is also an alternate design which is very interesting since it has no threshold. In this design, the rubber skin is molded on one side to have cone shaped protrusions. When no pressure is applied, the tip of the cone touches the probes but as more pressure is applied, the cone deforms to make contact with more probes. It is not too clear how it will respond to tangential forces but intuitively, one can imagine a response similar to that exhibited in our sensor, *i.e.* a tangential force will cause an offset in the center–of–mass of the region of contact in the direction of the force. Two possible designs are sketched below.

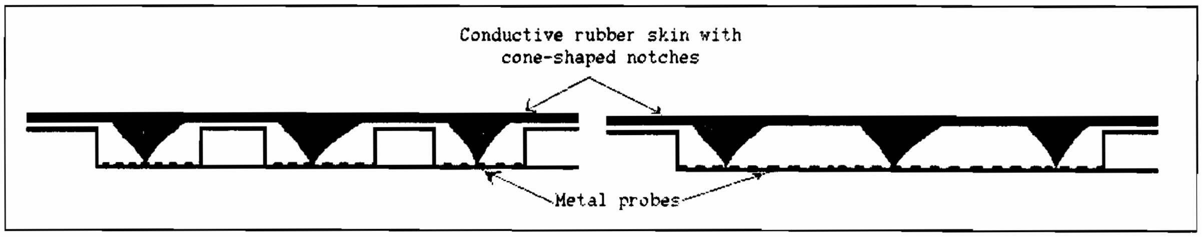

Figure 9.1 An alternate design with notched rubber skin.

The first sensor is identical in design to our chip with the exception of the conic protrusions in the skin. The polyimide coating is not strictly necessary and that is the difference in the second design. In the second design, the entire surface of the chip is completely covered by probes. It has an advantage over the first design in that it is 'self–aligning.' That is to say, it is not necessary, as in the first design, to align the skin so that the cones are over the holes. On the other hand, in the first design, once aligned, the skin can be permanently kept in place by glueing it to the polyimide coating. Furthermore, it is necessary that the second design be laid out in two metal layers, reserving the upper layer for the probes. This is to prevent the rubber from shorting the entire circuit. This is not necessary in the first as one can hide the active circuitry, as we did, under the polyimide coating. Finally, it must be emphasized that these proposals are purely speculatory and all hang on the assumption that it is possible to mold rubber skin accurately in such small dimensions.

Another extreme approach would be to use the principle of our sensor applied so that we only detect normal pressures in a binary fashion, forgetting about tangential forces. Instead of having an array of probes at the bottom of the sensor holes, one could just have a single probe so that the response of the sensor is on/off—when the normal pressure exceeds some threshold, the rubber touches the single probe. Such a sensor can be fabricated to extremely high resolutions. Also, the sensor could be made to give a graded response by having different sized holes which would result in different thresholds.

Indeed, since in the thesis, we have demonstrated the feasibility of constructing an entirely VLSI based digital tactile sensor, the horizons for future development are wide open. It would be quite exciting to try out various such designs, giving us sensors which, though based on the same principle, have different responses and are suitable for a great variety of different tasks.

Chapter 10 Conclusion

In summary, the objectives of this thesis, to design, implement and test a novel shear sensitive tactile sensor have all, to a certain extent, been met. We have demonstrated that the basic working principle of the sensor is sound and have been able to achieve a calibration by experimentally deriving a functional relationship between the sensor's response and the normal and tangential pressures applied to it.

The sensor is still in the very early stages of development and there will have to be many more design iterations before all the bugs are removed and there is a working, marketable product. In this project, we have completed two of these iterations. Several flaws have been discovered in the course of testing the sensor though none seem fatal—solutions to these problems have been proposed and should be very easy to implement in future designs.

Having, thus, demonstrated the feasibility of constructing such a VLSI based tactile sensor the chief effort in future designs will have to focus upon several details, though important, either omitted or not tested in our design. One very important part of the sensor which must be improved is the rubber skin. This task can be simplified by following the recommendation of decreasing the sensitivity of the sensor by increaing its 'cut–off resistance.' Also, considerable attention must be paid to the packaging of the sensor; this was completely ignored in the thesis. This step would depend a great deal upon the application chosen for the sensor, whether it be as a force sensor for a robot or as a mouse–like device for graphic input.

In closing, we have explored the fabrication of a completely new tactile sensing device and have found it to hold a lot of promise. We have shown that it is sensitive to both normal and shear forces and also offer several variant designs as well as improvements. The facts presented in this thesis lay the groundwork for future work and it is hoped that the thesis will be useful to others undertaking similar endeavours.

both normal and shear forces and also offer several variant designs as well as improvements. The facts presented in this thesis lay the groundwork for future work and it is hoped that the thesis will be useful to others undertaking similar endeavours.

Appendix A. Experimental Results

The Setup:

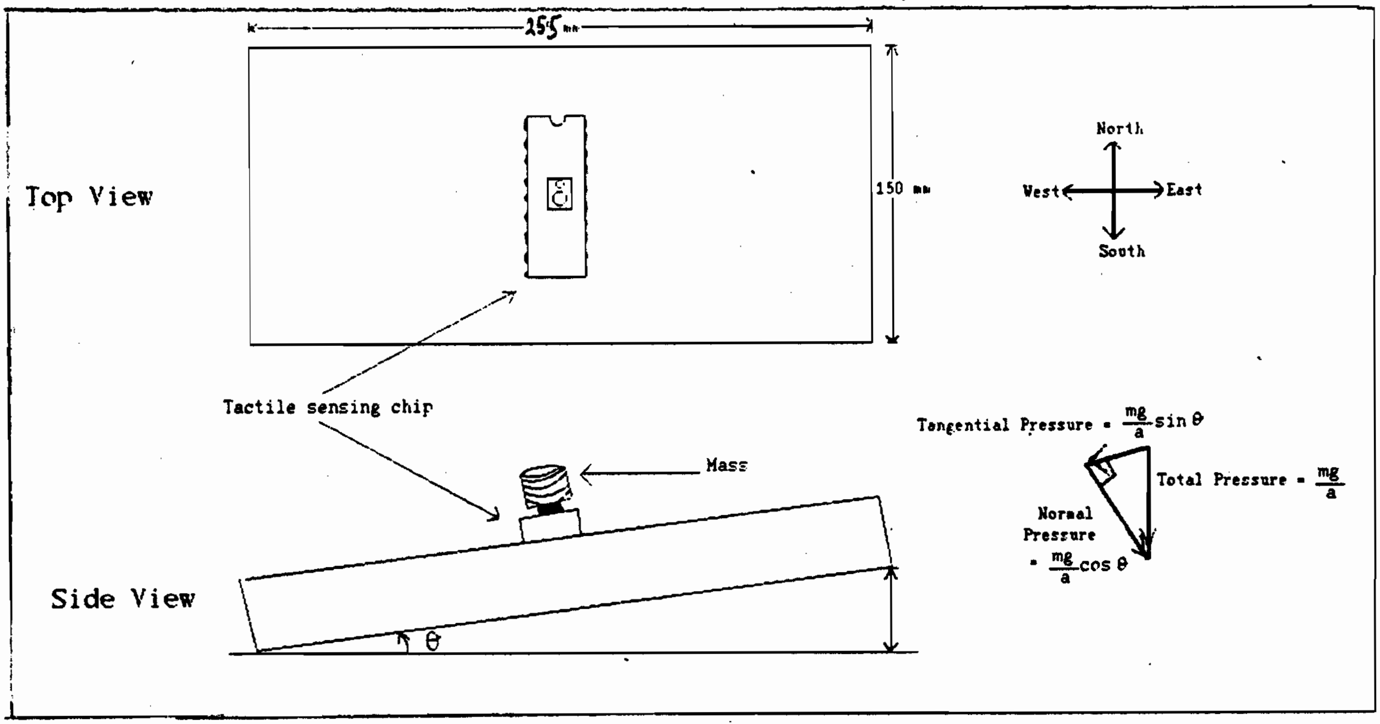

Figure A.1 The testing setup

"Qualitative" Results

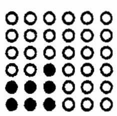

Mass= 7
Center–of–mass= (-163μ, -214μ)
Offset of the center of mass= 269μ in direction -127^o

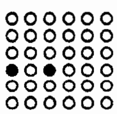

Mass= 2
Center–of–mass= (-180μ, -60μ)
Offset of the center of mass= 190μ in direction -162^o

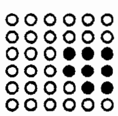

Mass= 8
Center–of–mass= (195μ, -45μ)
Offset of the center of mass= 200μ in direction -13^o

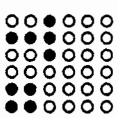

Mass= 9
Center–of–mass= (-180μ, -7μ)
Offset of the center of mass= 180μ in direction -178^o

Responses to Different Normal Forces

Pressure = $12952 N/m^2$

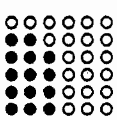

Mass= 14
Center–of–mass= (-189μ, -77μ)
Offset of the center of mass= 204μ in direction -158^o

Pressure $= 12952 N/m^2$

○○○○○○
○○○○○○
●●○○○○
●●●○○○
●●●○○○
●●●●○○

Mass= 12
Center–of–mass= (-170μ, -150μ)
Offset of the center of mass= 227μ in direction -139^o

Pressure $= 9706 N/m^2$

○○○○○○
●●○○○○
●●●○○○
●●●●●○
●●●●●●
●●●●●●

Mass= 22
Center–of–mass= (-60μ, -120μ)
Offset of the center of mass= 134μ in direction -117^o

Pressure $= 17384 N/m^2$

○○○○○○
●●○○○●
●●●●●●
●●●●●●
●●●●●●
●●●●●●

Mass= 27
Center–of–mass= (-7μ, -87μ)
Offset of the center of mass= 87μ in direction -94^o

Pressure $= 32833 N/m^2$

○○○○●●
●●○○○●
●●●●●●
●●●●●●
●●●●●●
●●●●●●

Mass= 29
Center–of–mass= (10μ, -60μ)
Offset of the center of mass= 61μ in direction -80^o

Responses to Forces with Different Tangential Components

South Inclined by $10.5mm$ Total Pressure= $12952 N/m^2$
Normal Pressure= $12920 N/m^2$ Tangential Pressure= $906 N/m^2$
Angle of Inclination= 4.01^o Direction of Pressure= 90^o

○○○●●●
●●○○●●
●●●●●●
●●●●●●
●●●●●●
●●●●●●

Mass= 31
Center–of–mass= (17μ, -41μ)
Offset of the center of mass= 44μ in direction -67^o

South Inclined by $10.5mm$ Total Pressure= $9706 N/m^2$
Normal Pressure= $9682 N/m^2$ Tangential Pressure= $679 N/m^2$
Angle of Inclination= 4.01^o Direction of Pressure= 90^o

○○○○●●
●●○○○●
●●●●●●
●●●●●●
●●●●●●
●●●●●●

Mass= 29
Center–of–mass= (10μ, -60μ)
Offset of the center of mass= 61μ in direction -80^o

South Inclined by $10.5mm$ Total Pressure= $17384 N/m^2$
Normal Pressure= $17341 N/m^2$ Tangential Pressure= $1216 N/m^2$
Angle of Inclination= 4.01^o Direction of Pressure= 90^o

○○○●●●
●●○○●●
●●●●●●
●●●●●●
●●●●●●
●●●●●●

Mass= 31
Center–of–mass= (17μ, -41μ)
Offset of the center of mass= 44μ in direction -67^o

At this point the chip latched up very badly. The current rose to 0.5 amps and the output became stuck high. The following experiments had to performed on another sensor.

A Continuation of the Analysis of the Sensor's Response to Forces with Different Tangential Components

Sensor Flat   Total Pressure= $17384 N/m^2$

Normal Pressure= 17384N/m^2 Tangential Pressure= 0N/m^2
Angle of Inclination= 0^o Direction of Pressure= n/a^o

○○○○○○
●●○○○●
●●●●●●
●●●●●●
●●●●●●
●●●●●●

Mass= 27
Center–of–mass= (-7μ, -87μ)
Offset of the center of mass= 87μ in direction -94^o

Sensor Flat Total Pressure= 17384N/m^2
Normal Pressure= 17384N/m^2 Tangential Pressure= 0N/m^2
Angle of Inclination= 0^o Direction of Pressure= n/a^o

○○○○○○
●●○○○●
●●●●●●
●●●●●●
●●●●●●
●●●●●●

Mass= 27
Center–of–mass= (-7μ, -87μ)
Offset of the center of mass= 87μ in direction -94^o

South Inclined by 20mm Total Pressure= 17384N/m^2
Normal Pressure= 17229N/m^2 Tangential Pressure= 2317N/m^2
Angle of Inclination= 7.66^o Direction of Pressure= 90^o

○○○○○○
●●○○○○
●●●○○○
●●●○○○
●○○○○○
●●○○○○

Mass= 11
Center–of–mass= (-213μ, -38μ)
Offset of the center of mass= 216μ in direction -170^o

South Inclined by 35mm Total Pressure= 17384N/m^2
Normal Pressure= 16904N/m^2 Tangential Pressure= 4055N/m^2
Angle of Inclination= 13.49^o Direction of Pressure= 90^o

○○○○○○
○○○○○○
●●○○○○
○○○○○○
○○○○○○
○○○○○○

Mass= 2
Center–of–mass= (-240μ, 60μ)
Offset of the center of mass= 247μ in direction 166^o

South Inclined by 35mm Total Pressure= 17384N/m^2
Normal Pressure= 16904N/m^2 Tangential Pressure= 4055N/m^2
Angle of Inclination= 13.49^o Direction of Pressure= 90^o

○○○○○○
●●○○○○
●●●○○○
●●●○○○
○○○○○○
○○○○○○

Mass= 8
Center–of–mass= (-195μ, 45μ)
Offset of the center of mass= 200μ in direction 167^o

South Inclined by 45mm Total Pressure= 17384N/m^2
Normal Pressure= 16583N/m^2 Tangential Pressure= 5216N/m^2
Angle of Inclination= 17.46^o Direction of Pressure= 90^o

○○○○○○
○●○○○○
○○○○○○
○○○○○○
○○○○○○
○○○○○○

Mass= 1
Center–of–mass= (-180μ, 180μ)
Offset of the center of mass= 255μ in direction 135^o

South Inclined by 45mm Total Pressure= 17384N/m^2
Normal Pressure= 16583N/m^2 Tangential Pressure= 5216N/m^2
Angle of Inclination= 17.46^o Direction of Pressure= 90^o

○○○○○○
●●○○○○
●●●○○●
●●●●●●
●●●●●●
●●●●●●

Mass= 24
Center–of–mass= (-30μ, -110μ)
Offset of the center of mass= 114μ in direction -105^o

South Inclined by 45mm Total Pressure= 17384N/m^2
Normal Pressure= 16583N/m^2 Tangential Pressure= 5216N/m^2

Angle of Inclination= 17.46^o Direction of Pressure= 90^o

○○○○○○
●●○○○○
●●●○○●
●●●●●●
●●●●●●
●●●●●●

Mass= 24
Center–of–mass= (-30μ, -110μ)
Offset of the center of mass= 114μ in direction -105^o

East Inclined by 35mm Total Pressure= 17384N/m^2
Normal Pressure= 17219N/m^2 Tangential Pressure= 2386N/m^2
Angle of Inclination= 7.89^o Direction of Pressure= 180^o

○○○○○○
●●○○○○
●●●○○○
○○○○○○
○○○○○○
○○○○○○

Mass= 5
Center–of–mass= (-204μ, 108μ)
Offset of the center of mass= 231μ in direction 152^o

East Inclined by 35mm Total Pressure= 17384N/m^2
Normal Pressure= 17219N/m^2 Tangential Pressure= 2386N/m^2
Angle of Inclination= 7.89^o Direction of Pressure= 180^o

○○○○●●
●●○○○●
●●●●●●
●●●●●●
●●●●●●
●●●●●●

Mass= 29
Center–of–mass= (10μ, -60μ)
Offset of the center of mass= 61μ in direction -80^o

Sensor Flat Total Pressure= 27090N/m^2
Normal Pressure= 27090N/m^2 Tangential Pressure= 0N/m^2
Angle of Inclination= 0^o Direction of Pressure= n/a^o

○○○○○○
●●○○○○
●●●○○○
●●●○○○
○○○○○○
○○○○○○

Mass= 8
Center–of–mass= (-195μ, 45μ)
Offset of the center of mass= 200μ in direction 167^o

South Inclined by 45mm Total Pressure= 27090N/m^2
Normal Pressure= 25842N/m^2 Tangential Pressure= 8128N/m^2
Angle of Inclination= 17.46^o Direction of Pressure= 90^o

○○○○○○
●●○○○○
●●●○○○
○○○○○○
○○○○○○
○○○○○○

Mass= 5
Center–of–mass= (-204μ, 108μ)
Offset of the center of mass= 231μ in direction 152^o

East Inclined by 45mm Total Pressure= 27090N/m^2
Normal Pressure= 26665N/m^2 Tangential Pressure= 4779N/m^2
Angle of Inclination= 10.16^o Direction of Pressure= 180^o

○○○○○○
●●○○○○
○●●○○○
○○○○○○
○○○○○○
○○○○○○

Mass= 4
Center–of–mass= (-180μ, 120μ)
Offset of the center of mass= 216μ in direction 146^o

East Inclined by 45mm Total Pressure= 27090N/m^2
Normal Pressure= 26665N/m^2 Tangential Pressure= 4779N/m^2
Angle of Inclination= 10.16^o Direction of Pressure= 180^o

○○○○○○
●●○○○○
●●●○○○
○○○○○○
○○○○○○
○○○○○○

Mass= 5
Center–of–mass= (-204μ, 108μ)
Offset of the center of mass= 231μ in direction 152^o

East Inclined by 45mm Total Pressure= 27090N/m^2
Normal Pressure= 26665N/m^2 Tangential Pressure= 4779N/m^2
Angle of Inclination= 10.16^o Direction of Pressure= 180^o

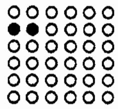

Mass= 2
Center–of–mass= (-240μ, 180μ)
Offset of the center of mass= 300μ in direction 143^o

East Inclined by 45mm Total Pressure= 27090N/m^2
Normal Pressure= 26665N/m^2 Tangential Pressure= 4779N/m^2
Angle of Inclination= 10.16^o Direction of Pressure= 180^o

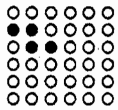

Mass= 4
Center–of–mass= (-180μ, 120μ)
Offset of the center of mass= 216μ in direction 146^o

Appendix B. SPICE Simulation Results

B.1 The Cut-off Resistance of the Shift Register

SPICE Program listing

```
*** SPICE DECK created from shift.sim, tech=cmos3
* Steady state analysis of the shift register to find the cut-off resistance
* of the pull-up circuitry.
*
* Circuit exracted by 'mextra'
*
* Gnd=0 Vdd=1 in=9 out=4 nload=7 pload=10 phi1=8 phi2=12 probe=11
*
********************CMOS TRANSISTOR MODELS********************************
.MODEL   NMOS NMOS (LEVEL=2      VTO=0.7     KP=50U      GAMMA=1.1   PHI=0.6
+                  LAMBDA=10M RD=40       RS=40       PB=0.7      CGSO=0.3N
+                  CGDO=0.3N  CGBO=0.5N   RSH=25      CJ=0.44M    MJ=0.5
+                  CJSW=0.4N  MJSW=0.3    JS=10U      TOX=50N     NSUB=1.7E16
+                  NSS=0      NFS=0       TPG=1       XJ=0.6U     LD=0.35U
+                  U0=775     VMAX=1.0E5 )
.MODEL   PMOS PMOS (LEVEL=2      VTO=-0.8    KP=16U      GAMMA=0.6   PHI=0.6
+                  LAMBDA=30M RD=100      RS=100      PB=0.6      CGSO=0.25N
+                  CGDO=0.25N CGBO=0.5N   RSH=80      CJ=0.15M    MJ=0.6
+                  CJSW=0.4N  MJSW=0.6    JS=10U      TOX=50N     NSUB=5.0E15
+                  NSS=0      NFS=0       TPG=1       XJ=0.5U     LD=0.25U
+                  U0=250     VMAX=0.7E5 )
********************CONTROL SIGNALS*************************************
*
*  vnload   01111000000000000000
*  vpload   10000111111111111111
*  vphi1    01000100010001000100      vphi1 goes low during loading
*  vphi2    00010001000100010001      vphi2 remains unchanged
*           01234567890123456789
*           0         1
vdd 1 0 dc 5v
rvpload   7   0    10K
vnload    8   0    dc 5v
rvphi1    10  0    10K
vphi2   12  0   dc 5v
* Input to shift register is grounded
rin 11 1 50K
* Resistance from the probe to ground (through the rubber skin)
rprobe 9 0 1K
* Print the steady state voltages
.print dc v(7) v(8) v(10) v(12) v(9) v(4)
.width out=80
.OPTIONS      NOMOD   LIMTIM=100   LIMPTS=99999
+             PIVREL=0.100   VNTOL=0.100   RELTOL=0.100 abstol=100e-12
+             ITL1=9999   ITL2=9999   ITL5=0
+             method=gear   maxord=3   numdgt=2
*
* Nodes are : 1=vdd 9=probe 4=out 7=pload 10=phi1 8=nload 12=phi2 11=in
M1 2 0 1 1 PMOS L=5.0U W=5.0U
M2 4 3 1 1 PMOS L=5.0U W=9.0U
M3 6 5 1 1 PMOS L=5.0U W=9.0U
M4 5 7 2 1 PMOS L=5.0U W=15.0U
M5 9 8 5 0 NMOS L=5.0U W=5.0U
M6 0 3 4 0 NMOS L=5.0U W=5.0U
M7 0 5 6 0 NMOS L=5.0U W=5.0U
M8 11 10 5 0 NMOS L=5.0U W=5.0U
M9 6 12 3 0 NMOS L=5.0U W=5.0U
C10 12 0 106.0F
C11 11 0 78.0F
C12 8 0 91.0F
C13 10 0 81.0F
C14 0 0 181.0F
C15 3 0 69.0F
C16 6 0 104.0F
C17 5 0 110.0F
C18 4 0 51.0F
C19 9 0 37.0F
C20 7 0 80.0F
C21 2 0 15.0F
```

```
C22 1 0 116.0F
* Slowly increment the resistance to find the 'cut--of resistance'
.alter
rprobe 9 999 2K
.alter
rprobe 9 999 3K
.alter
rprobe 9 999 4K
.alter
rprobe 9 999 5K
.alter
rprobe 9 999 6K
.alter
rprobe 9 999 7K
.alter
rprobe 9 999 8K
.alter
rprobe 9 999 9K
.alter
rprobe 9 999 10K
.alter
rprobe 9 999 11K
.alter
rprobe 9 999 12K
.alter
rprobe 9 999 13K
.alter
rprobe 9 999 14K
.alter
rprobe 9 999 15K
.alter
rprobe 9 999 16K
.alter
rprobe 9 999 17K
.alter
rprobe 9 999 18K
.alter
rprobe 9 999 19K
.alter
rprobe 9 999 20K
.end
```

Probe Resistance	Output Voltage
1KΩ	0.1085 V
2KΩ	0.1085 V
3KΩ	0.1085 V
4KΩ	0.1085 V
5KΩ	0.1085 V
6KΩ	0.1085 V
7KΩ	0.1087 V
8KΩ	0.1088 V
9KΩ	0.1090 V
10KΩ	0.1091 V
11KΩ	0.1094 V
12KΩ	0.1097 V
13KΩ	0.1103 V
14KΩ	0.5507 V
15KΩ	4.9993 V
16KΩ	5.0000 V
17KΩ	5.0000 V
18KΩ	5.0000 V
19KΩ	5.0000 V
20KΩ	5.0000 V

Table B.1 Cut–Off Resistance

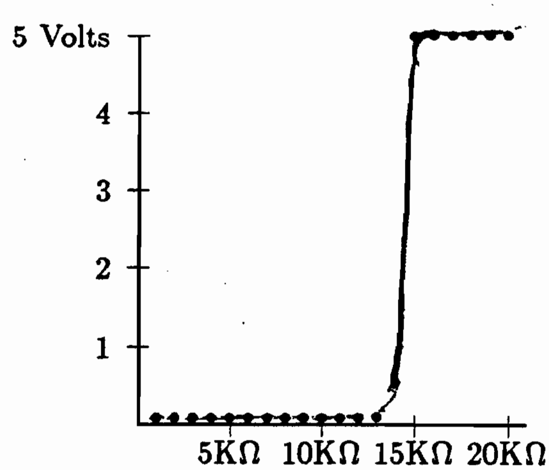

B.2 The Cut–off Resistance of the Negatively Biased Shift Register

SPICE Program listing

```
*** SPICE DECK created from shift.sim, tech=cmos3
* Steady state analysis of the shift register to find the effect of a
* negatively biased probe resistance on the cut-off resistance.
* In the simulations, we use a moderate bias of -1.5 volts as was used during
* the experiments.
*
* Circuit exracted by 'mextra'
*
* Gnd=0 Vdd=1 in=9 out=4 nload=7 pload=10 phi1=8 phi2=12 probe=11
*
********************CMOS TRANSISTOR MODELS*******************************
.MODEL   NMOS NMOS (LEVEL=2      VTO=0.7       KP=50U        GAMMA=1.1    PHI=0.6
+                   LAMBDA=10M  RD=40          RS=40           PB=0.7        CGSO=0.3N
+                   CGDO=0.3N   CGBO=0.5N    RSH=25          CJ=0.44M     MJ=0.5
+                   CJSW=0.4N   MJSW=0.3      JS=10U         TOX=50N       NSUB=1.7E16
+                   NSS=0          NFS=0          TPG=1          XJ=0.6U      LD=0.35U
+                   U0=775         VMAX=1.0E5 )
.MODEL   PMOS PMOS (LEVEL=2      VTO=-0.8      KP=16U        GAMMA=0.6    PHI=0.6
+                   LAMBDA=30M  RD=100         RS=100          PB=0.6        CGSO=0.25N
+                   CGDO=0.25N  CGBO=0.5N    RSH=80          CJ=0.15M     MJ=0.6
+                   CJSW=0.4N   MJSW=0.6      JS=10U         TOX=50N       NSUB=5.0E15
+                   NSS=0          NFS=0          TPG=1          XJ=0.5U      LD=0.25U
+                   U0=250         VMAX=0.7E5 )
*********************CONTROL SIGNALS***********************************
*
*   vnload   01111000000000000000
*   vpload   10000111111111111111
*   vphi1    01000100010001000100       vphi1 goes low during loading
*   vphi2    00010001000100010001       vphi2 remains unchanged
*             01234567890123456789
*             0         1
vdd 1 0 dc 5v
rvpload  7  0    10K
vnload   8  0    dc 5v
rvphi1   10  0    10K
vphi2   12  0    dc 5v
* Input to shift register is grounded
rin 11 1 50K
* Bias of -1.5 volts
vbias   999 0 dc -1.5v
* Resistance from the probe to ground (through the rubber skin)
rprobe 9 999 10K
* Print the steady state voltages
.print dc v(7) v(8) v(10) v(12) v(9) v(4)
.width out=80
.OPTIONS     NOMOD   LIMTIM=100   LIMPTS=99999
+              PIVREL=0.100    VNTOL=0.100    RELTOL=0.100 abstol=100e-12
+              ITL1=9999   ITL2=9999    ITL5=0
+              method=gear   maxord=3   numdgt=2
*
* Nodes are : 1=vdd 9=probe 4=out 7=pload 10=phi1 8=nload 12=phi2 11=in
M1  2  0  1  1  PMOS  L=5.0U  W=5.0U
M2  4  3  1  1  PMOS  L=5.0U  W=9.0U
M3  6  5  1  1  PMOS  L=5.0U  W=9.0U
M4  5  7  2  1  PMOS  L=5.0U  W=15.0U
M5  9  8  5  0  NMOS  L=5.0U  W=5.0U
M6  0  3  4  0  NMOS  L=5.0U  W=5.0U
M7  0  5  6  0  NMOS  L=5.0U  W=5.0U
M8  11  10  5  0  NMOS  L=5.0U  W=5.0U
M9  6  12  3  0  NMOS  L=5.0U  W=5.0U
C10  12  0  106.0F
C11  11  0  78.0F
C12  8  0  91.0F
C13  10  0  81.0F
C14  0  0  181.0F
C15  3  0  69.0F
C16  6  0  104.0F
C17  5  0  110.0F
C18  4  0  51.0F
C19  9  0  37.0F
C20  7  0  80.0F
C21  2  0  15.0F
C22  1  0  116.0F
* Slowly increment the resistance to find the 'cut--of resistance'
```

```
.alter
rprobe 9 999 11K
.alter
rprobe 9 999 12K
.alter
rprobe 9 999 13K
.alter
rprobe 9 999 14K
.alter
rprobe 9 999 15K
.alter
rprobe 9 999 16K
.alter
rprobe 9 999 17K
.alter
rprobe 9 999 18K
.alter
rprobe 9 999 19K
.alter
rprobe 9 999 20K
.alter
rprobe 9 999 21K
.alter
rprobe 9 999 22K
.alter
rprobe 9 999 23K
.alter
rprobe 9 999 24K
.alter
rprobe 9 999 25K
.alter
rprobe 9 999 26K
.alter
rprobe 9 999 27K
.alter
rprobe 9 999 28K
.alter
rprobe 9 999 29K
.alter
rprobe 9 999 30K
.alter
rprobe 9 999 31K
.alter
rprobe 9 999 32K
.alter
rprobe 9 999 33K
.alter
rprobe 9 999 34K
.alter
rprobe 9 999 35K
.end
```

Probe Resistance	Output Voltage
10KΩ	0.1085 V
11KΩ	0.1085 V
12KΩ	0.1085 V
13KΩ	0.1085 V
14KΩ	0.1085 V
15KΩ	0.1085 V
16KΩ	0.1085 V
17KΩ	0.1085 V
18KΩ	0.1085 V
19KΩ	0.1086 V
20KΩ	0.1086 V
21KΩ	0.1086 V
22KΩ	0.1087 V
23KΩ	0.1089 V
24KΩ	0.1090 V
25KΩ	0.1092 V
26KΩ	0.1094 V
27KΩ	0.1097 V
28KΩ	0.1101 V
29KΩ	0.1107 V
30KΩ	4.9048 V
31KΩ	4.9993 V
32KΩ	5.0000 V
33KΩ	5.0000 V
34KΩ	5.0000 V
35KΩ	5.0000 V

Table B.2 Cut–Off Resistance With a Bias of -1.5 *Volts*

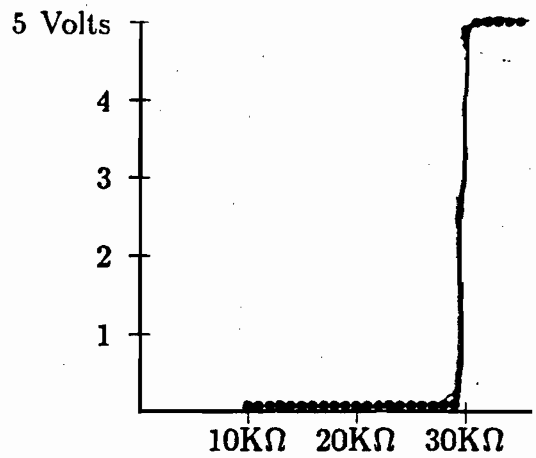
5 Volts
4
3
2
1
10KΩ
20KΩ
30KΩ

B.3 SPICE Simulations of a Five Bit Shift Register

SPICE Program Output

```
1*******07/16/87 ********  SPICE 2G.6     3/15/83 ********18:20:00*****
0* SIMULATION OF A 5 BIT SHIFT REGISTER
0****      INPUT LISTING                        TEMPERATURE =   27.000 DEG C
0***********************************************************************

 ***************************************************************
 * THE INPUT TO THE FIRST BIT IS GROUNDED.
 * THE PROBE RESISTANCES, FROM THE FIRST TO FIFTH BIT, ARE:
 *    100K, 10K, 5K, 50K  AND  30K OHMS
 * THE FIFTH BIT IS SHIFTED OUT  FIRST AND IS AVAILABLE WHEN PHI2 IS HIGH
 *  DURING THE LOADING PULSE. THE OTHER BITS ARE CONSEQUENTLY AVAILABLE
 *  WHEN  PHI2 IS HIGH.
 * THE OUTPUT SEEN SHOULD BE: HIGH, HIGH, LOW, LOW, HIGH FOLLOWED BY
 *  LOW BITS (SINCE THE INPUT TO THE FIRST BIT IS GROUNDED)
 *
 *********************TRANSISTOR MODELS***********************
 .MODEL   NMOS NMOS  (LEVEL=2      VTO=0.7      KP=50U       GAMMA=1.1   PHI=0.6
 +                      LAMBDA=10M RD=40          RS=40         PB=0.7        CGSO=0.3N
 +                      CGDO=0.3N   CGBO=0.5N   RSH=25        CJ=0.44M     MJ=0.5
 +                      CJSW=0.4N   MJSW=0.3     JS=10U       TOX=50N      NSUB=1.7E16
 +                      NSS=0        NFS=0          TPG=1         XJ=0.6U      LD=0.35U
 +                      UO=775       VMAX=1.0E5 )
 .MODEL   PMOS PMOS  (LEVEL=2      VTO=-0.8     KP=16U       GAMMA=0.6   PHI=0.6
 +                      LAMBDA=30M RD=100         RS=100        PB=0.6        CGSO=0.25N
 +                      CGDO=0.25N CGBO=0.5N   RSH=80        CJ=0.15M     MJ=0.6
 +                      CJSW=0.4N   MJSW=0.6     JS=10U       TOX=50N      NSUB=5.0E15
 +                      NSS=0        NFS=0          TPG=1         XJ=0.5U      LD=0.25U
 +                      UO=250       VMAX=0.7E5 )
 *******************CONTROL SIGNALS***************************
 *
 *   VNLOAD   01111000000000000000
 *   VPLOAD   10000111111111111111
 *   VPHI1    01000100010001000100        VPHI1 GOES LOW DURING LOADING
 *   VPHI2    00010001000100010001        VPHI2 REMAINS UNCHANGED
 *             01234567890123456789
 *             0          1
 VDD 1 0 DC 5V
 VPLOAD   7   0    PWL( ONS 5V      100NS 5V     105NS 0V      495NS 0V       500NS 5V )
 VNLOAD   8   0    PWL( ONS 0V      102NS 0V     107NS 5V      497NS 5V       502NS 0V )
 VPHI1   10   0    PWL( ONS 0V      502NS 0V     507NS 5V      597NS 5V       602NS 0V
 +                      902NS 0V      907NS 5V     997NS 5V     1002NS 0V     1302NS 0V
 +                     1307NS 5V     1397NS 5V    1402NS 0V     1702NS 0V     1707NS 5V
 +                     1797NS 5V     1802NS 0V    )
 VPHI2   12   0    PWL( ONS 0V      300NS 0V     305NS 5V      395NS 5V       400NS 0V
 +                                    700NS 0V     705NS 5V      795NS 5V       800NS 0V
 +                     1100NS 0V     1105NS 5V    1195NS 5V     1200NS 0V     1500NS 0V
 +                     1505NS 5V     1595NS 5V    1600NS 0V     1900NS 0V     1905NS 5V
 +                     1995NS 5V     2000NS 0V    )
 ******************5 SHIFT REGISTER STRUNG TOGETHER*************
 *             VDD PROBE  OUT PLOAD PHI1 NLOAD PHI2 IN
 XSHIFT1        1   111    41    7     10    8     12   91 SHIFT
 XSHIFT2        1   112    42    7     10    8     12   41 SHIFT
 XSHIFT3        1   113    43    7     10    8     12   42 SHIFT
 XSHIFT4        1   114    44    7     10    8     12   43 SHIFT
 XSHIFT5        1   115    45    7     10    8     12   44 SHIFT
 RIN           91  0  5
 RPROBE1      111  0  100K
 RPROBE2      112  0  10K
 RPROBE3      113  0  5K
 RPROBE4      114  0  50K
 RPROBE5      115  0  30K
 .TRAN  20NS  2000NS  UIC
 ***PRINT  THE  OUTPUTS:
 *** V(45)  = SHIFTED OUTPUT
 *** V(7)   = PLOAD (=LOAD BAR= THE INPUT TO THE GATE OF THE PMOS TRANSISTOR)
 *** V(8)   = NLOAD (=LOAD      = THE INPUT TO THE GATE OF THE NMOS TRANSISTOR)
 *** V(10)  = PHI1
 *** V(11)  = PHI2
 .PRINT  TRANS  V(45)  V(7)  V(8)  V(10)  V(12)
 .WIDTH  OUT=80
 .OPTIONS    NOMOD   LIMTIM=200   LIMPTS=99999
 +              PIVREL=0.200   VNTOL=0.100    RELTOL=0.200 ABSTOL=200E-12
 +              ITL1=9999  ITL2=9999   ITL5=0
 +              METHOD=GEAR    NUMDGT=2
 *
 .SUBCKT SHIFT 1 9 4 7 10 8 12 11
```

```
* NODES ARE : 1=VDD 9=PROBE 4=OUT 7=PLOAD 10=PHI1 8=NLOAD 12=PHI2 11=IN
M1 2 0 1 1 PMOS L=5.0U W=5.0U
M2 4 3 1 1 PMOS L=5.0U W=9.0U
M3 6 5 1 1 PMOS L=5.0U W=9.0U
M4 5 7 2 1 PMOS L=5.0U W=15.0U
M5 9 8 5 0 NMOS L=5.0U W=5.0U
M6 0 3 4 0 NMOS L=5.0U W=5.0U
M7 0 5 6 0 NMOS L=5.0U W=5.0U
M8 11 10 5 0 NMOS L=5.0U W=5.0U
M9 6 12 3 0 NMOS L=5.0U W=5.0U
C10 12 0 106.0F
C11 11 0 78.0F
C12 8 0 91.0F
C13 10 0 81.0F
C14 0 0 181.0F
C15 3 0 69.0F
C16 6 0 104.0F
C17 5 0 110.0F
C18 4 0 51.0F
C19 9 0 37.0F
C20 7 0 80.0F
C21 2 0 15.0F
C22 1 0 116.0F
.ENDS SHIFT
.END
1*******07/16/87 ********  SPICE 2G.6     3/15/83 ********18:20:00*****
0* SIMULATION OF A 5 BIT SHIFT REGISTER
0****      TRANSIENT ANALYSIS                    TEMPERATURE =   27.000 DEG C
0***********************************************************************
```

	<OUTPUT>	$\overline{\text{LOAD}}$	LOAD	PHI1	PHI2	<--Comments by
TIME	V(45)	V(7)	V(8)	V(10)	V(12)	Author
X						
0.000e+00	1.2e-01	5.0e+00	0.0e+00	0.0e+00	0.0e+00	V
2.000e-08	4.8e+00	5.0e+00	0.0e+00	0.0e+00	0.0e+00	
4.000e-08	4.8e+00	5.0e+00	0.0e+00	0.0e+00	0.0e+00	
6.000e-08	4.8e+00	5.0e+00	0.0e+00	0.0e+00	0.0e+00	
8.000e-08	4.8e+00	5.0e+00	0.0e+00	0.0e+00	0.0e+00	
1.000e-07	4.8e+00	5.0e+00	0.0e+00	0.0e+00	0.0e+00	
1.200e-07	4.8e+00	0.0e+00	5.0e+00	0.0e+00	0.0e+00	<--Loading Starts
1.400e-07	4.8e+00	0.0e+00	5.0e+00	0.0e+00	0.0e+00	
1.600e-07	4.8e+00	0.0e+00	5.0e+00	0.0e+00	0.0e+00	
1.800e-07	4.8e+00	0.0e+00	5.0e+00	0.0e+00	0.0e+00	
2.000e-07	4.8e+00	0.0e+00	5.0e+00	0.0e+00	0.0e+00	
2.200e-07	4.8e+00	0.0e+00	5.0e+00	0.0e+00	0.0e+00	
2.400e-07	4.8e+00	0.0e+00	5.0e+00	0.0e+00	0.0e+00	
2.600e-07	4.8e+00	0.0e+00	5.0e+00	0.0e+00	0.0e+00	
2.800e-07	4.8e+00	0.0e+00	5.0e+00	0.0e+00	0.0e+00	
3.000e-07	4.8e+00	0.0e+00	5.0e+00	0.0e+00	0.0e+00	
3.200e-07	5.0e+00	0.0e+00	5.0e+00	0.0e+00	5.0e+00	
3.400e-07	5.0e+00	0.0e+00	5.0e+00	0.0e+00	5.0e+00	
3.600e-07	5.0e+00	0.0e+00	5.0e+00	0.0e+00	5.0e+00	
3.800e-07	5.0e+00	0.0e+00	5.0e+00	0.0e+00	5.0e+00	<--First bit shifted out is HIGH
4.000e-07	5.0e+00	0.0e+00	5.0e+00	0.0e+00	1.1e-19	
4.200e-07	5.0e+00	0.0e+00	5.0e+00	0.0e+00	0.0e+00	
4.400e-07	5.0e+00	0.0e+00	5.0e+00	0.0e+00	0.0e+00	
4.600e-07	5.0e+00	0.0e+00	5.0e+00	0.0e+00	0.0e+00	
4.800e-07	5.0e+00	0.0e+00	5.0e+00	0.0e+00	0.0e+00	<--Loading Finished
5.000e-07	5.0e+00	5.0e+00	2.0e+00	0.0e+00	0.0e+00	
5.200e-07	5.0e+00	5.0e+00	0.0e+00	5.0e+00	0.0e+00	
5.400e-07	5.0e+00	5.0e+00	0.0e+00	5.0e+00	0.0e+00	
5.600e-07	5.0e+00	5.0e+00	0.0e+00	5.0e+00	0.0e+00	
5.800e-07	5.0e+00	5.0e+00	0.0e+00	5.0e+00	0.0e+00	
6.000e-07	5.0e+00	5.0e+00	0.0e+00	2.0e+00	0.0e+00	
6.200e-07	5.0e+00	5.0e+00	0.0e+00	0.0e+00	0.0e+00	
6.400e-07	5.0e+00	5.0e+00	0.0e+00	0.0e+00	0.0e+00	
6.600e-07	5.0e+00	5.0e+00	0.0e+00	0.0e+00	0.0e+00	
6.800e-07	5.0e+00	5.0e+00	0.0e+00	0.0e+00	0.0e+00	
7.000e-07	5.0e+00	5.0e+00	0.0e+00	0.0e+00	0.0e+00	
7.200e-07	5.0e+00	5.0e+00	0.0e+00	0.0e+00	5.0e+00	
7.400e-07	5.0e+00	5.0e+00	0.0e+00	0.0e+00	5.0e+00	
7.600e-07	5.0e+00	5.0e+00	0.0e+00	0.0e+00	5.0e+00	
7.800e-07	5.0e+00	5.0e+00	0.0e+00	0.0e+00	5.0e+00	<--Second bit is HIGH
8.000e-07	5.0e+00	5.0e+00	0.0e+00	0.0e+00	1.1e-19	
8.200e-07	5.0e+00	5.0e+00	0.0e+00	0.0e+00	0.0e+00	
8.400e-07	5.0e+00	5.0e+00	0.0e+00	0.0e+00	0.0e+00	
8.600e-07	5.0e+00	5.0e+00	0.0e+00	0.0e+00	0.0e+00	
8.800e-07	5.0e+00	5.0e+00	0.0e+00	0.0e+00	0.0e+00	
9.000e-07	5.0e+00	5.0e+00	0.0e+00	0.0e+00	0.0e+00	
9.200e-07	5.0e+00	5.0e+00	0.0e+00	5.0e+00	0.0e+00	
9.400e-07	5.0e+00	5.0e+00	0.0e+00	5.0e+00	0.0e+00	
9.600e-07	5.0e+00	5.0e+00	0.0e+00	5.0e+00	0.0e+00	
9.800e-07	5.0e+00	5.0e+00	0.0e+00	5.0e+00	0.0e+00	
1.000e-06	5.0e+00	5.0e+00	0.0e+00	2.0e+00	0.0e+00	

1.020e-06	5.0e+00	5.0e+00	0.0e+00	0.0e+00	0.0e+00	
1.040e-06	5.0e+00	5.0e+00	0.0e+00	0.0e+00	0.0e+00	
1.060e-06	5.0e+00	5.0e+00	0.0e+00	0.0e+00	0.0e+00	
1.080e-06	5.0e+00	5.0e+00	0.0e+00	0.0e+00	0.0e+00	
1.100e-06	5.0e+00	5.0e+00	0.0e+00	0.0e+00	0.0e+00	
1.120e-06	2.7e-01	5.0e+00	0.0e+00	0.0e+00	5.0e+00	
1.140e-06	1.3e-01	5.0e+00	0.0e+00	0.0e+00	5.0e+00	
1.160e-06	1.4e-01	5.0e+00	0.0e+00	0.0e+00	5.0e+00	
1.180e-06	1.2e-01	5.0e+00	0.0e+00	0.0e+00	5.0e+00	<--Third bit
1.200e-06	1.3e-01	5.0e+00	0.0e+00	0.0e+00	0.0e+00	is LOW
1.220e-06	1.3e-01	5.0e+00	0.0e+00	0.0e+00	0.0e+00	
1.240e-06	1.7e-01	5.0e+00	0.0e+00	0.0e+00	0.0e+00	
1.260e-06	1.6e-01	5.0e+00	0.0e+00	0.0e+00	0.0e+00	
1.280e-06	1.6e-01	5.0e+00	0.0e+00	0.0e+00	0.0e+00	
1.300e-06	1.6e-01	5.0e+00	0.0e+00	0.0e+00	0.0e+00	
1.320e-06	1.5e-01	5.0e+00	0.0e+00	5.0e+00	0.0e+00	
1.340e-06	1.5e-01	5.0e+00	0.0e+00	5.0e+00	0.0e+00	
1.360e-06	1.5e-01	5.0e+00	0.0e+00	5.0e+00	0.0e+00	
1.380e-06	1.5e-01	5.0e+00	0.0e+00	5.0e+00	0.0e+00	
1.400e-06	1.5e-01	5.0e+00	0.0e+00	2.0e+00	0.0e+00	
1.420e-06	1.5e-01	5.0e+00	0.0e+00	0.0e+00	0.0e+00	
1.440e-06	1.4e-01	5.0e+00	0.0e+00	0.0e+00	0.0e+00	
1.460e-06	1.4e-01	5.0e+00	0.0e+00	0.0e+00	0.0e+00	
1.480e-06	1.4e-01	5.0e+00	0.0e+00	0.0e+00	0.0e+00	
1.500e-06	1.4e-01	5.0e+00	0.0e+00	0.0e+00	0.0e+00	
1.520e-06	1.3e-01	5.0e+00	0.0e+00	0.0e+00	5.0e+00	
1.540e-06	1.3e-01	5.0e+00	0.0e+00	0.0e+00	5.0e+00	
1.560e-06	1.2e-01	5.0e+00	0.0e+00	0.0e+00	5.0e+00	
1.580e-06	1.2e-01	5.0e+00	0.0e+00	0.0e+00	5.0e+00	<--Fourth bit
1.600e-06	1.2e-01	5.0e+00	0.0e+00	0.0e+00	0.0e+00	is LOW
1.620e-06	1.1e-01	5.0e+00	0.0e+00	0.0e+00	0.0e+00	
1.640e-06	1.0e-01	5.0e+00	0.0e+00	0.0e+00	0.0e+00	
1.660e-06	1.0e-01	5.0e+00	0.0e+00	0.0e+00	0.0e+00	
1.680e-06	1.0e-01	5.0e+00	0.0e+00	0.0e+00	0.0e+00	
1.700e-06	1.0e-01	5.0e+00	0.0e+00	0.0e+00	0.0e+00	
1.720e-06	1.0e-01	5.0e+00	0.0e+00	5.0e+00	0.0e+00	
1.740e-06	9.9e-02	5.0e+00	0.0e+00	5.0e+00	0.0e+00	
1.760e-06	1.0e-01	5.0e+00	0.0e+00	5.0e+00	0.0e+00	
1.780e-06	1.0e-01	5.0e+00	0.0e+00	5.0e+00	0.0e+00	
1.800e-06	1.0e-01	5.0e+00	0.0e+00	2.0e+00	0.0e+00	
1.820e-06	1.0e-01	5.0e+00	0.0e+00	0.0e+00	0.0e+00	
1.840e-06	1.0e-01	5.0e+00	0.0e+00	0.0e+00	0.0e+00	
1.860e-06	1.0e-01	5.0e+00	0.0e+00	0.0e+00	0.0e+00	
1.880e-06	1.0e-01	5.0e+00	0.0e+00	0.0e+00	0.0e+00	
1.900e-06	1.0e-01	5.0e+00	0.0e+00	0.0e+00	0.0e+00	
1.920e-06	5.0e+00	5.0e+00	0.0e+00	0.0e+00	5.0e+00	
1.940e-06	5.0e+00	5.0e+00	0.0e+00	0.0e+00	5.0e+00	
1.960e-06	5.0e+00	5.0e+00	0.0e+00	0.0e+00	5.0e+00	
1.980e-06	5.0e+00	5.0e+00	0.0e+00	0.0e+00	5.0e+00	<--Fifth bit
2.000e-06	5.0e+00	5.0e+00	0.0e+00	0.0e+00	0.0e+00	is HIGH

Y
0 JOB CONCLUDED
0 TOTAL JOB TIME 569.97

Appendix C. Chip Pinout

This section contains the pinout for the chip that was successfully tested. It is read off from the KiC layout, clockwise starting from the top of the left hand corner.

Pin	Cell	Name	Description
15	Single Test Cell	$\overline{\text{Load}}$	Inverter Load Pulse
14	Global	GND	Ground
13	Single Test Cell	OUT	Output of Shift Register
12	Single Test Cell	Φ_2	Clock
11	Single Test Cell	Φ_1	Clock
10	Single Test Cell	Load	Load Pulse
9	Single Test Cell	IN	Input to Shift Register
8	Inpad Test Cell	IN	Input
7	Inpad Test Cell	OUT	Ouput of the Input Pad
6	Rpad Test Cell	OUT	Output of diodeless Input Pad
5	Rpad Test Cell	IN	Input of diodeless Input Pad
4	Outpad Test Cell	IN	Input to Output Pad Driver
3	Outpad Test Cell	OUT	Output of Output Pad Driver
2	Small Tactile Sensor	OUT	Output of the smaller sensor
1	Small Tactile Sensor	IN	Input to the first ~~bit~~
40	Small Tactile Sensor	Φ_1	Clock
39	Small Tactile Sensor	Load	Loading Pulse
38	Small Tactile Sensor	Φ_2	Clock
37	Global	GND	Ground
36	Global	V_{DD}	5 Volt Power Supply
35	Small Tactile Sensor	$\overline{\text{Load}}$	Inverted Loading Pulse
34	Three Bit Cell	OUT	Output
33	Three Bit Cell	Φ_1	Clock
32	Three Bit Cell	Φ_2	Clock
31	Three Bit Cell	P3	Probe of third bit
30	Three Bit Cell	P2	Probe of second bit
29	Three Bit Cell	P1	Probe of first bit
28	Three Bit Cell	Load	Loading Pulse
27	Global	GND	Ground
26	Three Bit Cell	$\overline{\text{Load}}$	Inverted Loadind Pulse
25	Large Tactile Sensor	$\overline{\text{Load}}$	Inverted Loading Pulse
24	Large Tactile Sensor	GND	Ground
23	Large Tactile Sensor	Φ_2	Clock
22	Large Tactile Sensor	Load	Loading Pulse
21	Large Tactile Sensor	Φ_1	Clock
20	Large Tactile Sensor	IN	Input to the first bit
19	Large Tactile Sensor	OUT	Output of the larger sensor
18	Single Test Cell	I1	Internal Probe Point #1

Appendix D. Photographs

This section contains photographs of the sensor in various stages of its development.

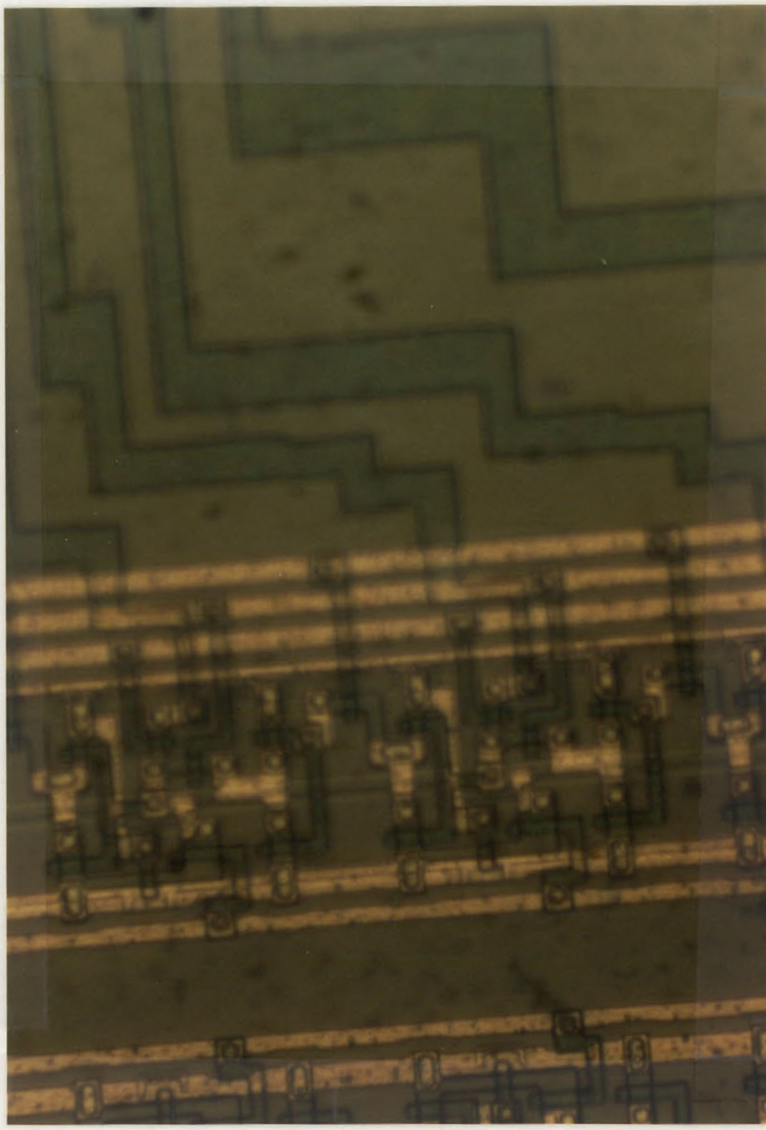

Three Bits of the Shift Register.

At the top are the polysilicon lines leading to the probes.

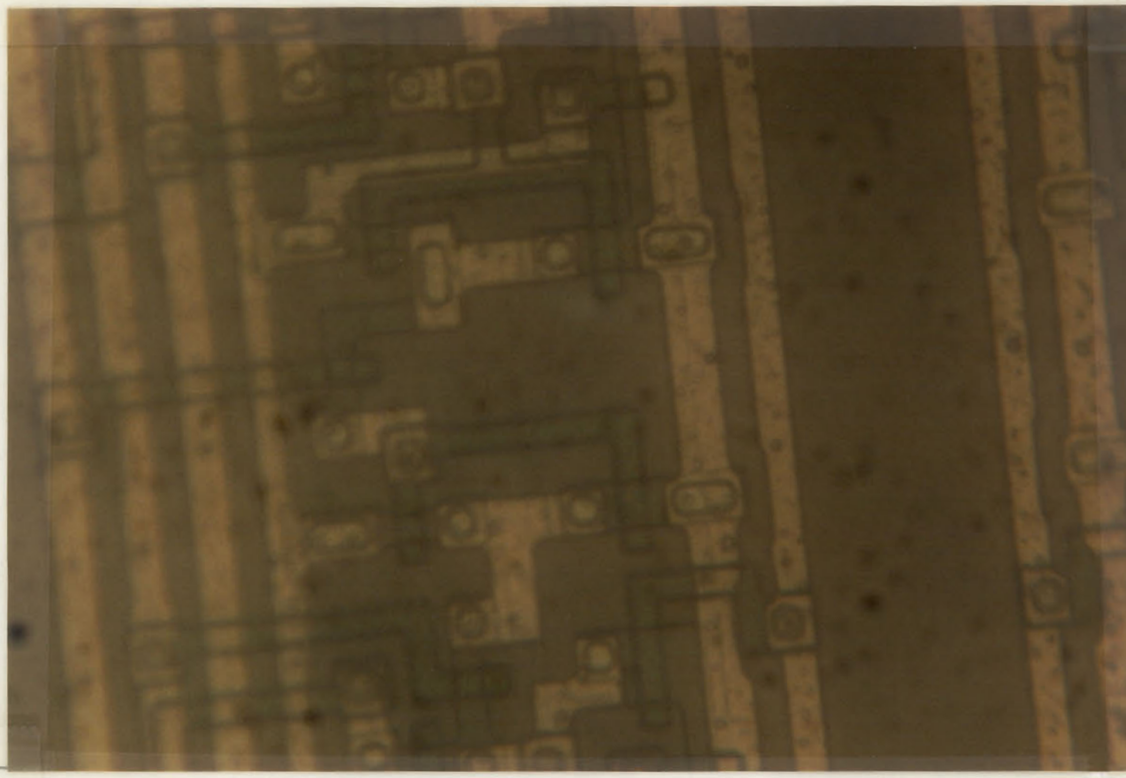

A shift register under higher magnification.

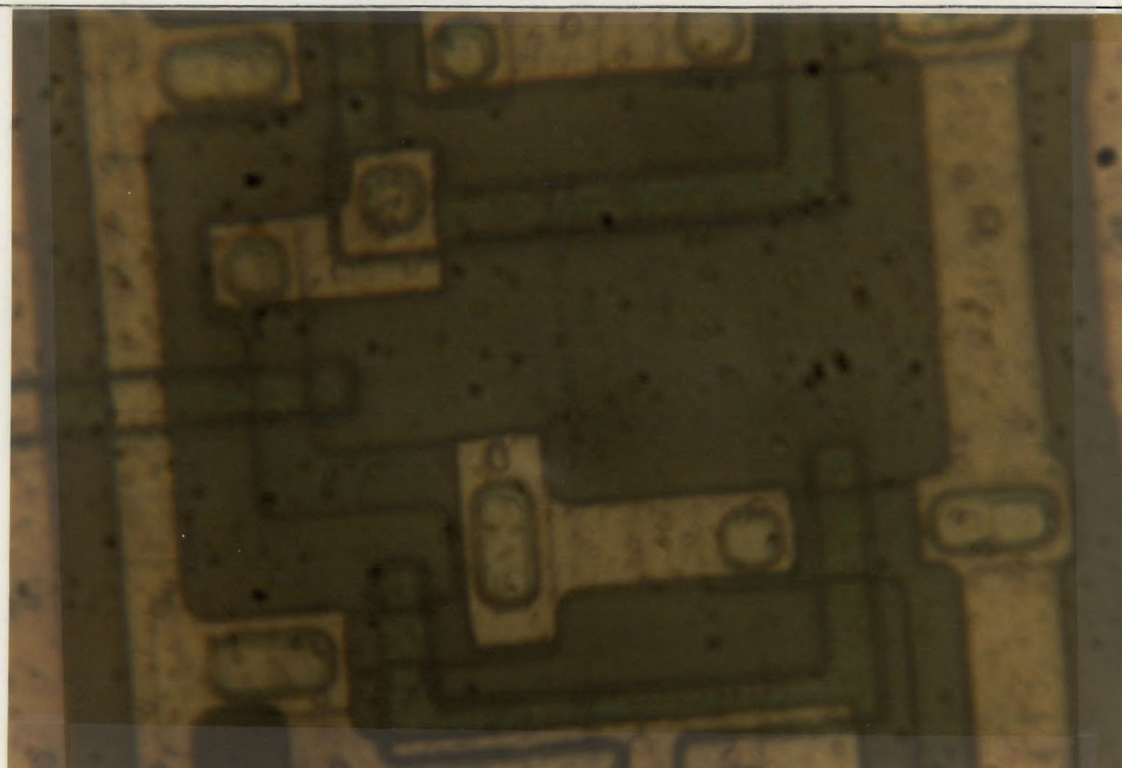

A shift register under the highest magnification.

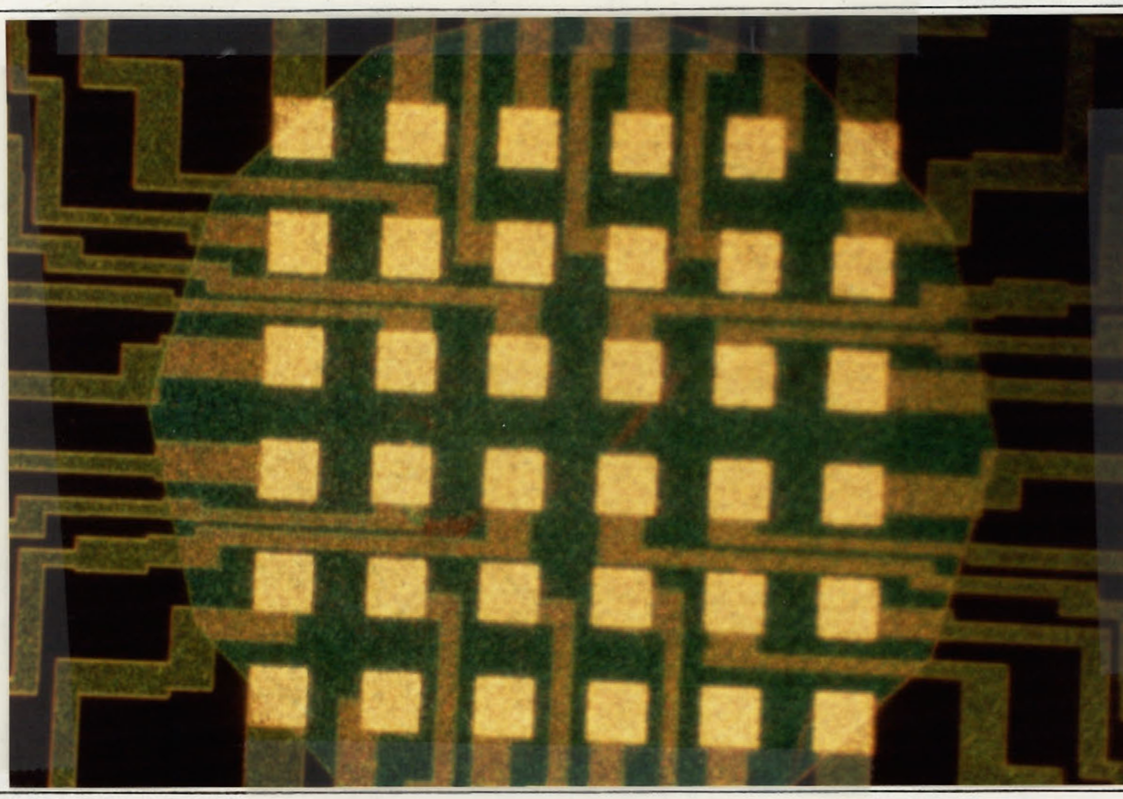

The large sensor before the application of the polyimide.

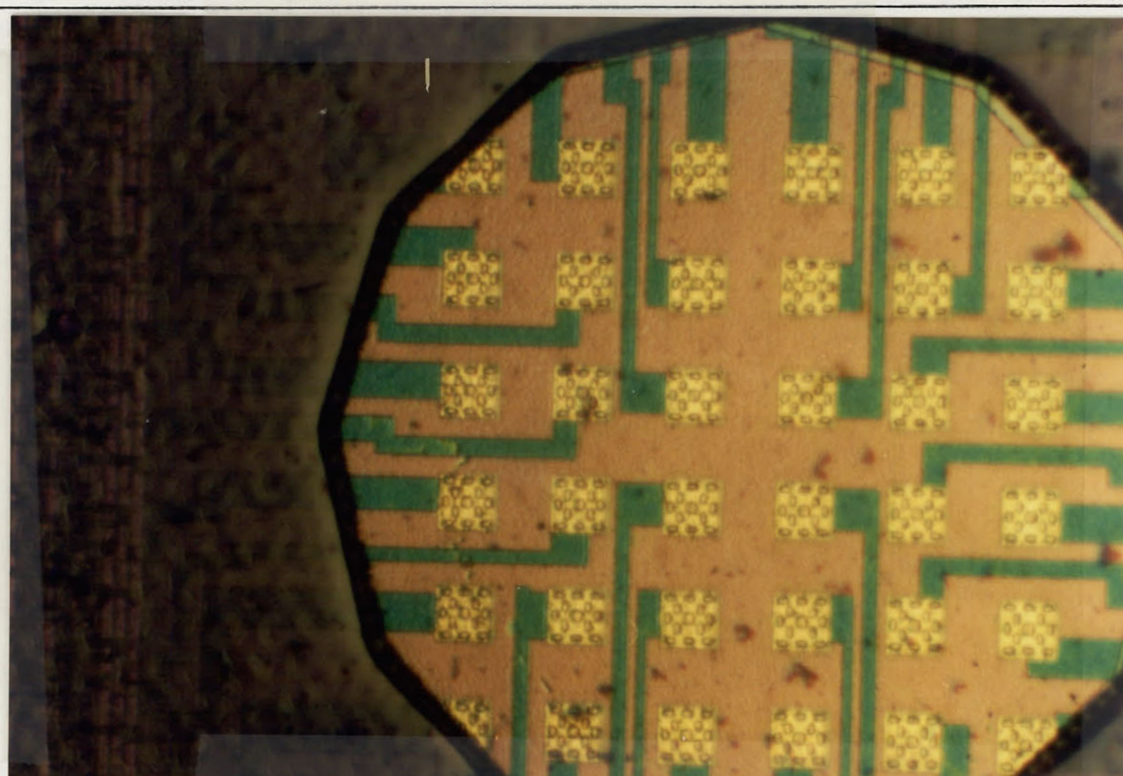

The large sensor after the application of the polyimide.

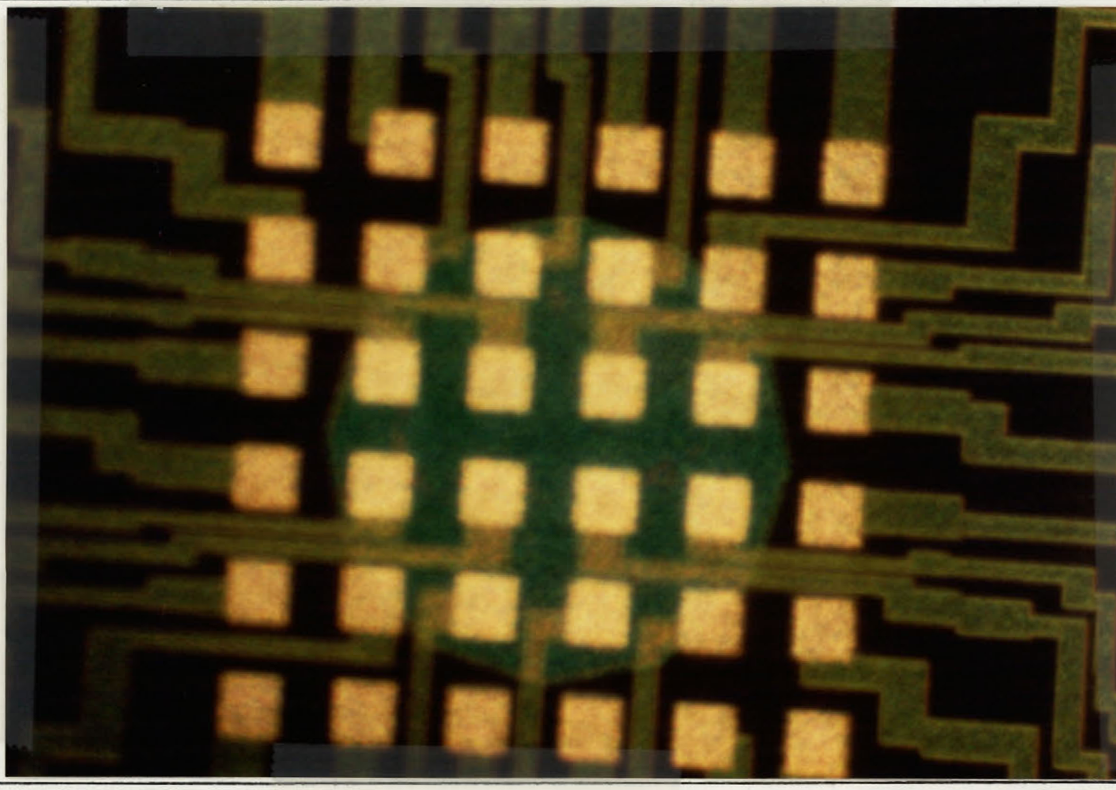

The small sensor before the application of the polyimide.

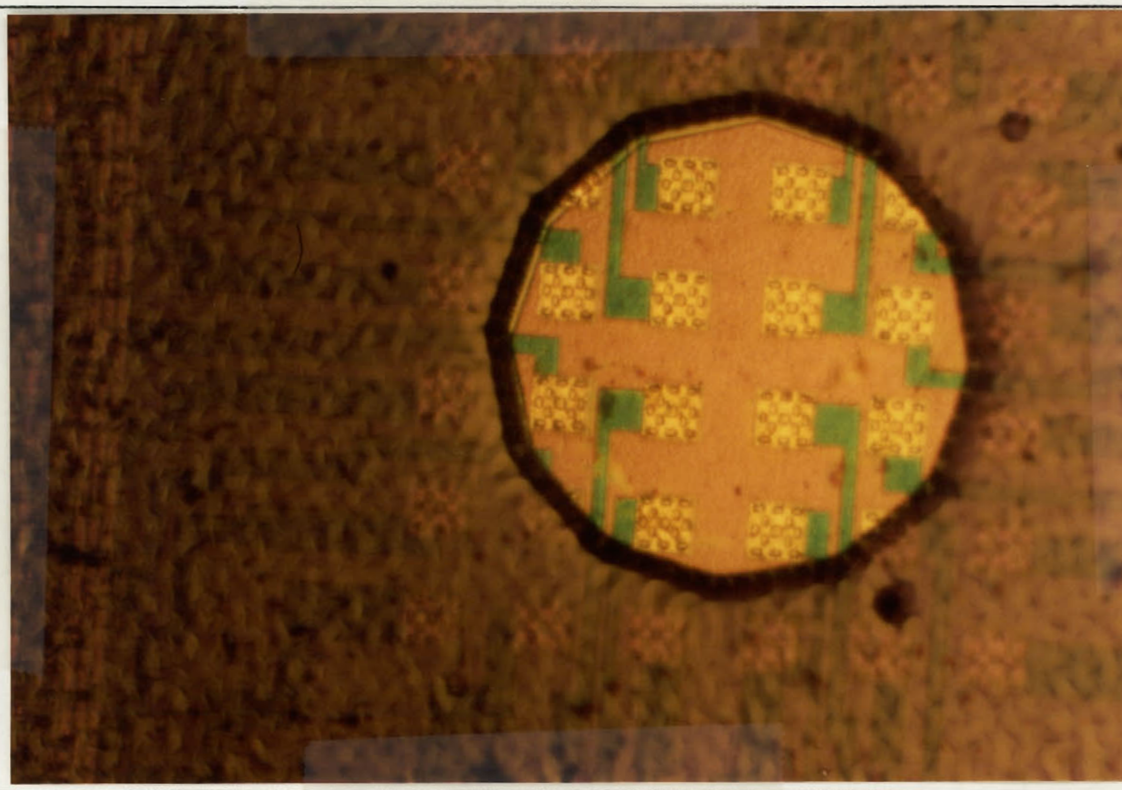

The small sensor after the application of the polyimide.

References

Bajczy Ruzena 1983 What Can We Learn form One Finger Experiments? *ISRR.*

Barth Phillip W.1986. Sensor Applications in Robotics. *Robotics Engineering.* Sept.:17–20

Bejczy Antal K. 1984. New Tactile Sensor Models for Robot Hands *U.S.A.—France Robotics Workshop.* U. of Penn, PA:1–13

Boie R.A. 1984. Capacitive Impedance Readout Tactile Image Sensor *IEEE International Conference on Robotics.*:370–375

Brock D. and Chiu S. Environment Perception of an Articulated Robot Hand Using Contact Sensors.

Buxton William, Hill Ralph and Rowley Peter 1985. Issues and Techniques in Touch–Sensitive Tablet Input. *SIGGRAPH.* 19(3):215–223

Fearing Ronald S. and Hollerbach John M. 1985. Basic Solid Mechanics for Tactile Sensing. *The International Journal for Robotics Research.* 4(3):40–54

Gaston Peter C. and Lozano-Pérez Tomás 1984. Tactile Recognition and Localization Using Object Models: The Case of Polyhedra on a Plane. *IEEE Trans. on Pattern Analysis and Machine Intelligence.* 6(3):257–265

Greene Richard 1985. The Drawing Prism: A Versatile Graphic Input Device. *SIGGRAPH.* 19(3):103–111

Grimson W. Eric L. and Lozano-Pérez Tomás 1984. Model–Based Recognition and Localization from Sparse Range or Tactile Data. *The International Journal for Robotics Research.* 3(3):3–35

Kinoshita Genichiro and Hattori Kiyoshi 1985. Tactile Sensor Design and Tactile Sensing on 3–D Objects. *Journal of Robotic Systems.* 2(1):41–52

Hackwood S., Beni G., Hornak L. A., Wolfe R., Nelson T. J. 1983. A Torque–Sensitive Tactile Array for Robotics. *The International Journal for Robotics Research.* 2(2):46–50

Hanafusa Hideo and Asada Haruhiko 1977. *A robot Hand with Elastic Fingers and its Application to Assembly Process.* IFAC Symposium on Information and control problems in Manufacturing technology. Tokyo:127–138.

Hillis William Daniel 1981. *Active Touch Sensing.* M.I.T A.I. Memo 629.

Hillis W. Daniel 1982. A High–Resolution Imaging Touch Sensor *The International Journal for Robotics Research.* 1(2):33–44

Hummel Robert A., Kimia B. and Zucker Steven W. 1983. *Deblurring Gaussian Blur.* Technical Report 83-15R. McGill University.

Keller Ken and Billingsley Giles. KIC: A Graphics Editor for Integrated Circuits. University of California at Berkeley.

Marr David 1982. *Vision.* W. H. Freenam and Company, New York

Merck Electronic Chemicals. *Photoresists: Selectilux© HTR 3* EM Industries, Inc. Hawthorne,N

Mott D. H., Lee M. H. and Nicholls H. R. An Experimental Very High Resolution Tactile Sensor Array.

Nevatia Ramkant 1982. *Machine Perception.* Prentice–Hall

Nishimura K., Nakagawa M. and Kawasaki H.. Mechanism and Control of a Page–Turning Robot.

Raibert Marc H. 1984. An All Digital VLSI Tactile Array Sensor. *IEEE International Conference on Robotics.*:314–319

Raibert Marc H. and Tanner John E. 1982. Design and Implementation of a VLSI Tactile Sensing Computer. *The International Journal for Robotics Research.* 1(3):3–18

Salisbury J. Kenneth Jr. 1983. Interpretation of Contact Geometries from Force Measurements. *ISSR.*

Tanigawa H., Ishihara T.,Hirata M. and Suzuki K. 1984. MOS Integrated Silicon Pressure Sensor. *IEEE Custom Integrated Circuits Conference.*:91–95

Vladimirescu A. et al. SPICE User's Guide. University of California at Berkeley.

Wallace Robert A. D. and Goldenberg Andrew A. A Tactile Sensor Incorporating PVF_2 as the Transduction Medium. *Towards the Factory of the Future.* eds. H.–J. Bullinger, H. J. Warnecke.

West H. and Asada H. Kinematic Analysis and Mechanical Advantage of Manipulators Constrained by Contact with the Environment.

Weste Neil and Eshraghian Kamran 1985. *Principles of CMOS VLSI Design: A Systems Perspective.* Addison–Wesley Publishing.

Yabuta T., Tsujimura T. and Morimitsu T. A Manipulator Control Method Using a Shape Recognition Systems with an Ultrasonic Distance Sensor. *Robotics and Manufacturing Automation.* eds. M. Donath and M. Leu.

THE END!